
PORTABLE SEISMIC PROPERTY ANALYZER

Identification of Asphalt Pavement Layers

Publication No. FHWA-CFL/TD-09-002

July 2009



U.S. Department
of Transportation
**Federal Highway
Administration**

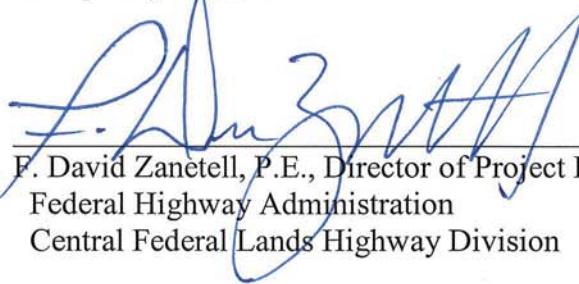


Central Federal Lands Highway Division
12300 West Dakota Avenue
Lakewood, CO 80228

FOREWORD

The Federal Lands Highway (FLH) of the Federal Highway Administration (FHWA) promotes development and deployment of applied research and technology applicable to solving transportation related issues on Federal Lands. The FLH provides technology delivery, innovative solutions, recommended best practices, and related information and knowledge sharing to Federal agencies, Tribal governments, and other offices within the FHWA.

This study evaluates the Portable Seismic Property Analyzer (PSPA) and its effectiveness in identifying pavement thickness. The results of this technique compare accurately to those from cores, and therefore the PSPA is a viable tool for transportation engineers responsible for pavement design and construction quality control.



F. David Zanetell, P.E., Director of Project Delivery
Federal Highway Administration
Central Federal Lands Highway Division

Notice

This document is disseminated under the sponsorship of the U.S. Department of Transportation in the interest of information exchange. The U.S. Government assumes no liability for the use of the information contained in this document. This report does not constitute a standard, specification, or regulation.

The U.S. Government does not endorse products or manufacturers. Trademarks or manufacturers' names appear in this report only because they are considered essential to the objective of the document.

Quality Assurance Statement

The FHWA provides high-quality information to serve Government, industry, and the public in a manner that promotes public understanding. Standards and policies are used to ensure and maximize the quality, objectivity, utility, and integrity of its information. FHWA periodically reviews quality issues and adjusts its programs and processes to ensure continuous quality improvement.

Technical Report Documentation Page

1. Report No. FHWA-CFL/TD-09-002		2. Government Accession No.		3. Recipient's Catalog No.	
4. Title and Subtitle <i>Portable Seismic Property Analyzer Identification of Asphalt Pavement Layers</i>			5. Report Date July 2009		
			6. Performing Organization Code		
7. Author(s) Manuel Celaya, Gary Young, and Soheil Nazarian			8. Performing Organization Report No.		
9. Performing Organization Name and Address Geomeia Research and Development 7225 Bosque Road Canutillo, TX 79835			10. Work Unit No. (TRAIS)		
			11. Contract or Grant No. DTFH68-03-P-00182		
12. Sponsoring Agency Name and Address Federal Highway Administration Central Federal Lands Highway Division 12300 W. Dakota Avenue, Suite 210 Lakewood, CO 80228			13. Type of Report and Period Covered Final Report, October 2003		
			14. Sponsoring Agency Code HFTS-16.4		
15. Supplementary Notes COTR: Matt DeMarco, FHWA CFLHD. Advisory Panel Members: Mike Voth, FHWA-FLH; Khamis Haramy, Michael Peabody, Steve Deppmeier, and Roger Surdahl, FHWA-CFLHD. This project was funded under the FHWA Federal Lands Highway Technology Deployment Initiatives and Partnership Program (TDIPP).					
16. Abstract The focus of the study was to evaluate the effectiveness of the Portable Seismic Property Analyzer (PSPA) to rapidly and nondestructively measure thickness and in situ moduli of asphalt pavement layers. These procedures are presented to calibrate and validate the results in the laboratory with simplified seismic tests on extracted cores and determine the design modulus from measured values. Performing these simplified laboratory and field tests along with more traditional tests may result in a database that can be used to smoothly unify the design procedures with pavement evaluation. Specifically, six sites with different pavement conditions and structures throughout Colorado were tested October 2003, and the results summarized in this report. Based on the results, the PSPA is proposed as a viable tool for immediate implemetation by the Federal Highway Administration, Federal Lands Highway.					
17. Key Words NONDESTRUCTIVE TESTING, SEISMIC, ASPHALT CONCRETE, PORTABLE SEISMIC PROPERTY ANALYZER			18. Distribution Statement No restriction. This document is available to the public from the sponsoring agency at the website http://www.cflhd.gov .		
19. Security Classif. (of this report) Unclassified		20. Security Classif. (of this page) Unclassified		21. No. of Pages 96	22. Price

SI* (MODERN METRIC) CONVERSION FACTORS

APPROXIMATE CONVERSIONS TO SI UNITS

Symbol	When You Know	Multiply By	To Find	Symbol
LENGTH				
in	inches	25.4	Millimeters	mm
ft	feet	0.305	Meters	m
yd	yards	0.914	Meters	m
mi	miles	1.61	Kilometers	km
AREA				
in ²	square inches	645.2	Square millimeters	mm ²
ft ²	square feet	0.093	Square meters	m ²
yd ²	square yard	0.836	Square meters	m ²
ac	acres	0.405	Hectares	ha
mi ²	square miles	2.59	Square kilometers	km ²
VOLUME				
fl oz	fluid ounces	29.57	Milliliters	mL
gal	gallons	3.785	Liters	L
ft ³	cubic feet	0.028	cubic meters	m ³
yd ³	cubic yards	0.765	cubic meters	m ³
NOTE: volumes greater than 1000 L shall be shown in m ³				
MASS				
oz	ounces	28.35	Grams	g
lb	pounds	0.454	Kilograms	kg
T	short tons (2000 lb)	0.907	megagrams (or "metric ton")	Mg (or "t")
TEMPERATURE (exact degrees)				
°F	Fahrenheit	5 (F-32)/9 or (F-32)/1.8	Celsius	°C
ILLUMINATION				
fc	foot-candles	10.76	Lux	lx
fl	foot-Lamberts	3.426	candela/m ²	cd/m ²
FORCE and PRESSURE or STRESS				
lbf	poundforce	4.45	Newtons	N
lbf/in ²	poundforce per square inch	6.89	Kilopascals	kPa

APPROXIMATE CONVERSIONS FROM SI UNITS

Symbol	When You Know	Multiply By	To Find	Symbol
LENGTH				
mm	millimeters	0.039	Inches	in
m	meters	3.28	Feet	ft
m	meters	1.09	Yards	yd
km	kilometers	0.621	Miles	mi
AREA				
mm ²	square millimeters	0.0016	square inches	in ²
m ²	square meters	10.764	square feet	ft ²
m ²	square meters	1.195	square yards	yd ²
ha	Hectares	2.47	Acres	ac
km ²	square kilometers	0.386	square miles	mi ²
VOLUME				
mL	Milliliters	0.034	fluid ounces	fl oz
L	liters	0.264	Gallons	gal
m ³	cubic meters	35.314	cubic feet	ft ³
m ³	cubic meters	1.307	cubic yards	yd ³
MASS				
g	grams	0.035	Ounces	oz
kg	kilograms	2.202	Pounds	lb
Mg (or "t")	megagrams (or "metric ton")	1.103	short tons (2000 lb)	T
TEMPERATURE (exact degrees)				
°C	Celsius	1.8C+32	Fahrenheit	°F
ILLUMINATION				
lx	lux	0.0929	foot-candles	fc
cd/m ²	candela/m ²	0.2919	foot-Lamberts	fl
FORCE and PRESSURE or STRESS				
N	newtons	0.225	Poundforce	lbf
kPa	kilopascals	0.145	poundforce per square inch	lbf/in ²

*SI is the symbol for the International System of Units. Appropriate rounding should be made to comply with Section 4 of ASTM E380.
(Revised March 2003)

TABLE OF CONTENTS

CHAPTER 1 – EXECUTIVE SUMMARY 1

CHAPTER 2 – INTRODUCTION 3

 OBJECTIVES 3

 ORGANIZATION 3

CHAPTER 3 – BACKGROUND 5

 METHODOLOGY FOR QUALITY CONTROL BASED ON SEISMIC METHOD 6

 Step 1: Selecting the Most Suitable Material 6

 Step 2: Selecting the Most Suitable Moduli 7

 Step 3: Characterizing the Variation in Modulus with Temperature 7

 Step 4: Determining Design Modulus of Material 7

 Step 5: Field Quality Control 8

 DESIGN MODULUS FROM SEISMIC MODULUS 9

CHAPTER 4 – TEST METHODS 11

 PORTABLE SEISMIC PROPERTY ANALYZER 11

 Ultrasonic Laboratory Test 17

 DIAMETRAL RESILIENT MODULUS 17

CHAPTER 5 – TEST PROTOCOL 21

 SELECTION AND MARKING OF TEST SITES 21

 PSPA TESTS 22

 RETRIEVAL OF CORES 24

 LAB TESTS 27

 RELATING LAB AND FIELD TEST RESULTS 27

CHAPTER 6 – PRESENTATION OF RESULTS 31

 DESCRIPTION OF SITES 31

 Site 1: Tarryall Road 31

 Site 2: Great Sand Dunes National Monument 32

 Site 3: Taylor River Road 32

 Site 4: Mesa Verde National Park 32

 Site 5: Canyonlands National Park – The Needles 32

 Site 6: Colorado National Monument 32

 VOLUMETRIC PROPERTIES 32

 PSPA MODULI 33

 DESIGN MODULI 41

 COMPARISON OF CORE MODULI WITH PSPA MODULI 41

CHAPTER 7 – SUMMARY AND CONCLUSIONS 43

REFERENCES 45

PORTABLE SEISMIC PROPERTY ANALYZER – TABLE OF CONTENTS

APPENDIX A – PHOTO ALBUM47

APPENDIX B – VOLUMETRIC INFORMATION59

APPENDIX C – PSPA RESULTS61

APPENDIX D – TYPICAL RESULTS FROM PSPA.....67

APPENDIX E – MASTER CURVES79

LIST OF FIGURES

Figure 1. Graph. Process of Determining Most Suitable Moduli.	7
Figure 2. Graph. Process of Characterizing Variation in Modulus with Temperature.	8
Figure 3. Graph. Process of Estimating Design Modulus.	8
Figure 4. Graph. Process of Field Testing for HMA Materials.	9
Figure 5. Graph. Master Curve Concept for Defining Design Modulus.	10
Figure 6. Photo. Portable Seismic Pavement Analyzer.	12
Figure 7. Graph. Typical Time Records from PSPA.	13
Figure 8. Schematic. Ultrasonic Surface Wave Method.	14
Figure 9. Graph. Typical Dispersion Curve Obtained from Time Records in Figure 7.	15
Figure 10. Graph. Typical Phase Spectra Obtained from Time Records in Figure 7.	15
Figure 11. Schematic. Impact Echo Method.	16
Figure 12. Schematic and Photo. Ultrasonic Test Device for AC Specimens.	18
Figure 13. Photo. Diametral Resilient Modulus Test.	19
Figure 14. Schematic. Specimen Subjected to Diametral Test.	19
Figure 15. Graph. Time Relationships for Repeated-Load Indirect Tension Test (after Roberts et al., 1996).	20
Figure 16. Schematic. Typical Marking of Sites.	21
Figure 17. Screen Shot. Typical Time Records as Demonstrated by PSPA Software.	22
Figure 18. Screen Shot. Typical Interpreted Results as Demonstrated by PSPA Software.	23
Figure 19. Graph. Typical Variation in Modulus along a Site.	25
Figure 20. Photo. Typical Coring Operation by CFLHD Staff.	26
Figure 21. Photo. Typical Core Retrieved from the Site.	26
Figure 22. Graph. Typical Master Curve to Combine all Test Results.	28
Figure 23. Graph. Typical Comparison of PSPA Field Moduli with Ultrasonic Lab Results.	29
Figure 24. Map. Location of Sites.	31
Figure 25. Graph. Variation in Modulus with PSPA along Site 1.	34
Figure 26. Graph. Variation in Modulus with PSPA along Site 2.	35
Figure 27. Graph. Variation in Modulus with PSPA along Site 3.	36
Figure 28. Graph. Variation in Modulus with PSPA along Site 4.	37
Figure 29. Graph. Variation in Modulus with PSPA along Site 5.	38
Figure 30. Graph. Variation in Modulus with PSPA along Site 6.	39
Figure 31. Graph. Comparison of Moduli Obtained by Ultrasonic Device and PSPA at all Sites.	42
Figure 32. Graph. Variation between Moduli Obtained by Ultrasonic Device and PSPA at all Sites.	42
Figure 33. Photo. Measuring with the PSPA on the Side of the Road at Site 1.	47
Figure 34. Photo. Coring at Site 1.	47
Figure 35. Photo. Cores from Site 1.	48
Figure 36. Photo. Coring at Site 2.	48
Figure 37. Photo. Examples of Cracks at Site 2.	49
Figure 38. Photo. View of Site 2.	49
Figure 39. Photo. Cores from Site 2.	50
Figure 40. Photo. View of Site 3.	50
Figure 41. Photo. Coring at Site 3.	51

PORTABLE SEISMIC PROPERTY ANALYZER – TABLE OF CONTENTS

Figure 42. Photo. Cores from Site 3.	51
Figure 43. Photo. Close up of Site 4.	52
Figure 44. Photo. View of Site 4.....	52
Figure 45. Photo. Coring at Site 4.....	53
Figure 46. Photo. Cores from Site 4.	53
Figure 47. Photo. Close up of Site 5.	54
Figure 48. Photo. View of Site 5.....	54
Figure 49. Photo. Coring at Site 5.....	55
Figure 50. Photo. Cores from Site 5.	55
Figure 51. Photo. Close up of Site 6.	56
Figure 52. Photo. Cracking at Site 6.	56
Figure 53. Photo. View of Site 6.....	57
Figure 54. Photo. Cores at Site 6.	57
Figure 55. Graph. Typical PSPA Results at Site 1.	67
Figure 56. Graph. Typical PSPA Results at Site 2.	69
Figure 57. Graph. Typical PSPA Results at Site 3.	71
Figure 58. Graph. Typical PSPA Results at Site 4.	73
Figure 59. Graph. Typical PSPA Results at Site 5.	75
Figure 60. Graph. Typical PSPA Results at Site 6.	77
Figure 61. Graph. Master Curves for Site 2.....	79
Figure 62. Graph. Master Curves for Site 3.....	80
Figure 63. Graph. Master Curves for Site 4.....	81
Figure 64. Graph. Master Curves for Site 5.....	82
Figure 65. Graph. Master Curves for Site 6.....	83

LIST OF TABLES

Table 1. Volumetric Information from Cores Retrieved from the Site.....27
Table 2. Volumetric Information from Cores Retrieved from Different Sites.33
Table 3. Seismic Moduli Obtained from PSPA at Different Sites.33
Table 4. Design Moduli Obtained from Integration of Lab and PSPA Tests at Different Sites...41
Table 5. Volumetric Information from Cores Retrieved at Site 2.59
Table 6. Volumetric Information from Cores Retrieved at Site 3.59
Table 7. Volumetric Information from Cores Retrieved at Site 4.59
Table 8. Volumetric Information from Cores Retrieved at Site 5.60
Table 9. Volumetric Information from Cores Retrieved at Site 6.60
Table 10. Seismic Moduli Measured at Site 1.61
Table 11. Seismic Moduli Measured at Site 2.62
Table 12. Seismic Moduli Measured at Site 3.63
Table 13. Seismic Moduli Measured at Site 4.64
Table 14. Seismic Moduli Measured at Site 5.65
Table 15..Seismic Moduli Measured at Site 6.66
Table 16. Master Curve Parameters for Site 2.84
Table 17. Master Curve Parameters for Site 3.84
Table 18. Master Curve Parameters for Site 4.84
Table 19. Master Curve Parameters for Site 5.84
Table 20. Master Curve Parameters for Site 6.85

CHAPTER 1 – EXECUTIVE SUMMARY

Depending upon the thickness of pavement layers and the mode(s) of failure, different structural parameters play dominant roles in the behavior of pavements. In general, the most important parameters are moduli of different layers. Currently, measuring moduli of asphalt concrete pavement (ACP) layers nondestructively, especially when they are thin, is difficult or impossible. The Portable Seismic Property Analyzer (PSPA), a seismic-based measurement device, provides a viable alternative for measuring pavement moduli in the field.

The major advantage of seismic methods is that similar results are obtained from field and laboratory tests as long as the material is tested under comparable conditions. This unique feature of seismic methods in material characterization is of particular significance to the implementation of performance-based design.

The focus of the study is on evaluating the utility of the PSPA for measuring moduli of ACP rapidly and nondestructively in situ. Procedures have been presented to measure the moduli of ACP with the PSPA, calibrate and validate the results in the laboratory with simplified seismic tests on extracted cores, and determining the design modulus from measured values. Performing the simplified laboratory and field tests, along with more traditional tests, will result in a database that can be used to smoothly unify design procedures with pavement evaluation.

This report presents the results of field investigations conducted in October 2003 at six sites with different pavement conditions and structures in Colorado and Utah. Based on the results presented, the PSPA is proposed as a viable tool for immediate implementation by CFLHD and other branches of the Federal Highway Administration.

CHAPTER 2 – INTRODUCTION

In many current procedures for structural design of pavements an accurate determination of layer moduli is required. These moduli can either be determined with field testing or laboratory testing. Laboratory tests are essential to study the parameters that affect the properties of materials. Laboratory tests on specimens prepared from material retrieved during construction or on cores is currently the most common way of obtaining pavement layer moduli. These test procedures are time consuming, and associated equipment costs are high. Practically speaking, no more than two specimens can be tested in one day. Moreover, the laboratory prepared specimens may not be representative of as-placed materials. Nondestructive field tests are more practical and desirable because they are rapid to perform and test the material in its natural state. The Portable Seismic Property Analyzer (PSPA) is an example of such a device.

Seismic methods, such as incorporated in the PSPA, can provide moduli of different pavement layers and have distinct advantages over other methods used in the state of practice. Seismic moduli are fundamentally-correct material properties, which can often be measured equally easily in the laboratory and in the field (see Chapter 3).

OBJECTIVES

The overall objective of this work was to compare field PSPA moduli and thickness data with laboratory data from cores. The study also addresses issues regarding how CFLHD engineers can implement techniques involving seismic measurements to improve design, construction, and maintenance programs. The PSPA was deployed at six sites in October 2003 to measure the modulus of several asphalt concrete pavement (ACP) sections that are part of the road network monitored by the CFLHD. Cores were also extracted from the sites for performing laboratory measurements using an ultrasonic device. Select cores were then subjected to diametral resilient modulus tests to relate the seismic moduli with the design moduli. This report presents the comparisons of field and laboratory data and the master curves.

ORGANIZATION

This report contains several chapters. Chapter 2 contains a brief introduction. The historical background behind the methodology is included in Chapter 3. In Chapter 4, the laboratory and field test methods used in this study are introduced. The test protocol is described in Chapter 5. The description of the sites tested is included in Chapter 6, along with the results from field and lab tests. Finally, in Chapter 7 conclusions are drawn and recommendations for future work are presented. Several appendices contain the test data.

CHAPTER 3 – BACKGROUND

Current mechanistic design procedures are based on modeling pavement as an elastic multi-layered system. Estimating the remaining life of flexible pavements is mainly based on predicting the strains or stresses at the interfaces of different layers. The two main strains considered are the tensile strain at the bottom of the AC layer and the compressive strain on top of the subgrade (Huang, 1993). These critical strains are strongly related to the moduli of all pavement layers.

Daniel and Kim (1998) defined several field and laboratory tests for determining AC moduli. The most common laboratory tests are the resilient modulus, creep, uniaxial frequency sweep, free-free resonant column, and ultrasonic wave velocity tests. The main field tests are the Falling Weight Deflectometer (FWD) and wave propagation (or seismic) tests.

Resilient modulus tests have been used by many researchers to measure the modulus of Hot Mix Asphalt (Roberts et al., 1996). These tests can be performed either in compression (similar to soil specimens) or diametrically. The diametral resilient modulus test will be discussed comprehensively in the next section since it was used in this study.

In the creep test, the specimen is subjected to a static load. The displacement of the specimen due to the applied load is measured with time. Using the variation in compliance (ratio of the strain and stress) with time, and the time-temperature superposition principle (Kim and Lee, 1995), the relaxation modulus can be determined and converted to a modulus.

In the uniaxial frequency sweep test, also known as the complex modulus test, the stresses and strains under sinusoidal loading are measured (ASTM D3497). Assuming that the material is linear viscoelastic, the dynamic modulus and viscous damping (or storage and loss moduli) are determined. By varying the frequency over a wide range, the variation in modulus with frequency can be determined. The method can be effective over a range of frequencies from 0.1 Hz to 50 Hz.

In the free-free resonant column test, also known as the impact resonance test, the specimen is impacted with a hammer, and the resonant frequency associated with the standing waves within the specimen is measured. The resonant frequency, along with the length of the specimen, can be used to determine the modulus (ASTM C215).

The ultrasonic wave velocity method will be discussed comprehensively in the next section. This method was used in this study.

Most of the laboratory tests discussed above are comprehensive and time-consuming. As such, they are not suitable for testing a large number of specimens. The free-free resonant column test is quite rapid. For this test to be effective, a specimen with a length-to-diameter ratio of at least two is required. Since preparing such specimens from the thin pavements tested in this study was not reasonable, this test method was not considered.

Several parameters affect the modulus of bituminous materials. The most important parameters are the rates and frequency of loading, temperature, air void content, binder content and gradation. The impact of each of these parameters is well published. An excellent review of this matter can be found in Roberts, et al. (1996).

Daniel and Kim (1998) and Kim and Lee (1995) used the results from several laboratory and field tests (such as FWD, ultrasonic, uniaxial sweep, and creep) to show the frequency-dependency of modulus. Aouad et al. (1993) clearly demonstrated the importance of considering the rate of loading. At a temperature of 77^oF, the modulus measured with seismic methods should be reduced by a factor of about three to account for the rate of loading.

The AC modulus is strongly dependent on temperature. Von Quintus and Killingworth (1998) demonstrate the importance of temperature correction, and the complexity involved in considering the temperature gradient within a pavement section. Aouad et al. (1993), Li and Nazarian (1994), and several other investigators have studied the variation in modulus with temperature for seismic methods.

METHODOLOGY FOR QUALITY CONTROL BASED ON SEISMIC METHOD

Nazarian et al. (2003) have proposed a comprehensive protocol for quality management of the ACP based on seismic methods. The proposed quality management procedure consists of five steps. The first step consists of selecting the most suitable material or mix for a given project. In the second step, a suitable modulus value is determined based on variation in modulus with the primary parameter of interest. For a particular hot mix asphalt (HMA) mixture, this step may consist of developing an air voids vs. modulus curve. In the third step, the variation in modulus with environmental factors is considered. In the case of an HMA layer, the variation in modulus with temperature is important. The fourth step consists of determining the design modulus for the material. The fifth and final step is to compare the field modulus with the acceptable laboratory modulus. All steps are briefly described below.

Step 1: Selecting the Most Suitable Material

Even though the durability of a material cannot be directly included in the structural design of a pavement, the durability definitely does impact performance. The process of volumetric design, from the simplest Marshall method to the most sophisticated, Strategic Highway Research Program (SHRP) method, ensures a constructible and durable material. However, the material selection and mix design should be based on the existing collective experience within the highway community. The following steps, even though more quantitative, do not replace this knowledge.

Step 2: Selecting the Most Suitable Moduli

After the material is selected and its constructability is ascertained, the next step is to determine its most suitable modulus. The modulus can be related to one of the primary construction parameters such as the compaction effort (i.e., air voids) similar to Figure 1. Two modulus values should be selected from the seismic modulus-air voids curves: the modulus corresponding to the air voids at placement (typically 7-8%), and the modulus at design air voids from the job mix formula (JMF, typically 4%). The modulus at placement is used by the construction engineer for field quality control as described in Step 5. The modulus at the design air voids is used by the pavement engineers to determine the modulus that should be used in structural design as discussed in Step 4.

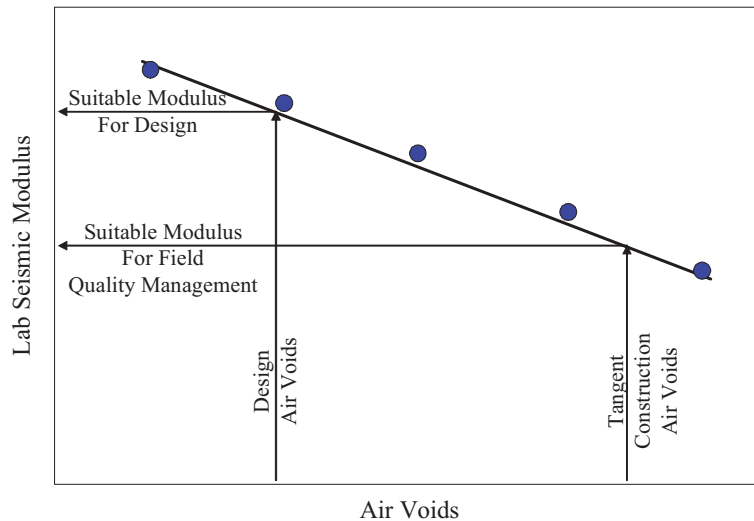


Figure 1. Graph. Process of Determining Most Suitable Moduli.

Step 3: Characterizing the Variation in Modulus with Temperature

After the compaction of a layer is completed, it may be exposed to different temperatures. The simplest method of relating modulus to temperature consists of preparing two specimens: one at the JMF air voids and another at the target placement air voids. These specimens are subjected to a sequence of temperatures. The suitable temperature range for the region being considered can be determined based on the guidelines set forward by SHRP for selecting the regional air temperature extremes to determine the appropriate PG grade for the binder. At the end of each temperature sequence, the specimens are tested as described in the next sections. An example for the variations in modulus with temperature for one mixture is shown in Figure 2.

Step 4: Determining Design Modulus of Material

The most suitable seismic modulus at JMF air voids, determined in Step 2, should be translated to a design modulus as will be discussed in the next section. As schematically shown in Figure 3, the most rigorous way of calculating the design modulus is to develop a master curve as advocated by the new 2002 Pavement Design Guide funded by the National Cooperative Highway Research (NCHRP) under Project 10-37.

If the modulus assumed by the designer and the one obtained from this analysis are significantly different, either an alternative material should be used, or the layer thickness should be adjusted. In that manner, the design and material selection can be harmonized.

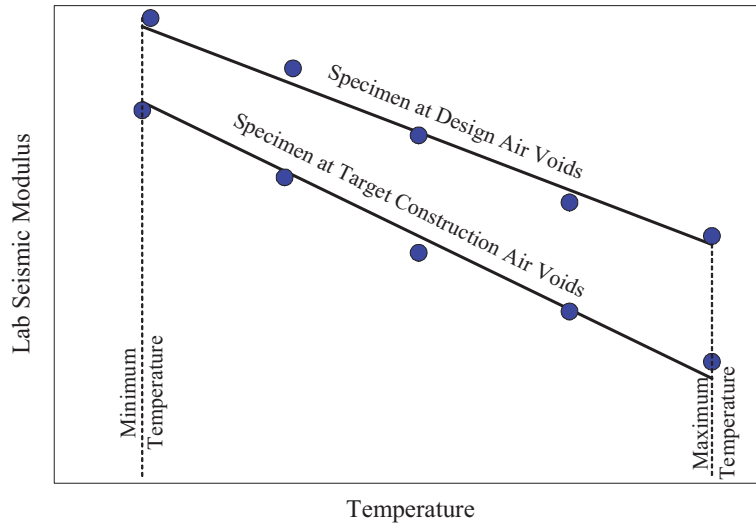


Figure 2. Graph. Process of Characterizing Variation in Modulus with Temperature.

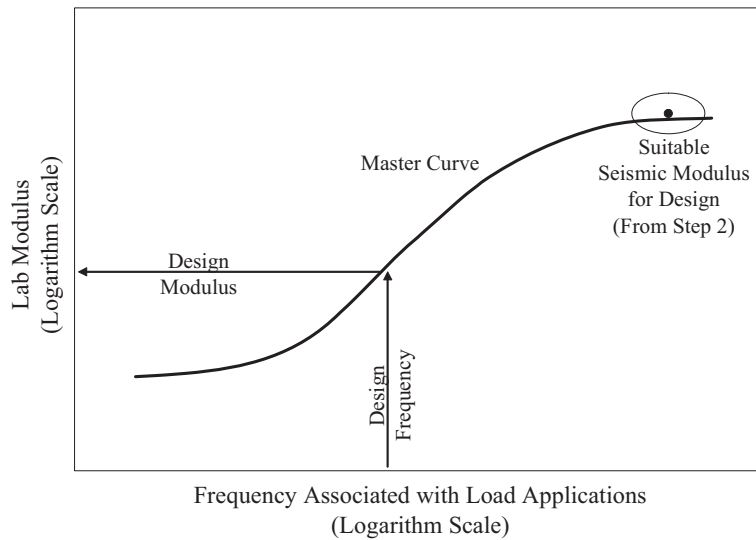


Figure 3. Graph. Process of Estimating Design Modulus.

Step 5: Field Quality Control

Tests are carried out at regular intervals or at any point that the construction inspector suspects segregation, lack of compaction, or any other construction related anomalies. The field moduli should be greater than the most suitable laboratory seismic modulus determined at the placement air voids in Step 2. An example is shown in Figure 4.

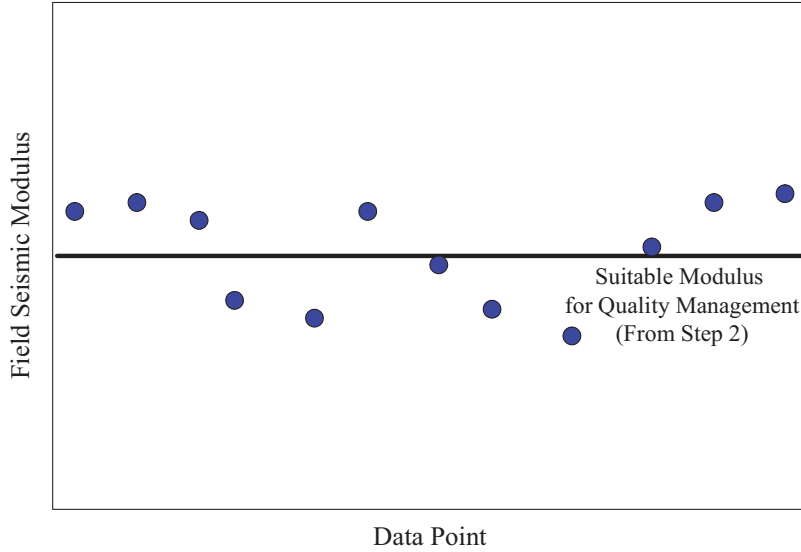


Figure 4. Graph. Process of Field Testing for HMA Materials.

As emphasized in Step 2, it is important to make a distinction between the most suitable modulus for design reported to the pavement engineer and the most suitable modulus used as a guideline for quality management.

The procedure described above was adapted to the study described here. The methodology followed is described in Chapter 4.

DESIGN MODULUS FROM SEISMIC MODULUS

Moduli obtained with seismic measurements are low-strain high-strain-rate values. Vehicular traffic causes high strain deformation at low strain rates. Because of the difference, there has been concern in the pavement community regarding how to implement seismic moduli in the design. This concern has been resolved by implementing a master curve concept, which tracks modulus over a wide frequency range.

The most desirable way of calculating the design modulus is to develop the master curve based on the recommendations of Witczak et al. (1999). The response of a viscoelastic material, such as AC, is dependent on the loading frequency and temperature. The general practice has been to perform the testing at various temperatures with similar loading frequencies. A master curve is generated at a reference temperature by using time-temperature shift factors. The following sigmoid function proposed by Ferry (1970) can be used to generate a master curve

$$\log(E^*) = \delta + \frac{\alpha}{1 + e^{\beta + \gamma \times \log t_r}} \tag{3.1}$$

where E^* = dynamic modulus, t_r = loading period, δ = minimum value of dynamic modulus, $\delta + \alpha$ = maximum value of dynamic modulus, and β and γ = sigmoidal function shape parameters. Once the master curve is established, the design modulus can be readily determined from the design vehicular speed and the design temperature as recommended in the 2002 Design Guide.

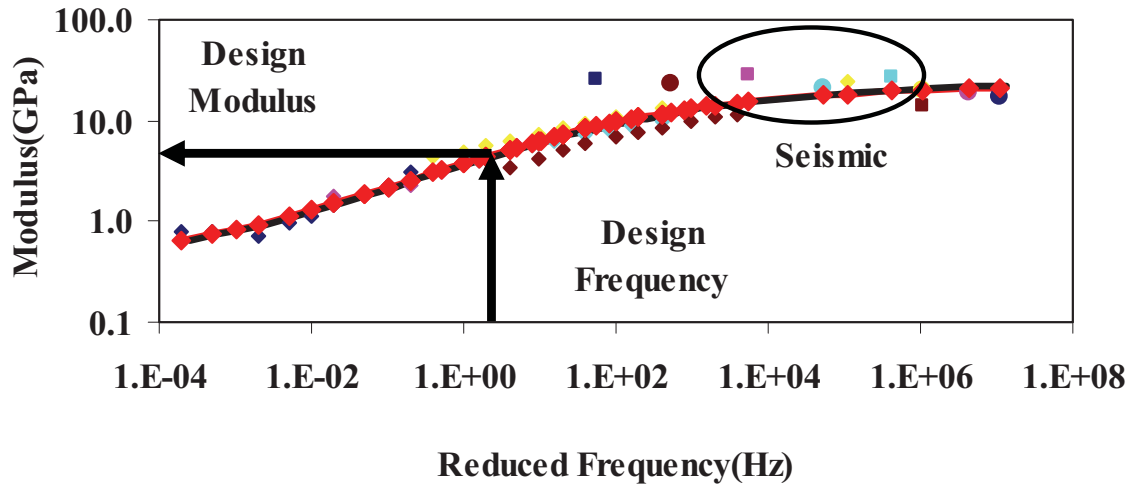


Figure 5. Graph. Master Curve Concept for Defining Design Modulus.

Tandon et al. (2004), have shown that the seismic modulus and the master curve from complex modulus correlate well. Typical results from one material when the seismic and dynamic moduli are combined are shown in Figure 5. First, a reference temperature is defined for the region. A design frequency is then determined based upon the vehicular speed. The desired design modulus based on these two input parameters can readily be determined from the master curve, as shown in the figure.

CHAPTER 4 – TEST METHODS

As indicated above, the methodology developed by Nazarian et al. (2003) for quality management of ACP was modified and applied to this study. The test methods employed in that work are introduced in this chapter. A laboratory and a field seismic device were used in this study and compared to traditional laboratory tests. These test methods and the theoretical backgrounds behind them are described below.

PORTABLE SEISMIC PROPERTY ANALYZER

With the PSPA, the average modulus of the exposed surface layers can be estimated within a few seconds in the field. The PSPA, shown in Figure 6, consists of two transducers (accelerometers in this case) and a source packaged into a hand-portable system, which can perform high frequency seismic tests. The source package is also equipped with a transducer for consistency in triggering and for some advanced analysis of the signals. The device is operable from a computer tethered to the hand-carried transducer unit through a cable that carries operational commands to the PSPA and returns the measured signals to the computer.

The operating principle of the PSPA is based on generating and detecting stress waves in a medium. The Ultrasonic Surface Wave (USW) interpretation method, which is implemented in the Spa Manager software in the PSPA computer, is used to determine the modulus of the material. Description of the measurement and implementation techniques is the subject of the next few pages.

To collect data with the PSPA, the technician only initiates the testing sequence through the computer. All the other data acquisition tasks are handled automatically by the computer. The high-frequency source is activated four to six times. Pre-recording impacts of the source are used to adjust the gains of the amplifiers in a manner that optimizes the dynamic range of the electronics. The outputs of the three transducers from the final three impacts are saved and stacked. Typical voltage outputs of the three accelerometers are shown in Figure 7.

The relationship between velocity, V , travel time, Δt , and receiver spacing, ΔX , can be written in the following form:

$$V = \frac{\Delta X}{\Delta t} \quad (4.1)$$

In this equation, V can be the propagation velocity of any of seismic waves [i.e. compression wave, V_P ; shear wave, V_S ; or surface (Rayleigh) wave, V_R]. Knowing any one wave velocity, the modulus can be determined, using appropriate transformations.

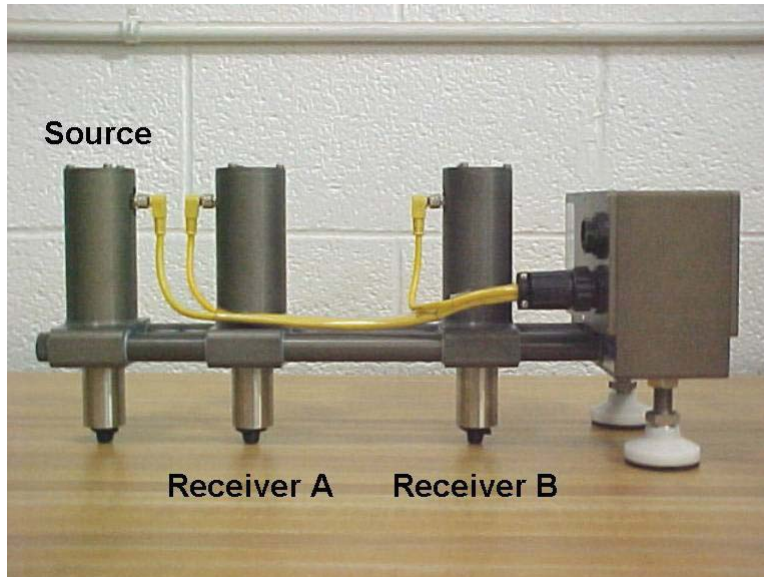
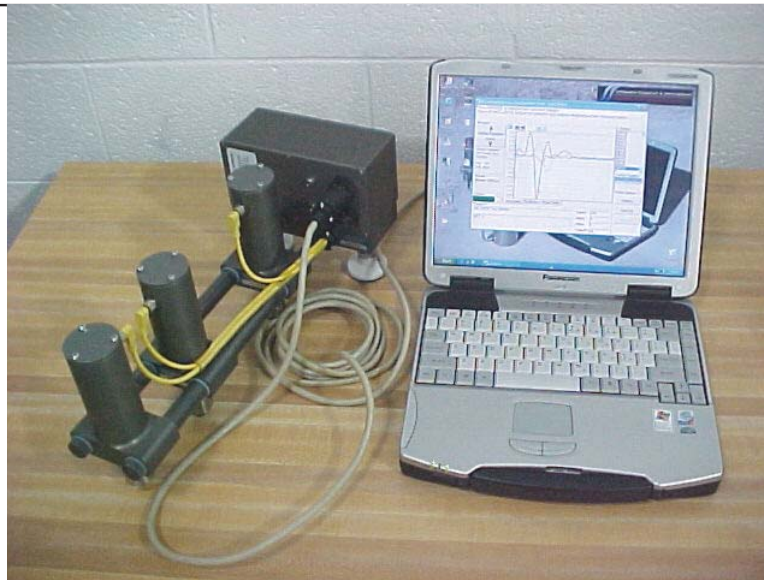


Figure 6. Photo. Portable Seismic Pavement Analyzer.

Shear velocity, V_s can be used to determine shear modulus, G , using:

$$G = \frac{\gamma}{g} V_s^2 \quad (4.2)$$

Young's modulus, E , can be determined from shear modulus, through the Poisson's ratio, ν , using:

$$E = 2(1 + \nu)G \quad (4.3)$$

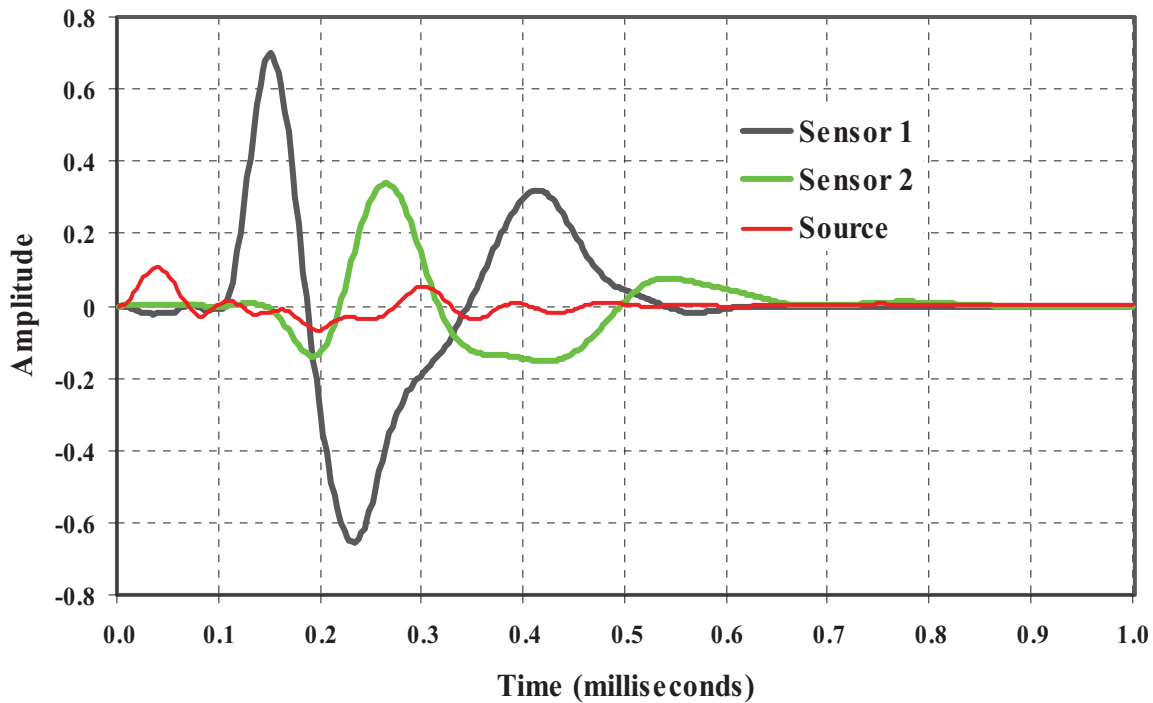


Figure 7. Graph. Typical Time Records from PSPA.

To obtain the modulus from surface wave velocity, V_R is first converted to shear wave velocity using:

$$V_S = V_R (1.13 - 0.16v) \quad (4.4)$$

The shear modulus is then determined by using Equation 4.2.

Surface waves (or Rayleigh, R-waves) contain about two-thirds of the seismic energy. Accordingly, the most dominant arrivals are related to the surface waves making them the easiest to measure. The Ultrasonic Surface Wave (USW) method¹ is an offshoot of the Spectral Analysis of Surface Waves (SASW) method (Nazarian et al., 1997). The major distinction between these two methods is that in the USW method the modulus of the top pavement layer can be directly determined without an inversion algorithm.

As sketched in Figure 8, at wavelengths less than or equal to the thickness of the uppermost layer, the velocity of propagation is independent of wavelength. Therefore, if one simply generates high-frequency (short-wavelength) waves and if one assumes that the properties of the

¹ Some organizations involved in seismic tests do not differentiate between the USW and the SASW methods. In our terminology, the SASW test is a comprehensive test that requires the development of an experimental dispersion curve and determining the modulus profile through an inversion process. The USW simply provides the modulus of the top layer without need for an inversion process and is much simpler to perform.

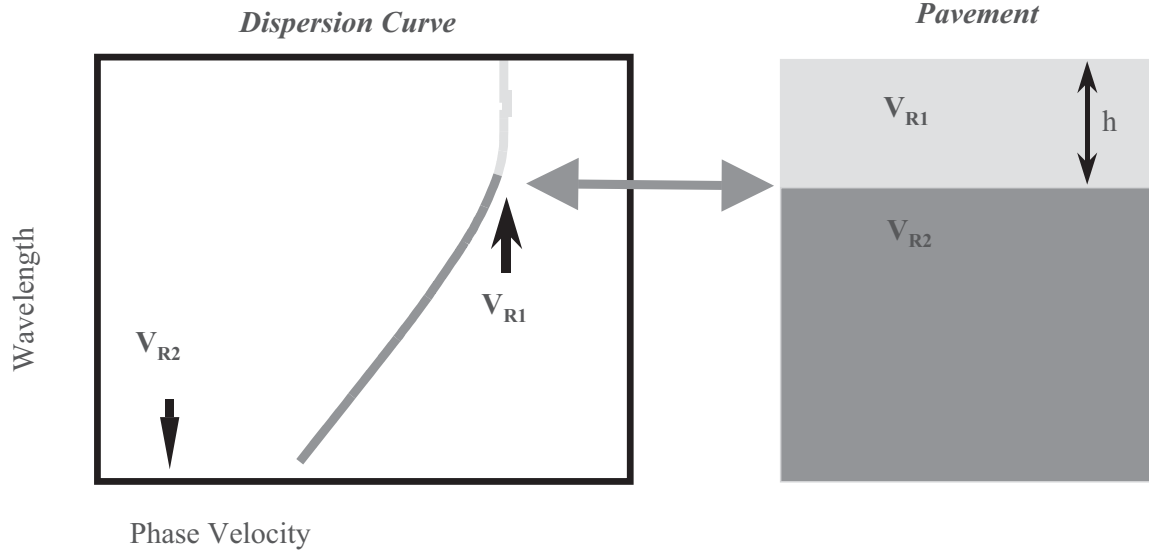


Figure 8. Schematic. Ultrasonic Surface Wave Method.

uppermost layer are uniform, the shear wave velocity of the upper layer, V_s , can be determined from

$$V_s = (1.13 - 0.16\nu) V_{ph} \quad (4.5)$$

The modulus of the top layer, E_{field} , can be determined from

$$E_{field} = 2 \rho V_s^2 (1 + \nu). \quad (4.6)$$

where V_{ph} = phase velocity of surface waves, ρ = mass density, and ν = Poisson's ratio.

The wavelength at which the phase velocity, i.e. velocity of individual frequency components, is no longer constant and closely related to the thickness of the top layer (NCHRP,1996).

Alternatively, the thickness of the ACP layer can be estimated from the impact-echo method as long as the layer is reasonably thick (thicker than 5 in.) and as long as there is enough contrast between the modulus of the ACP and the underlying layer.

An actual dispersion curve from the time record shown in Figure 7 is included in Figure 9a. As approximated by the solid line, the phase velocity is reasonably constant for the first 3 in. below which the phase velocity tends towards lower values with depth. By a comparison of this figure with the idealized one in Figure 8, one can conclude that the average phase velocity is about 4200 fps and the approximate thickness is about 3 in. To obtain the average modulus, the dispersion curve from a wavelength of about 1 in. to slightly less than the nominal thickness of the layer was used.

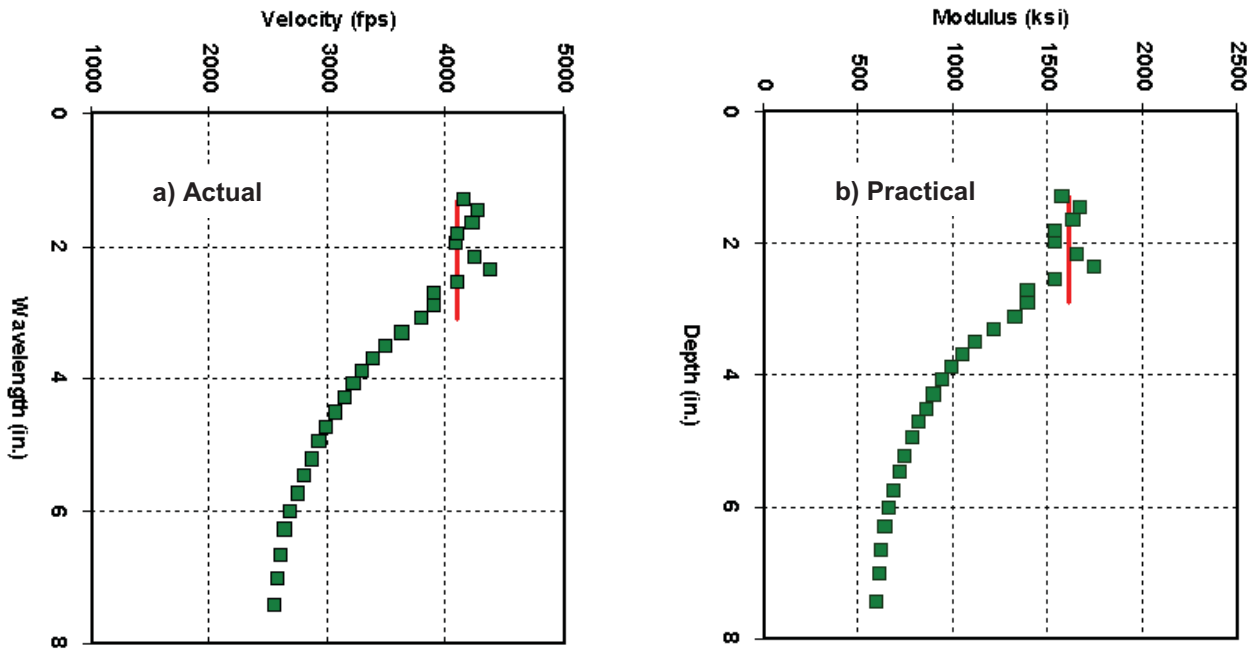


Figure 9. Graph. Typical Dispersion Curve Obtained from Time Records in Figure 7.

For practical inspection of dispersion curve in the field (see Figure 9b), the velocities in Figure 9a are converted to moduli using Equations 4.3 through 4.6, while the wavelength is simply relabeled as depth. In that manner, the operator of the PSPA can get a qualitative feel for the variation in modulus with depth.

The dispersion curve shown in Figure 9 is developed from the phase spectra shown in Figure 10. The phase spectrum, which can be considered as an intermediate step between the time records shown in Figure 8 and the dispersion curve shown in Figure 9 (Nazarian and Desai, 1993), is determined by conducting Fourier transform and spectral analysis on the time records from the two sensors. This step makes the determination of the velocity with wavelength much easier.

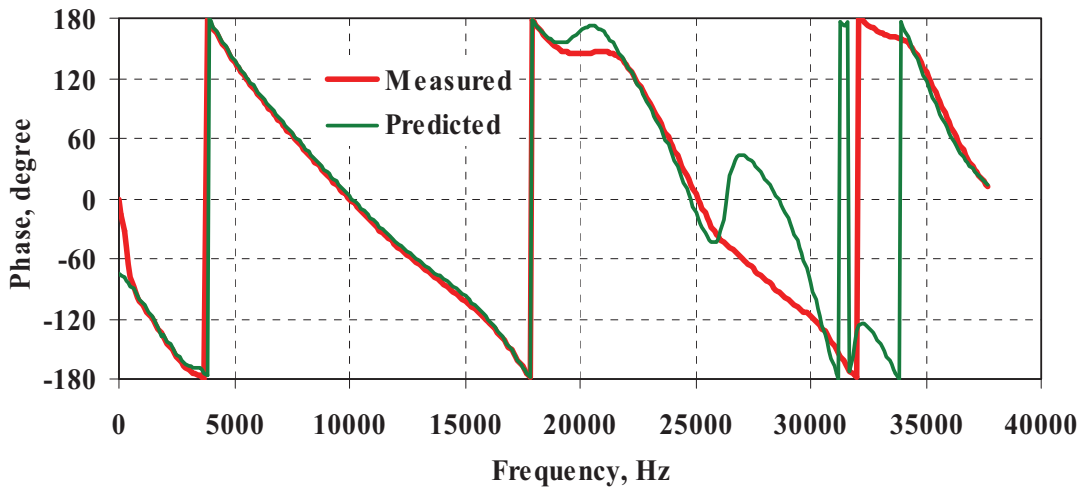


Figure 10. Graph. Typical Phase Spectra Obtained from Time Records in Figure 7.

Two phase spectra are shown, one measured from the time records, and the other that represents the best estimation of the phase when the effect of the body waves are removed. The second one is used to compute the dispersion curve as described above and detailed in Nazarian and Desai (1993).

The Impact Echo method primarily provides information about the thickness of a layer. Sansalone and Carino (1986) have also used the method to locate defects, voids, cracks, and zones of deterioration within concrete. As detailed in Nazarian et al. (1997), the method is not applicable to relatively thin layers and layers where the difference in moduli of adjacent layers is small. In ACP layers, getting accurate estimates of thickness is usually not possible due to scattering around aggregates. The PSPA computes Impact Echo data, but resultant thicknesses are not normally used in ACP applications. Its operation is described here for completeness.

The transducer closer to the source or the one embedded in the source of the PSPA, shown in Figure 6, is used. The method, as sketched in Figure 11, is based on detecting the frequency of the standing wave reflecting from the bottom and the top of the top pavement layer. Upon impact, some of the source energy is reflected from the bottom of the layer, and some is transmitted into the base and subgrade. Since the top of the layer is in contact with air, almost all of the energy is reflected from that interface. The receiver senses the reflected energy at periodic time intervals. The period depends on the thickness and compression wave velocity of the layer. To conveniently determine the frequency associated with the periodic arrival of the signal, one can use a fast Fourier transform algorithm. The frequency associated with the reflected wave appears as a peak in the amplitude spectrum. Using the compression wave velocity of the layer, V_p , the depth-to-reflector, h , can be determined from

$$h = V_p / 2f \tag{4.7}$$

where f is the resonant frequency obtained by transforming the time record into the frequency domain. The compression wave velocity can be determined if the surface wave velocity is known from

$$V_P = V_R [(1 - \nu) / (0.5-\nu)]^{0.5} / (1.13 - 0.16 \nu) \tag{4.8}$$

Since all sites visited for this study contained thin ACP layers, the impact echo results were not used. A new algorithm is currently under development at this time that may enable the reliable detection of the thickness of thin layers.

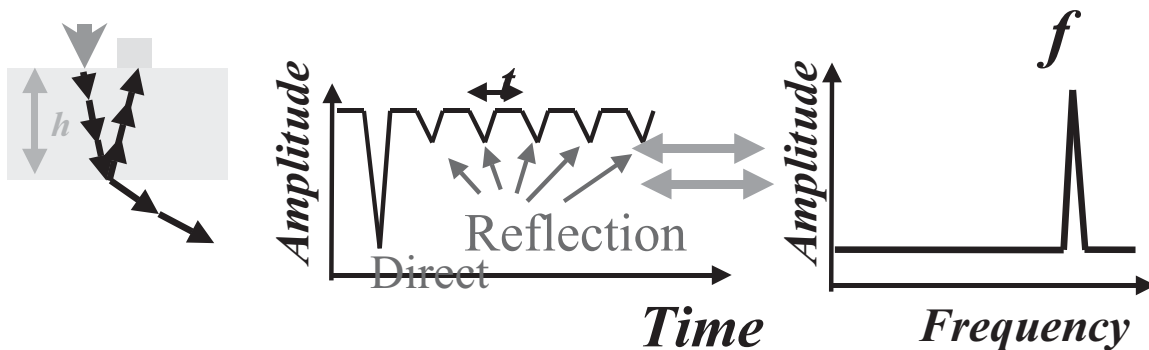


Figure 11. Schematic. Impact Echo Method.

Ultrasonic Laboratory Test

The laboratory setup used in this study is shown in Figure 12. The elastic modulus of a specimen is measured using a device (marketed as a V-meter) containing a pulse generator and a timing circuit, coupled with piezoelectric transmitter. To ensure full contact between the transducers and a specimen, special removable epoxy coupling caps are used on both transducers. To secure the specimen between the transducers, a loading plate is placed on top of it, and a spring-supporting system is placed underneath the transmitting transducer. The compression wave (P-wave) receiving transducer is placed on top of the specimen, on the opposite end from the transmitter. The dominant frequency of the energy imparted to the specimen is 54 kHz. The timing circuit digitally displays the time needed for a wave to travel through and a velocity, V_p , is calculated by dividing the length of the specimen by the corresponding travel time. The modulus, M_v , is then calculated using

$$M_v = \rho V_p^2 \quad (4.9)$$

where ρ is the bulk density of the specimen. For practical use, Equation 4.9 can be rewritten as

$$M_v = \frac{WH}{(\pi R^2 t_v^2)}, \quad (4.10)$$

where W , R and H are the mass, radius and height of the specimen, and t_v = travel time. The size of the sensors used with the test device is large relative to the wave travel path. The modulus measured with the V-meter, M_v , is the so-called constraint modulus. The constraint modulus, M_v can then be converted to Young's modulus, E_v through a theoretically-correct relationship in the form of

$$E_v = M_v \frac{(1+\nu)(1-2\nu)}{(1-\nu)} \quad (4.11)$$

where ν is Poisson's ratio.

DIAMETRAL RESILIENT MODULUS

Measuring resilient modulus is one of the current states of practice for characterizing the modulus of ACP mixtures. This test may be performed either axially or diametrically. Axial resilient modulus tests are conducted on specimens with the length-to-diameter of about two. Because of the sizes of the cores retrieved for this project, only diametral resilient modulus tests could be carried out. ASTM D4123 contains a thorough description of the test procedure.

A picture of a resilient modulus test setup, used in this study, is shown in Figure 13. All tests were carried out with a servo-control dynamic testing device retrofitted in a temperature-controlled chamber.

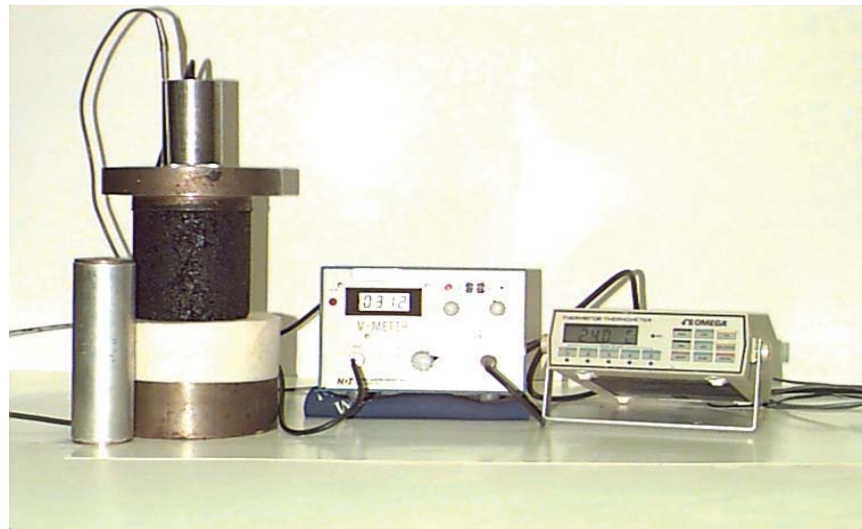
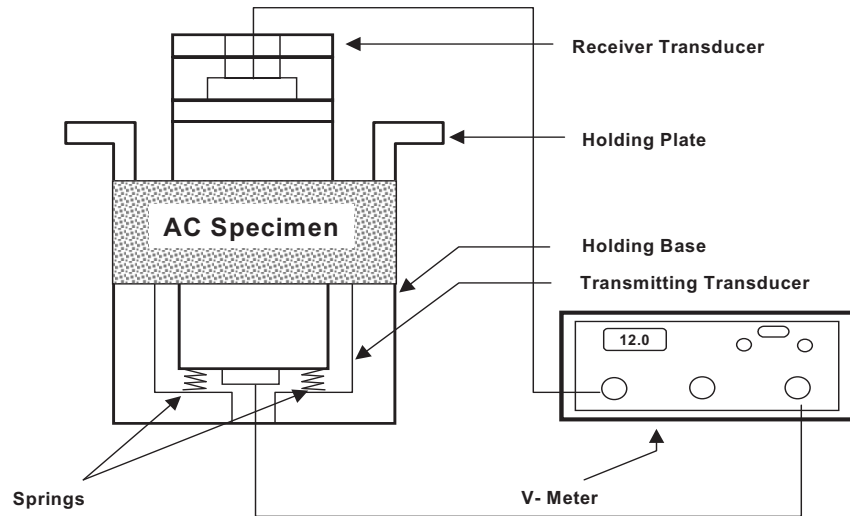


Figure 12. Schematic and Photo. Ultrasonic Test Device for AC Specimens.

A schematic of a specimen being tested is shown in Figure 14. A cyclic compressive load, P , is applied to the specimen vertically along one diameter. This compressive load induces tensile stresses along the diameter of the specimen in line with the load. These tensile stresses cause horizontal deformation of the specimen, ΔH . The resilient modulus of the specimen, E_{RT} is calculated from

$$E_{RT} = P (v + 0.27) / t \quad (4.12)$$

where t = core thickness and v = Poisson's ratio.

A typical load and deformation versus time relationships is shown in Figure 15. The ACP core is subjected to a cyclic haversine deviatoric stress applied for 0.1 seconds followed by a 0.9 sec



Figure 13. Photo. Diametral Resilient Modulus Test.

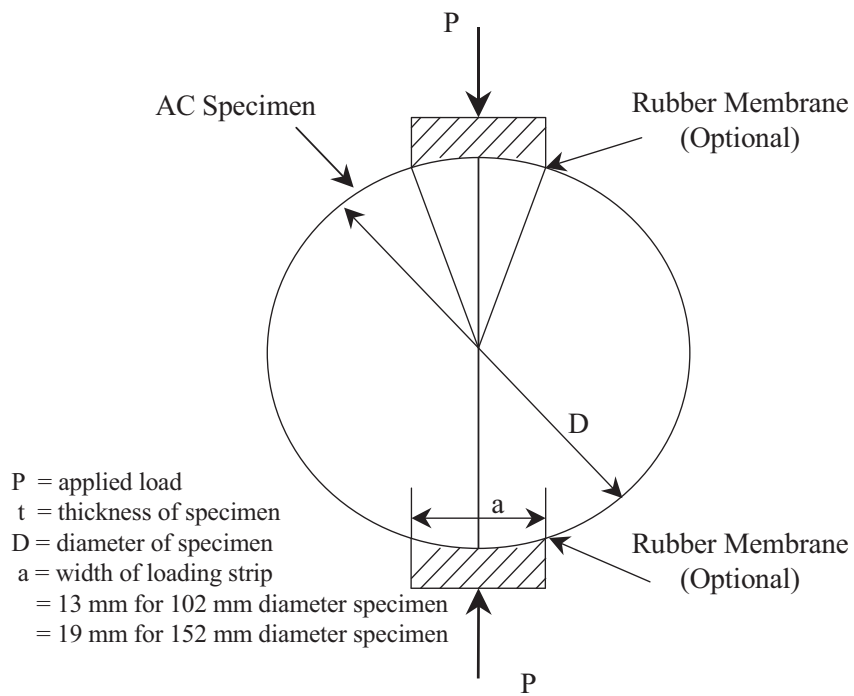


Figure 14. Schematic. Specimen Subjected to Diametral Test.

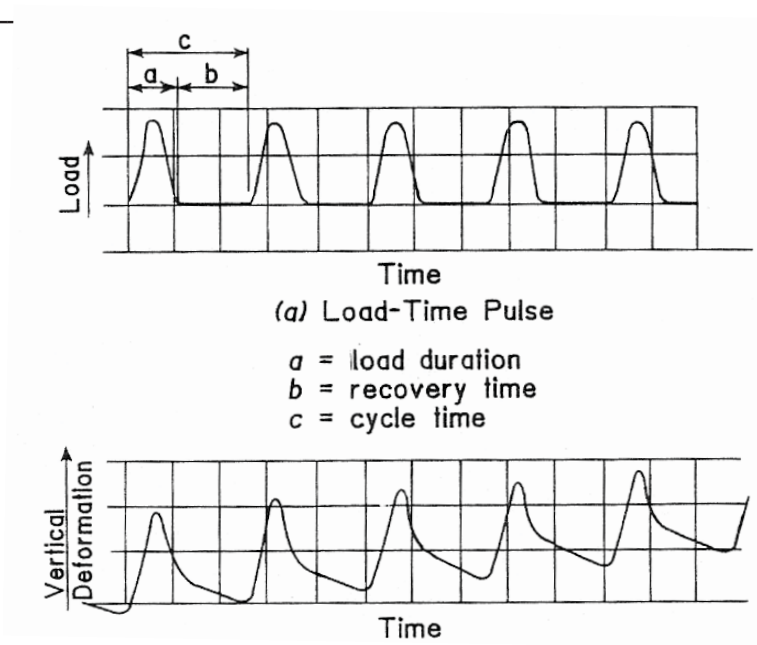


Figure 15. Graph. Time Relationships for Repeated-Load Indirect Tension Test (after Roberts et al., 1996).

rest period. The tests were performed at three temperatures 5 °C, 25 °C, and 45 °C.

At a workshop on resilient modulus testing held at Oregon State University in 1989, there was a strong consensus amongst pavement engineers that the testing procedure is rather time-consuming and results were not very repeatable (Shah, 1993). The estimated repeatability of the test is about 15% to 20%, depending on the sophistication of the test system, and the quality of the cores.

CHAPTER 5 – TEST PROTOCOL

As indicated before, the five-step procedure for quality management of the ACP was adapted for evaluating the modulus of the ACP layer in situ. The procedure followed here can be summarized in the following five steps:

1. Selection and Marking of Test Sites.
2. Conducting PSPA Tests.
3. Retrieval of Cores.
4. Conducting Lab Tests.
5. Relating Lab and Field Test Results.

Each step is described below. The results from one actual site, Taylor River Road, are also used to clarify the process.

SELECTION AND MARKING OF TEST SITES

At each site, the first step consisted of visually inspecting the pavement and selecting a test section. The main criteria for selecting the site were safety of the crew and reasonable uniformity of the section.

About 30 points were marked on the pavement as depicted in Figure 16. Of these points, fifteen were located in the wheel path and fifteen along the midlane of the road.

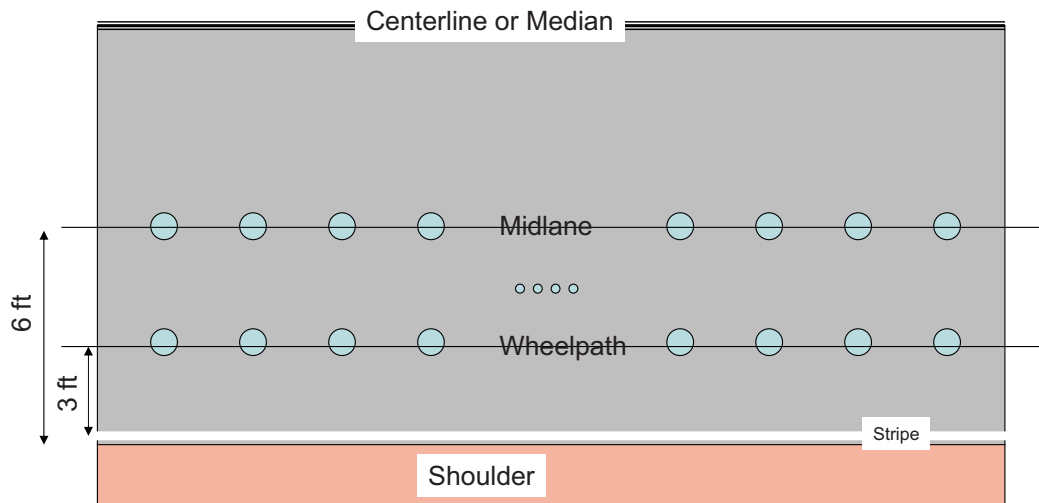


Figure 16. Schematic. Typical Marking of Sites.

PSPA TESTS

Each of the thirty points was tested with the PSPA four times, twice with the instrument oriented parallel to the centerline and twice perpendicular. Repeating the test at each point will provide information about the repeatability of the device as well as the variation in the properties in the two perpendicular directions due to the compaction pattern and the damage to the pavement. At each point, the temperature of the pavement was also measured with an infrared gun in addition to the thermistor measurement made by the PSPA.

A typical waveform collected at one point with the PSPA software is shown in Figure 17. Three time records are shown in the figure. The red record is the time history of the sensor placed in the source, with the amplitude heavily attenuated. This record is useful to the advanced user for ensuring that the source is functioning properly. Additionally, the record is used in the impact-echo analysis.

The black record depicts the time history as recorded by the sensor closer to the source (near receiver), and the green record is the time history from the far sensor. These two records are used in the determination of the modulus with the USW method. Both records demonstrate the typical arrival of the surface energy as depicted by the full sine-wave cycle in the left hand of the records, after which the energy attenuates rapidly. On the left side of the figure, under the “Results” section, the modulus obtained for this section (i.e. 1630 ksi) is presented as soon as the data collection is completed.

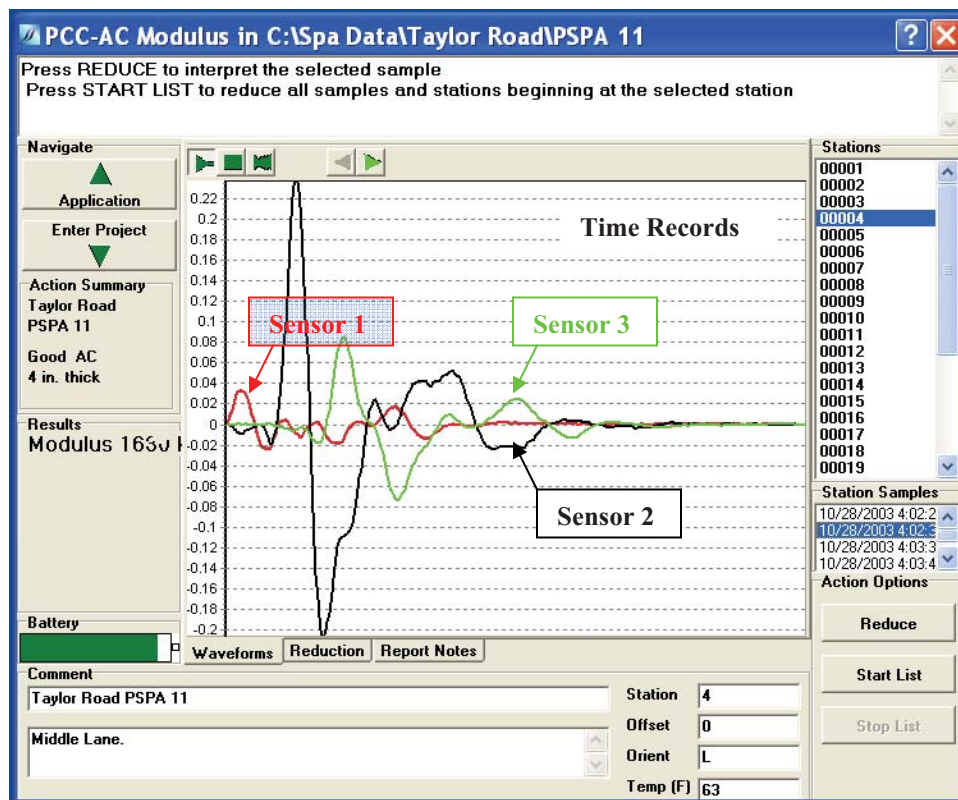


Figure 17. Screen Shot. Typical Time Records as Demonstrated by PSPA Software.

In the next step, the operator has the option of viewing the reduced data, as shown in Figure 18. Several items can be inspected in the figure. The graph at the bottom is the phase spectrum (a variation in phase delay due to propagation of wave with frequency). This is the intermediate result obtained from the analysis of the time records shown in Figure 17. As described in Nazarian et al. (1997), this curve should represent a saw-tooth pattern as it does in the figure. The green record is the measured phase spectrum and the red one is the best fit to the data by the software. The two curves follow one another quite well.

The upper graph labeled “Dispersion Curve is a representation of the variation in modulus (horizontal axis) with wavelength (vertical axis). As indicated before, for shorter wavelengths, the wavelength approximates the thickness of the layer. For this reason, the vertical axis is labeled as thickness. The dispersion curve, which is directly calculated from the phase spectrum, is represented by green dots. The red vertical solid line in this graph corresponds to the range of thickness along which the average modulus is calculated. This average value is the number shown in the “Results” section (i.e., 1630 ksi). The shortest thickness is controlled by the spacing between the receivers, the top size aggregate of the mixture and the shortest wavelengths measured by the PSPA at this transducer spacing. The longest thickness is input by the user as a nominal value. In this case the nominal thickness and the actual thickness of the layer coincide quite well, as the measured dispersion curve is uniform up to a thickness of 4 in. beyond which the curve breaks towards lower moduli.

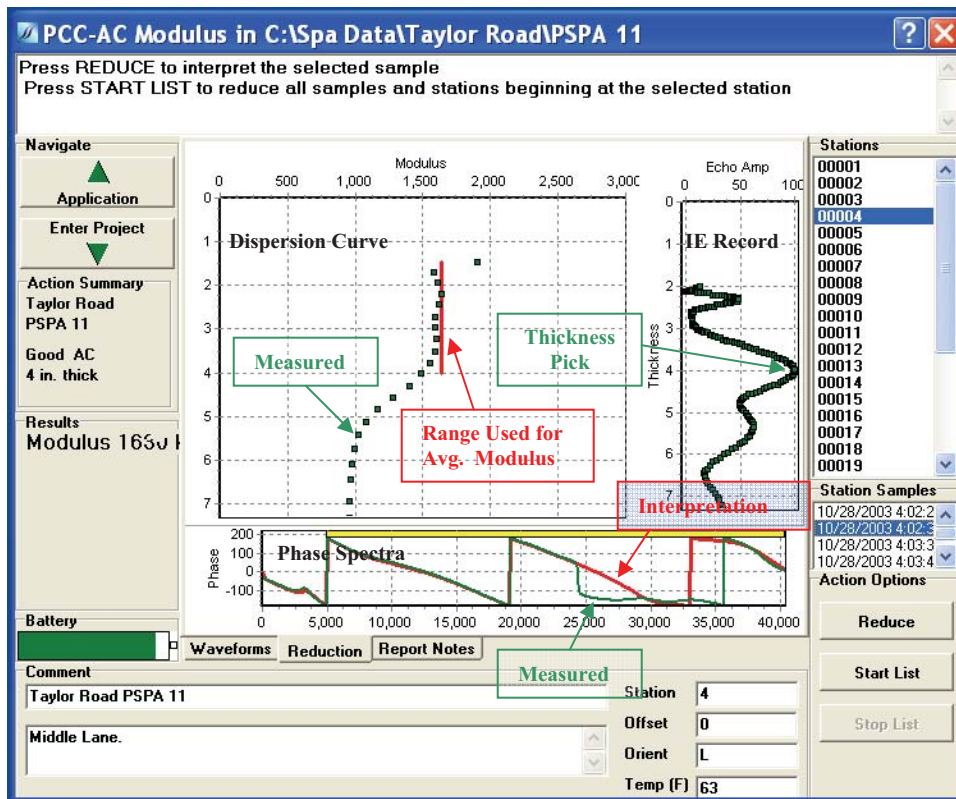


Figure 18. Screen Shot. Typical Interpreted Results as Demonstrated by PSPA Software.

On the right hand side of the graphs, the impact-echo results are shown. The most probable thickness corresponds to the pick of the curve as marked. Even though in this case, the results are quite close to the actual thickness, at this time this methodology will not provide consistent results on ACP layers. We feel that the change in the slope of the dispersion curve may be a better indicator of the thickness, especially in multi-course pavements.

The variations in seismic moduli along the wheel path and the midlane at this site are shown in Figure 19. For each test point, four numbers, corresponding to the four measurements, are shown. The two individual measurements corresponding to either the longitudinal or perpendicular measurements are almost always within 5% of one another. In some cases, the results from the two directions are different indicating heterogeneity of the material due to the compaction pattern, due to localized segregation, or due to load or environmental induced micro-cracking or cracking of the ACP. Hugo et al. (1997) have well documented this phenomenon. Six red circles in the figure correspond to the core locations.

The temperature varied from location to location. The temperature measured at each site was used to adjust the AC moduli to 77°F. The relationship suggested by Li and Nazarian (1994) for adjusting the modulus of AC to a reference temperature of 25° C (77° F) was used here. That relationship is in the form of

$$E_{25} = E_t / (1.35 - 0.014 t) \quad (4.11)$$

where E_{25} and E_t are the moduli at 25° C and temperature t (in Celsius). A temperature gun was used to measure the temperature at each test point. This relationship is approximate, but in the absence of data for developing temperature-modulus relationships, it was used in this study.

The measured seismic moduli along this site vary from a low of about 1600 ksi close to Station 1 to a high of about 2200 ksi towards the end of the tested section. To validate these variations, cores were retrieved and tested as discussed in the next section.

RETRIEVAL OF CORES

At each site six cores were retrieved, three along the wheel path and three along the midlane. In order to core in a systematic manner, the results from the PSPA were inspected in the field. The locations with the highest modulus and lowest modulus, as well as a location with an approximately average modulus were identified and cored. A picture of the coring operation is shown in Figure 20. The CFLHD staff kindly performed all the coring. The cores were clearly labeled, air-dried and packaged for shipment to El Paso for laboratory testing.

As soon as the cores were received in the laboratory, they were re-labeled, and the ends in contact with the base were saw-cut to obtain smooth ends. The cores as received in the lab and after saw-cut are shown in Figure 21.

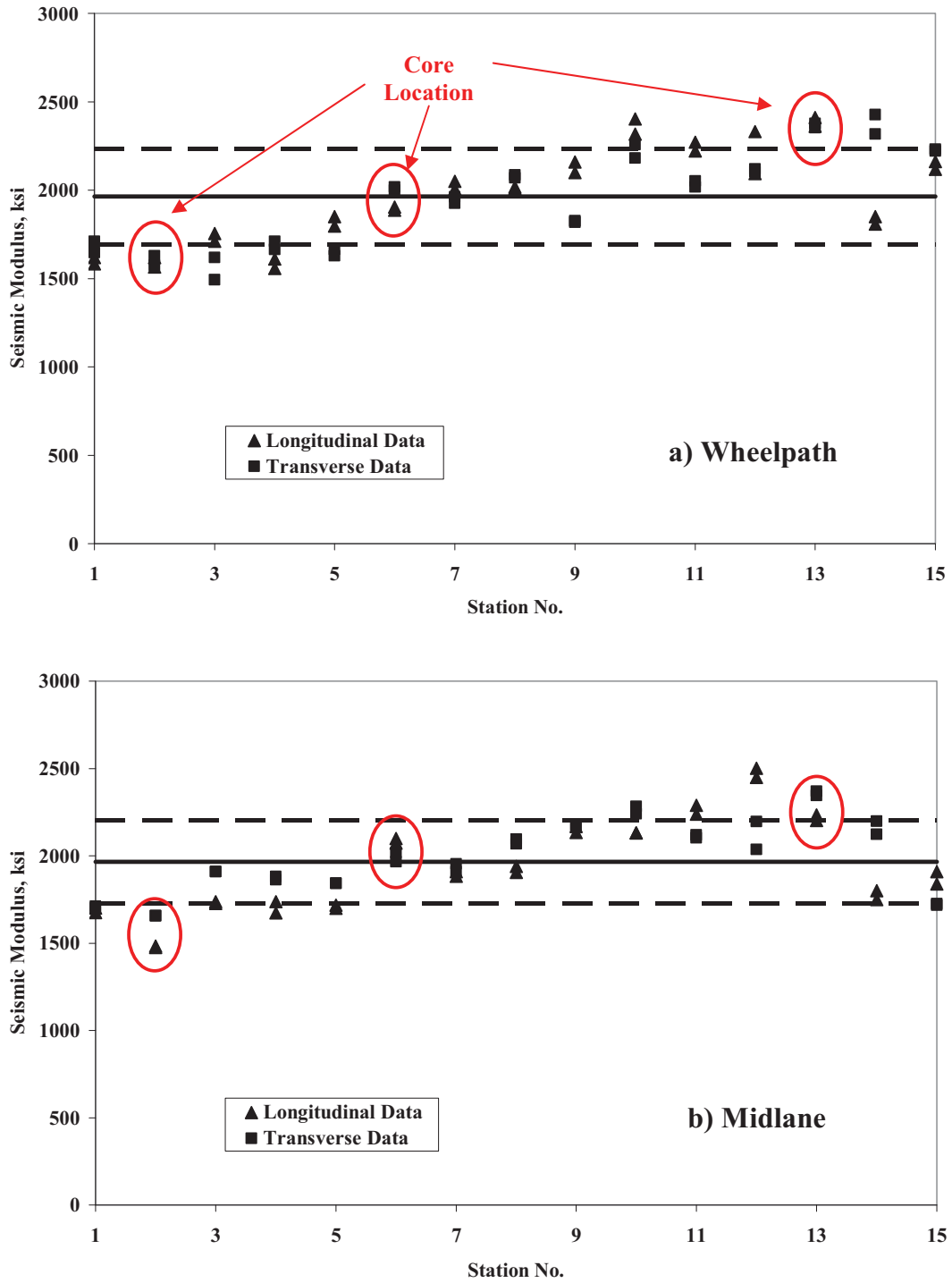


Figure 19. Graph. Typical Variation in Modulus along a Site.



Figure 20. Photo. Typical Coring Operation by CFLHD Staff.



Figure 21. Photo. Typical Cored Retrieved from the Site.

LAB TESTS

In this step, the six cores were tested at room temperature with the ultrasonic device shown in Figure 12 to determine their seismic moduli. Two to four specimens for each site were then subjected to the diametral resilient modulus tests as described in Chapter 4.

After the completion of the resilient modulus tests, the cores were then used to determine the volumetric properties of the specimens. The first step consisted of determining the air void content of the specimens. The specimens that underwent resilient modulus testing experienced excess deformation and could not be used for air void determination. Therefore, air voids were only determined for specimens that were not subjected to lab tests.

In the next step, the asphalt content of the material was determined using the NCAT ignition oven. In that test method, the specimen is placed in an oven for an extended period of time to burn the binder. The remaining aggregates after ignition oven test were sieved to obtain the gradation of the aggregates from each core.

The results from this activity for the site used as an example are included in Table 1. The asphalt content is reasonably uniform and the gradation is fairly similar. The voids in total mix (VTM), however, vary by about 1.5% between the two cores tested. As expected, the higher VTM is associated with the specimen with the lower modulus.

Table 1. Volumetric Information from Cores Retrieved from the Site.

Sample ID	AC Content	Voids in Total Mix	Modulus with Ultrasonic Device, ksi	Gradation (Percent Passing)						
				1/2 in.	3/8 in.	No. 4	No. 10	No. 40	No. 80	No. 200
1	6.2%	--	2142	97.9	83.3	53.7	30.6	13.5	7.9	3.0
2	6.1%	--	2177	100.0	82.3	52.8	31.6	14.5	8.6	4.2
3	5.6%	--	2286	98.7	74.9	45.9	28.7	13.5	8.0	3.7
4	6.2%	--	2312	100.0	83.6	53.3	30.9	14.2	9.1	4.2
5	--	6.13%	2058	--	--	--	--	--	--	--
6	--	4.77%	2275	--	--	--	--	--	--	--
Average	6.0%	5.45%	2208	99.2	81.0	51.4	30.4	13.9	8.4	3.8
COV	5%	17.6%	4.5%	1%	5%	7%	4%	4%	7%	15%

RELATING LAB AND FIELD TEST RESULTS

The results from the PSPA, ultrasonic lab device and resilient modulus tests are combined to obtain the master curve as described in Chapter 4. This curve can then be used to obtain the desired modulus for structural design of pavement.

A typical master curve is shown in Figure 22. As indicated before, the resilient modulus tests were carried out at three temperatures. The “reduced” or shifted data points are shown in the

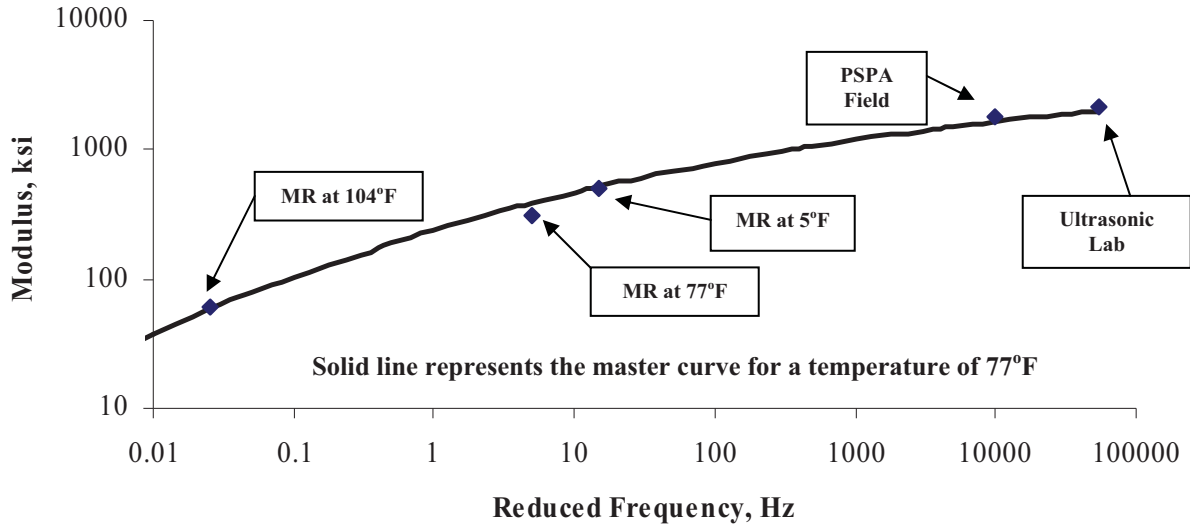


Figure 22. Graph. Typical Master Curve to Combine all Test Results.

figure. The number of data points from diametral resilient modulus tests, unlike from dynamic modulus tests shown in Figure 5, is limited. This is a limitation of the diametral resilient modulus test. As indicated before, it would have been desirable to conduct dynamic modulus tests on these specimens to get a complete master curve. Because of the length-to-diameter restrictions, this was not possible. For this example, the design modulus at a frequency of 15Hz is about 514 ksi while the PSPA modulus is about 2150 ksi.

In the next step the moduli from the ultrasonic tests on the cores and the PSPA were compared. Typical results from this activity are included in Figure 23. In this case, the two results are within 20% of one another. The reasons for the differences, aside from any errors in measurements and analyses, are the following.

- The use of approximate temperature correction method for converting the field modulus to lab modulus. As indicated in Chapter 3, modulus-temperature relationships could have been established in the laboratory if more material was available.
- The measurements with the PSPA are impacted by the micro-cracking and internal damage of the specimen, while the lab tests primarily characterize the material properties.
- Approximations due to the assumption of mass density and/or Poisson's ratio in the determination of moduli

It should be mentioned that the cores from the average modulus position on each pavement section were used for determining the density and Poisson's ratio.

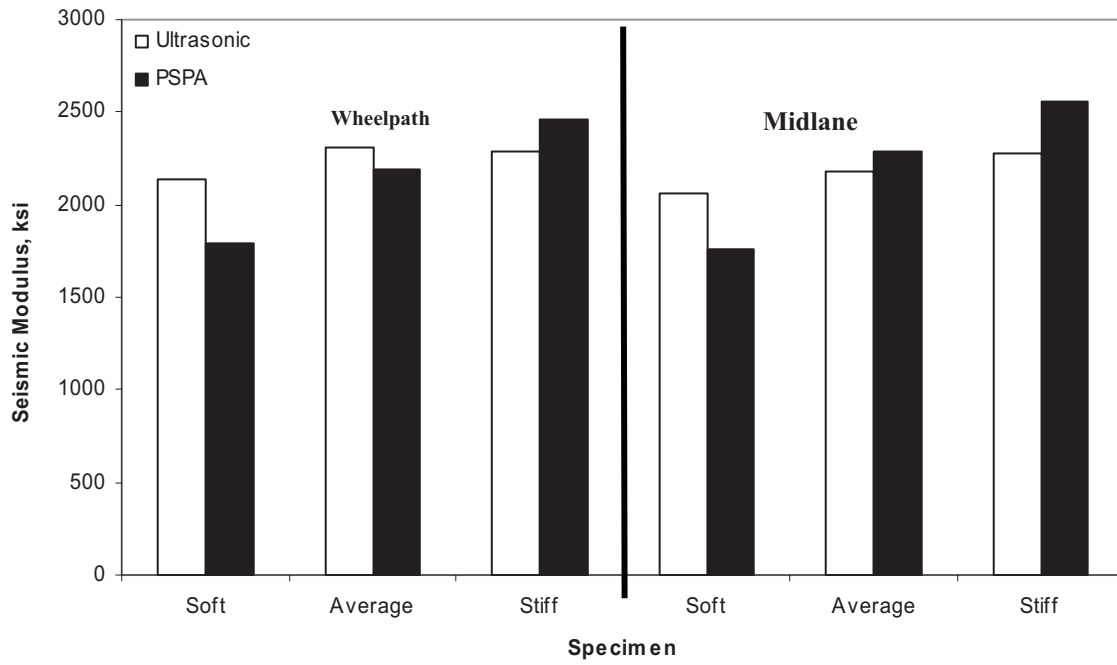


Figure 23. Graph. Typical Comparison of PSPA Field Moduli with Ultrasonic Lab Results.

CHAPTER 6 – PRESENTATION OF RESULTS

DESCRIPTION OF SITES

Five sites in Colorado and one site in Utah were tested. The locations of the sites are marked in Figure 24. Each site is described below. An extensive photo album of the sites and cores can be found in Appendix A.



Figure 24. Map. Location of Sites.

Site 1: Tarryall Road

Site 1 was located at Mile Post 2, measuring from US Highway 285 near Jefferson, CO just a few miles west of Kenosha Pass (about 70 miles Southwest of Denver). The top layer at this site was a double surface treatment about 0.75 in. to 1 in. thick. The road was in a fair condition. No significant cracks on the pavement were found. This site was tested on October 27, 2003. Laboratory tests were not feasible on the cores retrieved from this site because they were too thin and not structurally sound.

Site 2: Great Sand Dunes National Monument

Site 2 was located on the southbound lane of Route 150. Field tests started in front of the Amphitheater parking lot and extended to about 0.25 miles south of it. The thickness of the ACP layer was reported as 2 to 3 in. The road way was visually in a fair condition given that it had been placed several years ago. Transverse cracks were observed every 50 ft with some infrequent longitudinal cracks. No shoulder had been constructed on the side of the road.

Site 3: Taylor River Road

Site 3, located on Route 135, was a newly-constructed pavement section about 4 in. thick. The construction project covered from Mile Post 14 to Mile Post 19, starting from the town of Almont. Field tests were started at Mile Post 15.5 and covered about one-quarter of a mile, finishing at Mile Post 15.25. The first test point was located on a small parking area.

Site 4: Mesa Verde National Park

Site 4 was located about five miles south of the main entrance to the park. A newly overlaid section of the road was tested. Based on the visual observation immediately before and after the test section, the underlying ACP was heavily cracked. However, the section tested exhibited isolated cracks. The cores retrieved from the site demonstrated varying degrees of stripping in the underlying layer, especially towards the end of the test section.

Site 5: Canyonlands National Park – The Needles

The project, which covered the last 6 miles of the main road of the Park, was nominally 2 in. of new pavement over a recycled pavement. The road is visually in fair condition with isolated longitudinal and transverse cracks. The section tested did not contain any cracks and seemed in good condition.

Site 6: Colorado National Monument

The project covered the first 15 miles of the Monument Rimrock Drive, starting from the Fruita Entrance of IH-70. The section selected for field tests was a straight section of road in front of the Visitors Center. The test section was in poor condition with very frequent longitudinal and transverse cracks. The ACP was nominally 5 in. thick, with the top 2 in. being of significantly higher quality.

VOLUMETRIC PROPERTIES

The variation in gradation, AC content and air voids for all sites tested are summarized in Table 2. The detailed results can be found in Appendix B. The AC contents are in the range of 6% to 9%, which is typically greater than anticipated for normal mix designs. At Site 2, the coefficient of variation for the AC content is about 37%. This occurs because the AC content of one of the cores is about 3.6%. This point corresponds to the core with the lowest seismic modulus among the cores that were tested for AC content.

On the average, the voids in total mix (VTMs) at different sites vary from a low of about 2% at Site 6 to a high of about 8.5% at Site 5. The two highest air voids correspond to the two sites with the newer AC layer, with the lowest corresponding to Site 6 corresponding to one of the oldest.

Table 2. Volumetric Information from Cores Retrieved from Different Sites.

Site	AC Content	Voids in Total Mix	Modulus with Ultrasonic Device, ksi	Gradation (Percent Passing)						
				1/2 in.	3/8 in.	No. 4	No. 10	No. 40	No. 80	No. 200
1	No test was conducted because the site was covered with surface treatment only									
2	7.2% (37.2%)	3.3% (47.1%)	1619 (15.8%)	94.4 (4.6%)	83.4 (6.6%)	52.8 (9.9%)	33.0 (13.8%)	18.3 (20.7%)	11.8 (32.8%)	4.2 (56.7%)
3	6.0% (5%)*	5.45 (17.6%)	2208 (4.5)	99.2 (1%)	81.0 (5%)	51.4 (7%)	30.4 (4%)	13.9 (4%)	8.4 (7%)	3.8 (15%)
4	7.2% (13.1%)	6.8% (14.6%)	1388 (24.2%)	95.3 (5.7%)	81.0 (3.6%)	53.6 (4.9%)	34.5 (5.2%)	21.6 (11.7%)	12.2 (10.1%)	4.7 (12.5%)
5	7.3% (5.9%)	8.4% (6.7%)	1961 (6.1%)	98.2 (3.6%)	81.8 (1.8%)	48.4 (7.5%)	29.6 (10.4%)	18.1 (13.2%)	11.4 (24.9%)	5.5 (51.0%)
6	8.7% (10.8%)	2.1% (33.7%)	1841 (12.2%)	93.9 (4.7%)	79.2 (1.6%)	53.2 (5.2%)	37.2 (10.7%)	22.9 (16.5%)	11.5 (12.7%)	3.4 (55.1%)

* Numbers in parentheses are the coefficients of variation

The gradations seem to be fairly uniform within each site and between the sites. Large variability in the fines contents (i.e. materials passing No. 200 sieve) is apparent. Given the small amounts of fines present in the gradation, this can be due to experimental error during the sieving operations.

PSPA MODULI

The average moduli obtained at each site adjusted for temperature are reflected in Table 3. Point-by-point variation in moduli can be found graphically in Figures 6.2 through 6.7 and numerically in Appendix C. Typical time records, phase spectra and dispersion curves from the core locations at each site as seen in the PSPA software are included in Appendix D.

Table 3. Seismic Moduli Obtained from PSPA at Different Sites.

Site	Seismic Modulus					
	Wheel path		Midlane		Overall	
	Average, ksi	COV, %	Average, Ksi	COV, %	Average, ksi	COV, %
1	741	20.9%	794	18.8%	767	20.1%
2	1645	35.8%	1280	30.6%	1463	36.3%
3	1964	13.8%	1967	12.2%	1965	13.0%
4	1104	44.0%	1119	41.8%	1112	42.7%
5	1811	18.5%	1849	17.9%	1830	18.2%
6	1795	29.2%	1648	32.0%	1721	30.8%

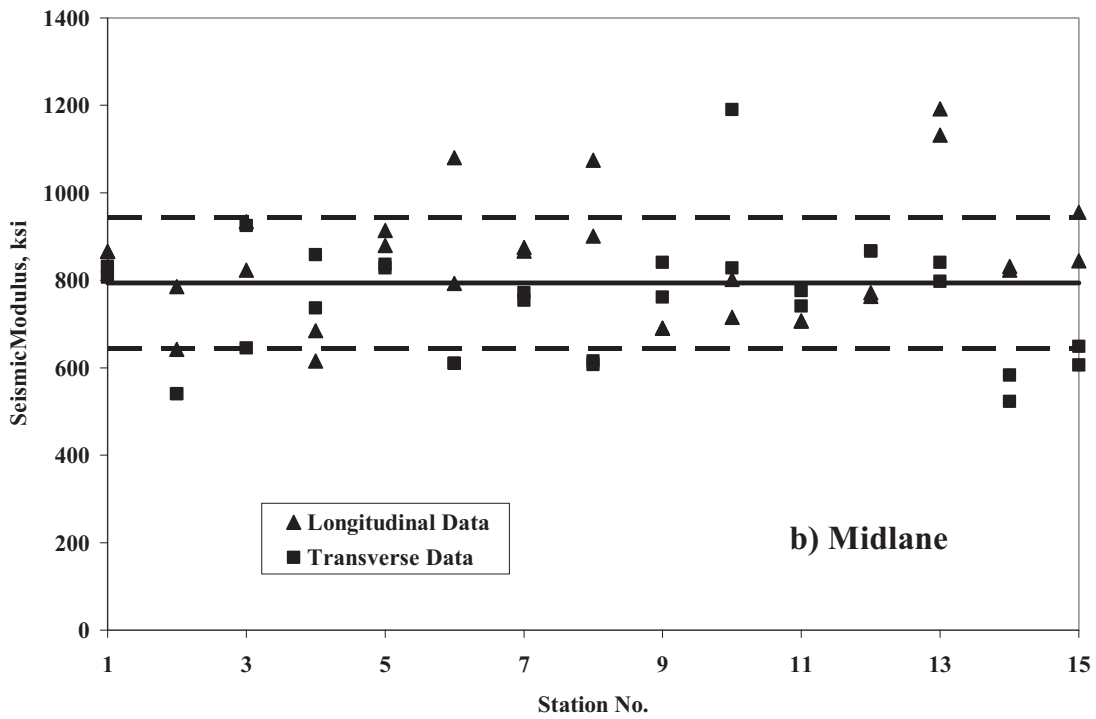
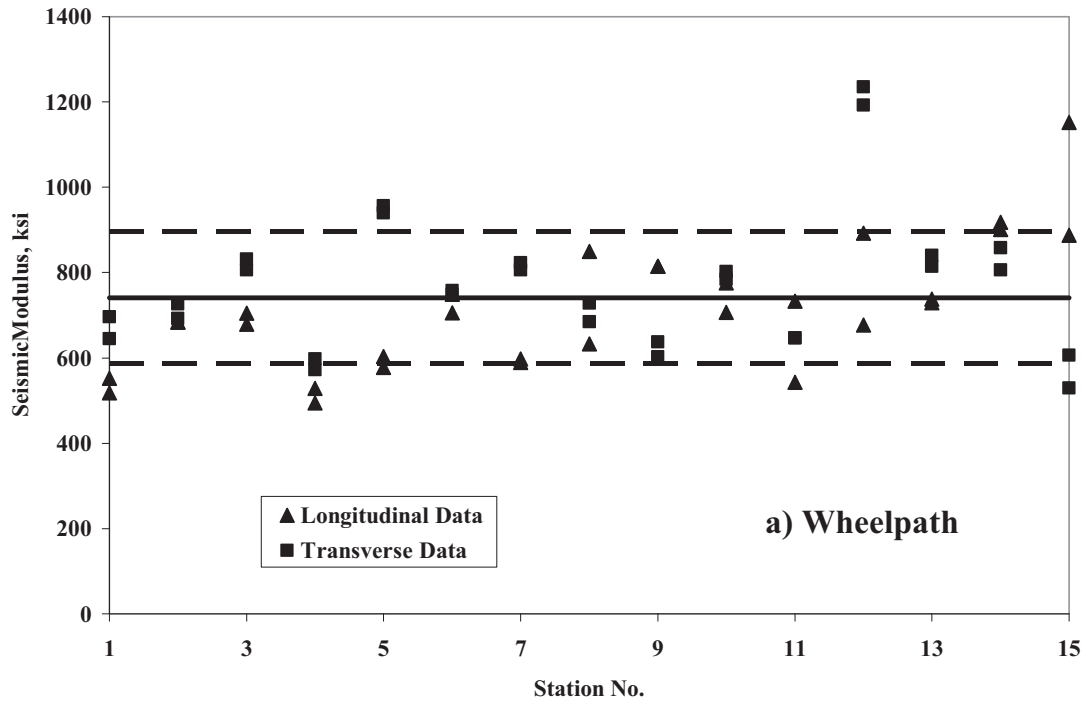


Figure 25. Graph. Variation in Modulus with PSPA along Site 1.

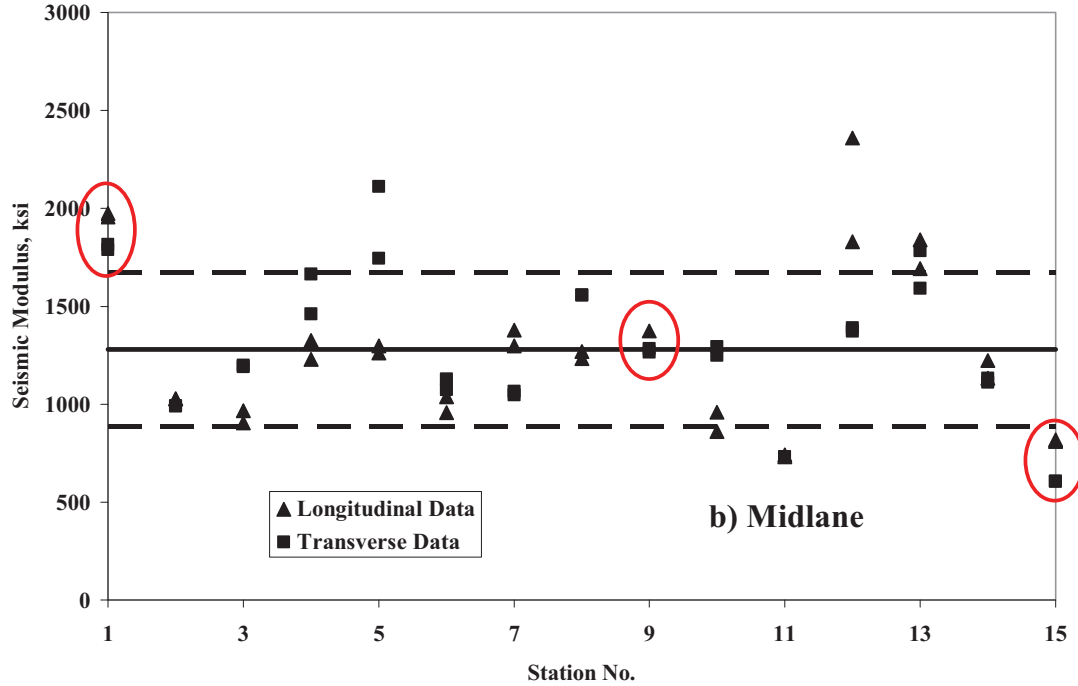
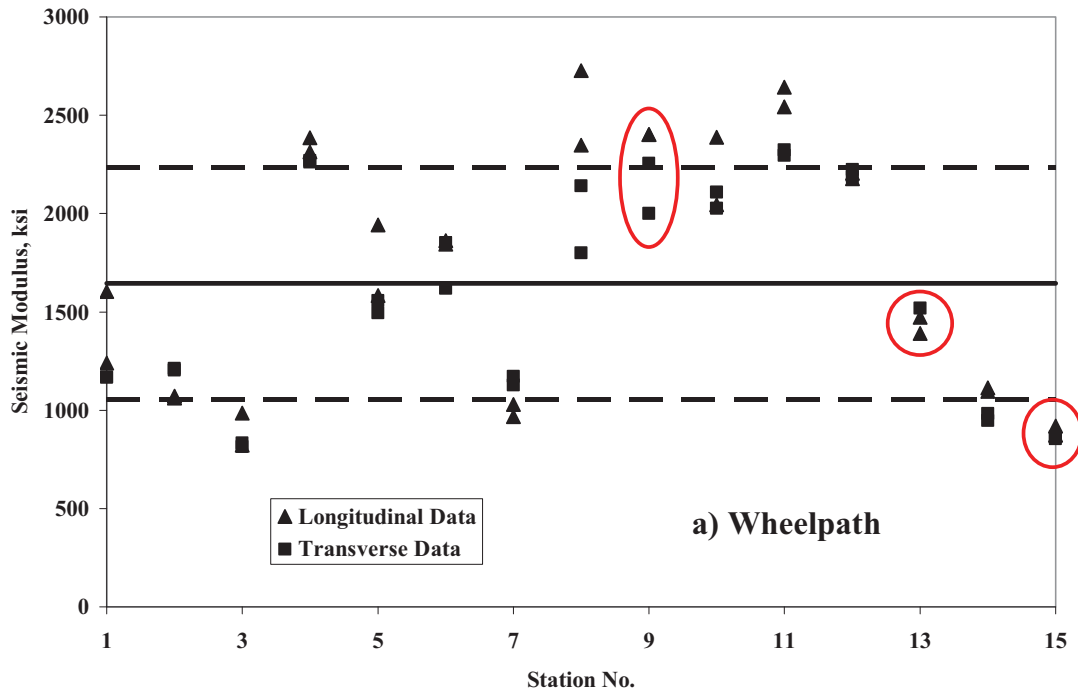


Figure 26. Graph. Variation in Modulus with PSPA along Site 2.

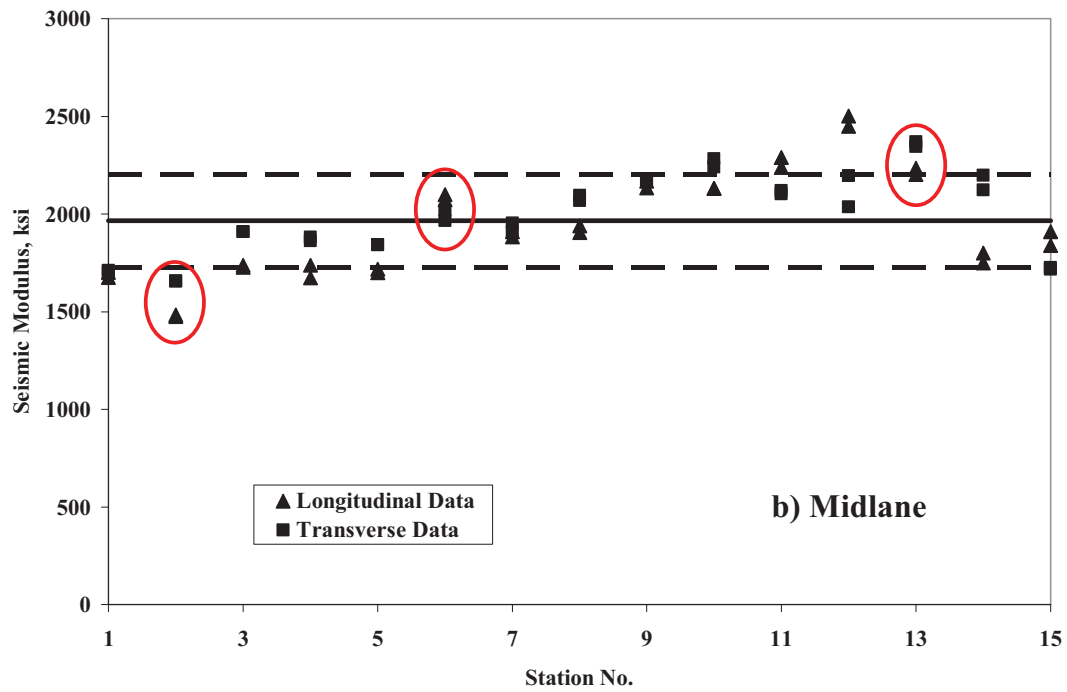
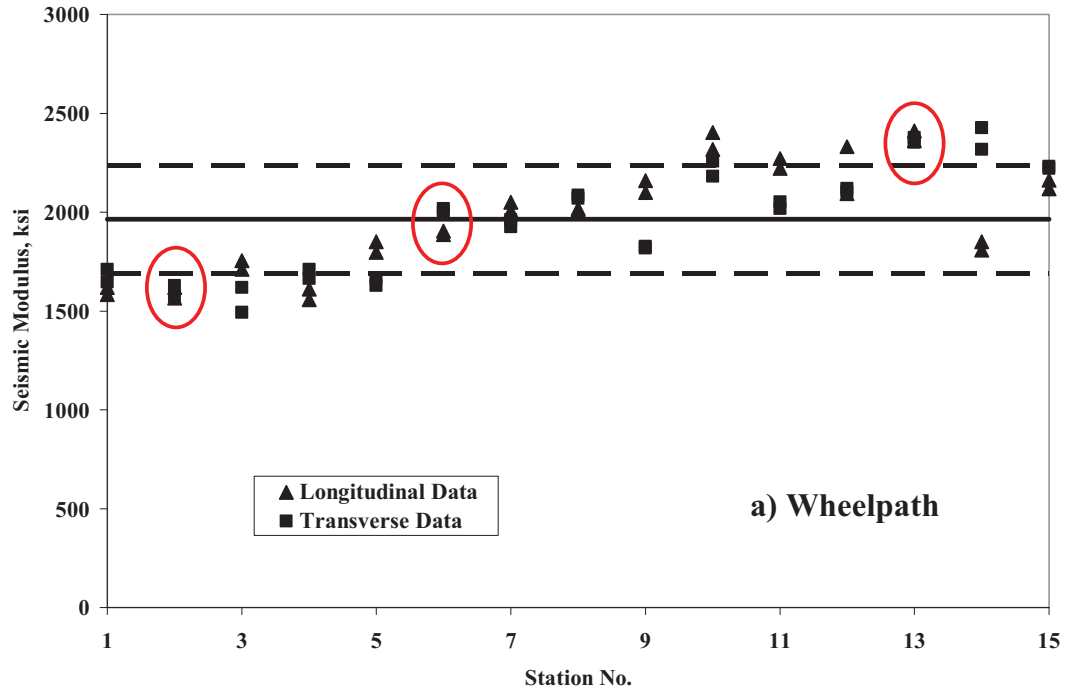


Figure 27. Graph. Variation in Modulus with PSPA along Site 3.

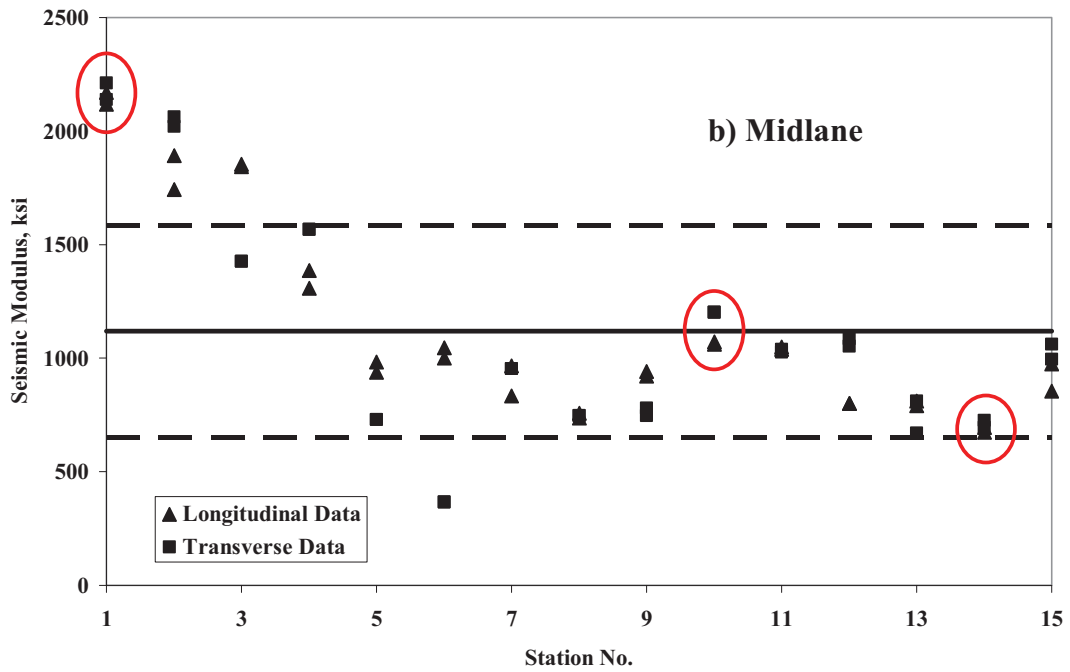
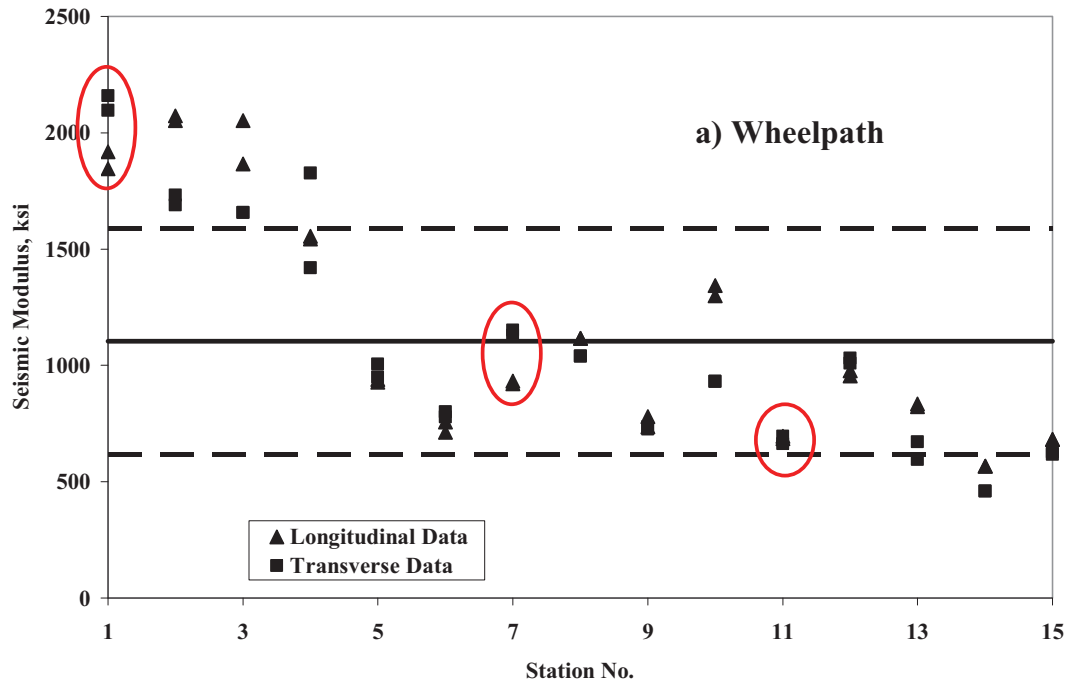


Figure 28. Graph. Variation in Modulus with PSPA along Site 4.

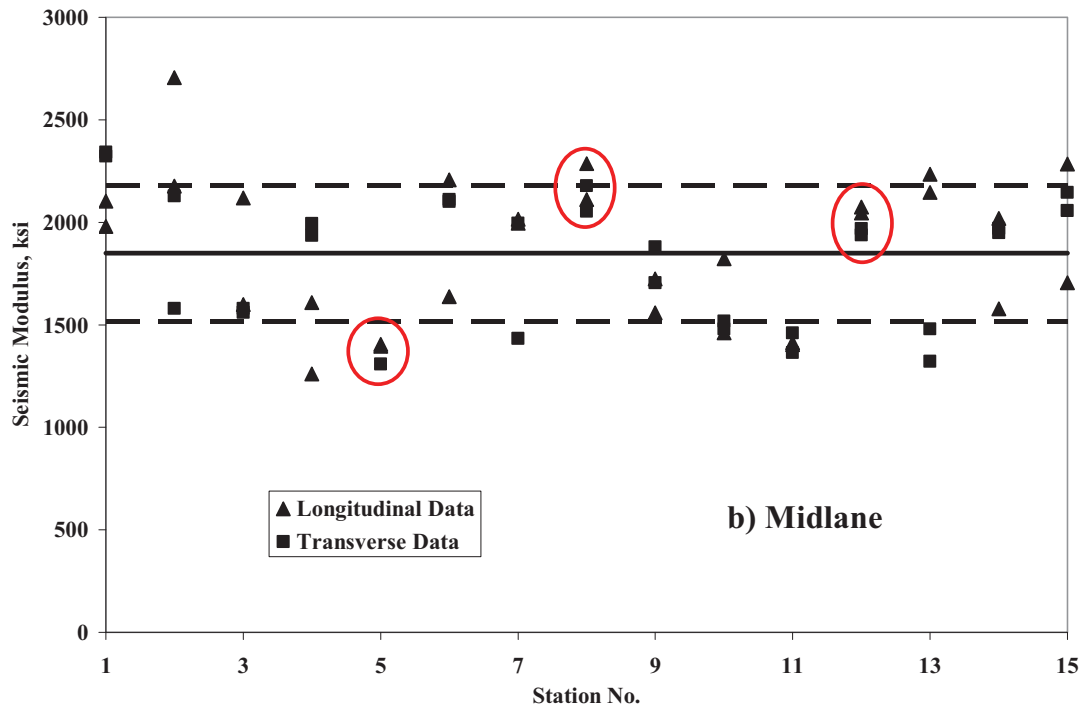
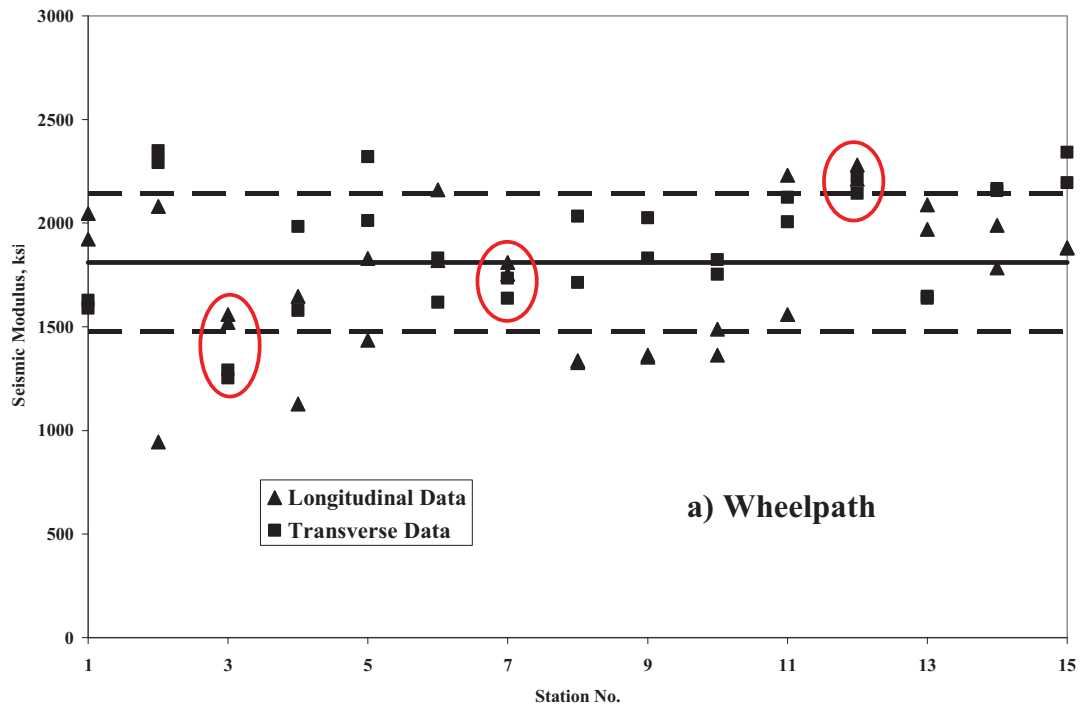


Figure 29. Graph. Variation in Modulus with PSPA along Site 5.

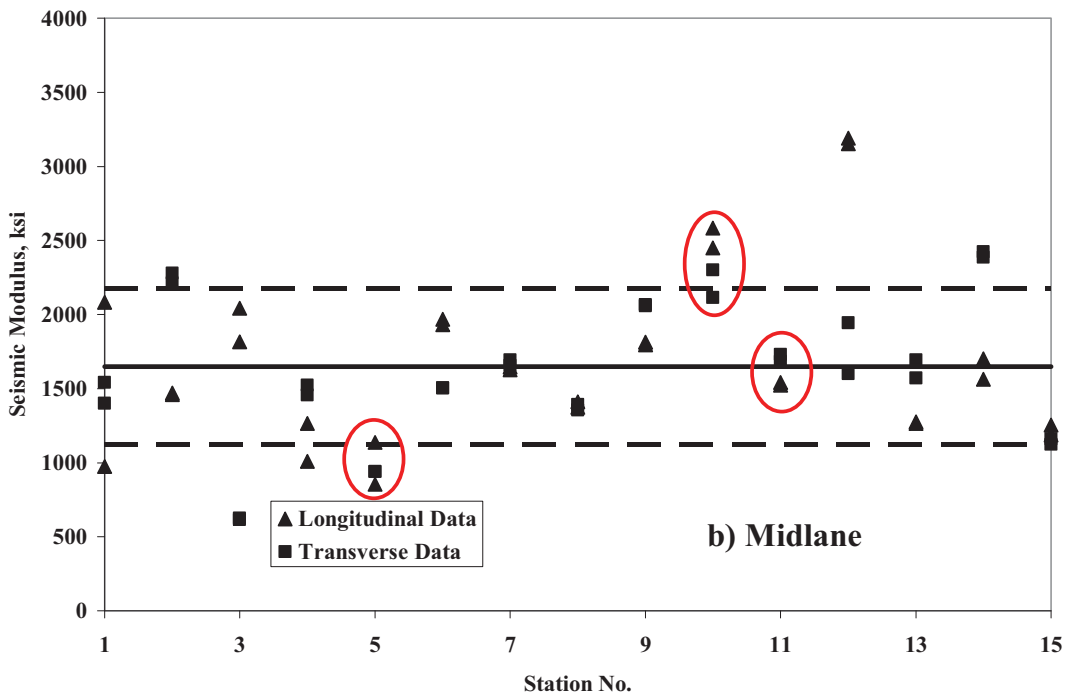
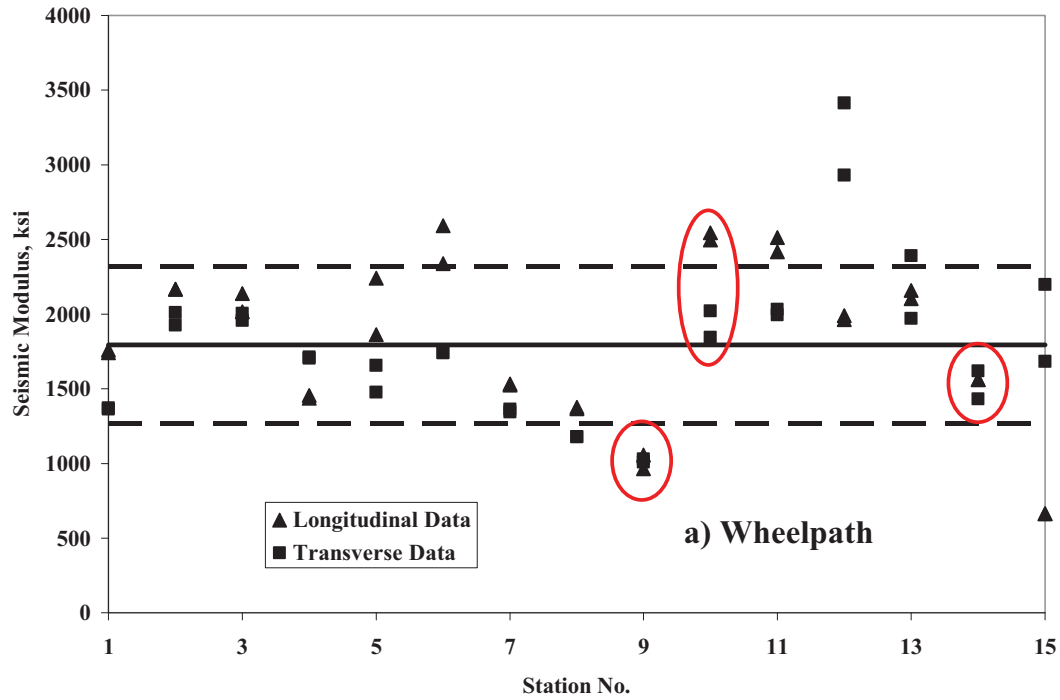


Figure 30. Graph. Variation in Modulus with PSPA along Site 6.

The variations in PSPA modulus along the wheel path and midlane for Site 1 are shown in Figure 25. As indicated before, the top layer at this site was a thin double surface treatment. The average seismic modulus at this site is about 760 ksi which translates to an approximate design modulus of about 250 ksi. This value seems to be reasonable for such a surface. The coefficient of variation is about 20% which reflects the quality anticipated from surface treatment.

At site 2, as reflected in Table 3, the average seismic modulus is about 1460 ksi. The variations in PSPA modulus along the site are shown in Figure 26. For the wheel path, the first three and last two points exhibit lower moduli with the middle points generally being significantly stiffer. Along the midlane, the moduli are more uniform and generally lower than the wheel path. This trend is typically observed on the older pavements, where the vehicular traffic would typically consolidate the material in the wheel path. The VTM for the wheel path, as shown in Table 5 is about 2% whereas for the midlane the VTM is closer to 4%. The observed point-to-point variability is also normal for aged pavements that contain micro-cracking and have experienced consolidation.

Contrary to Site 2, Site 3 exhibits fairly uniform behavior along the site (see Figure 27). This trend is also anticipated because Site 3 was newly constructed. The average seismic moduli along the wheel path and the midlane are fairly close since the site is not extensively trafficked. The quality of construction can be observed in Figure 27. The first half of the site demonstrates consistently lower moduli perhaps because of compaction efforts. This increase in modulus was not only apparent on the PSPA results but also on seismic tests performed on cores.

Site 4 consists of 2 in. of overlay over an old ACP. An inspection of cores (see Figure 46) and dispersion curves (see Appendix D) indicated that at the beginning of the section the overlay is thicker as compared to the remainder of the section. The inspection of the cores also indicated that the original ACP is of poor quality. The variations in PSPA modulus along the wheel path and midlane are shown in Figure 28. The moduli along the section are initially high. Past Point 5, the moduli are much lower than the initial points, indicating the lower quality materials. The close relationship, between the observed quality of the cores and the results from the PSPA is a good indication of the usefulness of the PSPA in determining the properties of an AC layer.

Site 5 again consists of 2 in. of overlay over a recycled asphalt layer. The average PSPA modulus at this site is about 1830 ksi with a coefficient of variation of about 18%. The variations in PSPA modulus along the wheel path and midlane are shown in Figure 29. The variation is rather random along the site, indicating variability in the properties of the recycled ACP layer. Also the moduli in the longitudinal and transverse directions at some points, especially along wheel path, are different, maybe demonstrating directionality of compactions of recycled materials.

Finally, the results from PSPA at Site 6 are shown in Figure 30. This site consisted of an old, cracked, road. As anticipated the coefficient of variation is rather high at about 31%. The average modulus of the wheel path is greater than the midlane, once again because of consolidation of the ACP under traffic.

DESIGN MODULI

The individual master curves from the cores subjected to resilient modulus are included in Appendix E. The procedure to obtain the design modulus was described in Chapter 5. The average master curve parameters associated with Equation 3.1 for each site are included in Table 4. The coefficient of determination, the R^2 value, associated with each curve fit is also included in the table. All R^2 values are greater than 0.94 indicating good agreement between the fitted curve and the data obtained from lab and field testing.

Based on these average master curve parameters, the average design moduli were obtained and reported in Table 4. For Site 1, the simplified procedure advocated by Aouad et al. (1993) was used because the cores were too thin for actual resilient modulus tests. The approximate design modulus for this site is about 250 ksi. For the other five sites, the modulus varied from about 500 ksi to 800 ksi.

Table 4. Design Moduli Obtained from Integration of Lab and PSPA Tests at Different Sites.

Site	Average Master Curve Parameters					Average Design Modulus, ksi
	δ	α	β	γ	R^2	
1	Specimens too thin for Testing					250*
2	-3.100	6.967	-1.600	0.147	0.978	713
3	-3.300	6.800	-1.600	0.390	0.960	523
4	-2.988	6.813	-1.600	0.119	0.944	582
5	-3.338	7.115	-1.600	0.228	0.981	709
6	-2.950	6.833	-1.600	0.160	0.977	811

* Based on simplified Method

COMPARISON OF CORE MODULI WITH PSPA MODULI

A comparison of the seismic moduli obtained with the ultrasonic device on the cores and the PSPA moduli obtained at the respective core location is presented in Figure 31. In general, close agreement between the two moduli was observed. The exception is Core 4 for Site 2 that contained micro-cracks and Core 1 of Site 4 that was badly stripped (see picture of cores in Appendix A). To further quantify the comparison between the two moduli, they are plotted against one another in Figure 32. The differences between the two moduli are generally less than 20%. The reasons for differences, aside from any experimental errors are itemized in Chapter 5.

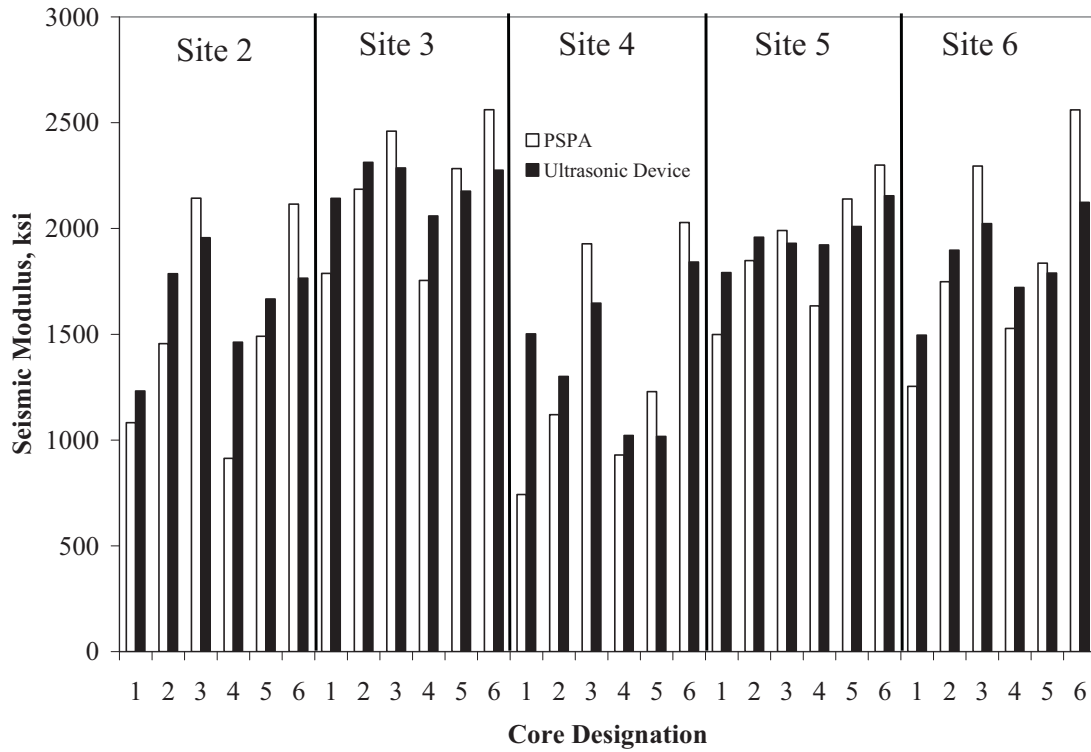


Figure 31. Graph. Comparison of Moduli Obtained by Ultrasonic Device and PSPA at all Sites.

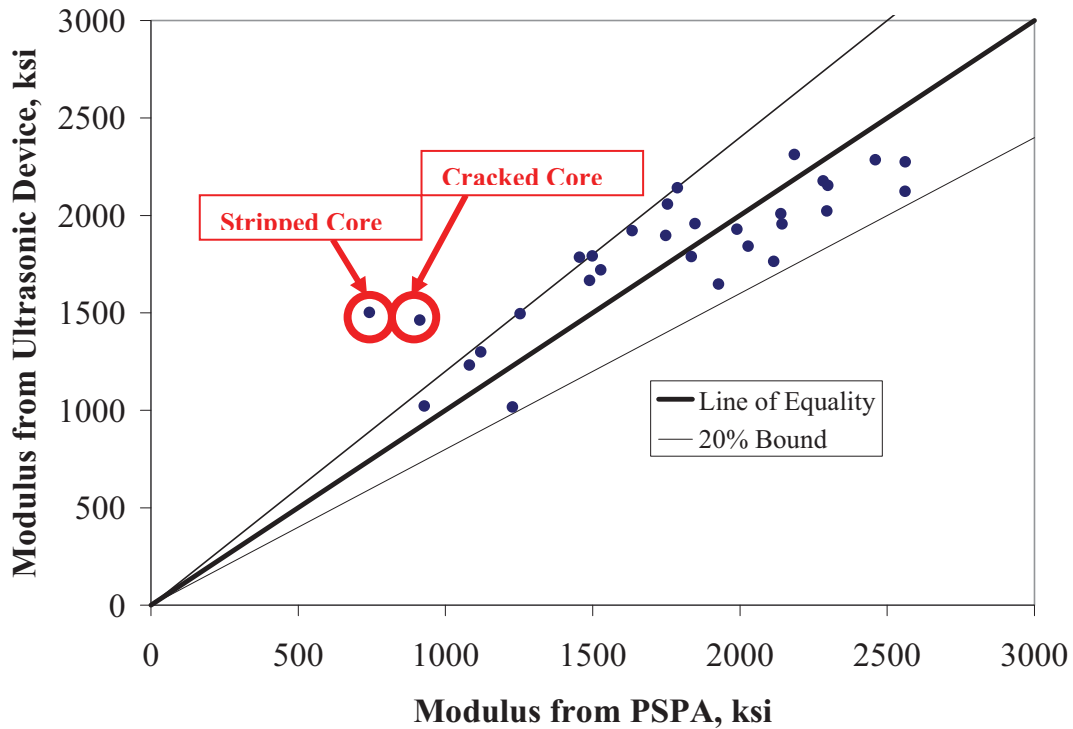


Figure 32. Graph. Variation between Moduli Obtained by Ultrasonic Device and PSPA at all Sites.

CHAPTER 7 – SUMMARY AND CONCLUSIONS

The Portable Seismic Property Analyzer (PSPA) was used at six sites in Colorado and Utah to demonstrate its applicability to the evaluation of typical asphalt-concrete pavements. To achieve this objective, each site was tested with the PSPA, representative cores were obtained, laboratory tests were carried out, and the results were analyzed.

The major findings are as follows.

- The field operation of the PSPA was practical and repeatable.
- The detrimental effects of microcracking and stripping are reflected in the PSPA moduli.
- The PSPA moduli and moduli from seismic lab tests on cores compare favorably since the two are generally within 20% of one another.
- Seismic moduli can be integrated with the lab testing to obtain a master curve that can be used in determining design moduli.

More extensive field and lab evaluation is desirable. However, this limited study demonstrates the viability of the PSPA in characterizing the AC layer at a number of sites with varying properties.

REFERENCES

1. Aouad, M. F., Stokoe, K. H., and Briggs, R. C. (1993), "Stiffness of Asphalt Concrete Surface Layer from Stress Wave Measurements," Transportation Research Board, No. 1384, Washington, DC, pp. 29-35.
2. Daniel, J. S., and Kim, Y. R. (1998), "Relationships Among Rate-Dependent Stiffness of Asphalt Concrete Using Laboratory and Field Test Methods," Journal of Transportation Research Record, No. 1630, Washington, DC, pp 3-9.
3. Ferry, J.D, Viscoelastic Properties of Polymers, 2nd edition, John Willy, New York, 1970.
4. Huang Y.H. (1993), Pavement Analysis and Design, Prentice Hall, Inc., Englewood Cliffs, NJ, 805 pp.
5. Lee, N-KJ; Hugo, F; Stokoe, KH, II (1997), "Detection and Monitoring of Cracks in Asphalt Pavement under Texas Mobile Load Simulator Testing," Journal of Transportation Research Record, No. 1570, Washington, DC, pp 10-22.
6. Kim Y.R. and Lee Y.C. (1995), "Interrelationships among Stiffnesses of Asphalt Aggregate Mixtures," Journal of Association of Asphalt Paving Technologists, Vol. 64., pp.575-609.
7. Li, Y. and Nazarian, S. (1994), "Evaluation of Aging of Hot-Mix Asphalt Using Wave Propagation Techniques,@ Engineering Properties of Asphalt Mixtures And the Relationship to Their Performance, ASTM STP 1265, Philadelphia, Pa., pp.166-179.
8. Nazarian, S. and Desai, M.R. (1993), "Automated Surface Wave Method: Field Testing," Journal of Geotechnical Engineering, Volume: 119 Issue: 7, ASCE, New York, NY, pp 1094-11.
9. Nazarian, S., Baker, M., and Crain, K. (1997), "Assessing Quality of Concrete with Wave Propagation Techniques," Materials Journal, American Concrete Institute, Farmington Hills, MI, Vol. 94, No. 4, pp. 296-306.
10. Nazarian S., Yuan D., Tandon V., and Arellano M. (2003) "Quality Management of Flexible Pavement Layers with Seismic Methods," Research Report 1735-3F, Center for Highway Materials Research, UTEP, El Paso, TX.
11. NCHRP (1996), "Nondestructive Testing to Determine Material Properties of Pavement Layers," Interim Report, NCHRP 10-44, Washington, DC.
12. Roberts, F. L., Kandhal, P. S., Brown, E. R., Lee, D., and Kennedy, T.W. (1996), Hot Mix Materials: Mixture Design and Construction, NAPA Education Foundation Lanham, Maryland.
13. Sansalone, M., and Carino, N. J. (1986), "Impact-Echo: A Method for Flaw Detection in Concrete Using Transient Stress Waves," Report NBSIR 86-3452. National Bureau of Standards, Gaithersburg, MD.
14. Tandon, T., Nazarian, S. and Bai X. (2004), "Assessment of Relationship between Seismic and Dynamic Modulus of Hot Mix Asphalt Concrete," International Journal of Road Materials and Pavement Design.
15. Von Quintus H.L. and Kilingsworth B. M. (1998), "Comparison of Laboratory and In Situ Determined Elastic Layer Moduli," presented in 77th Annual TRB Meeting, Washington, DC.
16. Witczak, M.W., Bonaquist, R., Von Quintus, H. and Kaloush, K. (1999), "Specimen Geometry and Aggregate Size Effects in Uniaxial Compression and Constant Height Shear Tests," *Journal of Association of Asphalt Paving Technologist*, Vol. 69, pp. 733-793.

APPENDIX A – PHOTO ALBUM



Figure 33. Photo. Measuring with the PSPA on the Side of the Road at Site 1.



Figure 34. Photo. Coring at Site 1.



Figure 35. Photo. Cores from Site 1.



Figure 36. Photo. Coring at Site 2.



Figure 37. Photo. Examples of Cracks at Site 2.



Figure 38. Photo. View of Site 2.



Figure 39. Photo. Cores from Site 2.



Figure 40. Photo. View of Site 3.



Figure 41. Photo. Coring at Site 3.



Figure 42. Photo. Cores from Site 3.



Figure 43. Photo. Close up of Site 4.



Figure 44. Photo. View of Site 4.



Figure 45. Photo. Coring at Site 4.



Figure 46. Photo. Cores from Site 4.



Figure 47. Photo. Close up of Site 5.



Figure 48. Photo. View of Site 5.



Figure 49. Photo. Coring at Site 5.



Figure 50. Photo. Cores from Site 5.



Figure 51. Photo. Close up of Site 6.



Figure 52. Photo. Cracking at Site 6.



Figure 53. Photo. View of Site 6.



Figure 54. Photo. Cores at Site 6.

APPENDIX B – VOLUMETRIC INFORMATION
Table 5. Volumetric Information from Cores Retrieved at Site 2.

Sample ID	AC Content	Voids in Total Mix	Modulus with Ultrasonic Device, ksi	Gradation (Percent Passing)						
				1/2 in.	3/8 in.	No. 4	No. 10	No. 40	No. 80	No. 200
1	8.6%	--	1758	100	89	52.38	30.02	15.74	9.00	3.15
2	9.7%	--	1641	95.45	86.47	59.37	39.00	23.83	17.42	3.92
3	3.6%	--	1440	90.22	76.57	46.60	28.99	16.08	9.59	7.62
4	6.8%	--	1737	91.90	81.62	52.88	34.07	17.44	11.08	2.15
5	--	2.2%	1926	--	--	--	--	--	--	--
6	--	4.4%	1213	--	--	--	--	--	--	--
Average	7.2%	3.3%	1619	94.4	83.4	52.8	33.0	18.3	11.8	4.2
COV	37.2%	47.1%	15.8%	4.6%	6.6%	9.9%	13.8%	20.7%	32.8%	56.7%

Table 6. Volumetric Information from Cores Retrieved at Site 3.

Sample ID	AC Content	Voids in Total Mix	Modulus with Ultrasonic Device, ksi	Gradation (Percent Passing)						
				1/2 in.	3/8 in.	No. 4	No. 10	No. 40	No. 80	No. 200
1	6.2%	--	2142	97.9	83.3	53.7	30.6	13.5	7.9	3.0
2	6.1%	--	2177	100.0	82.3	52.8	31.6	14.5	8.6	4.2
3	5.6%	--	2286	98.7	74.9	45.9	28.7	13.5	8.0	3.7
4	6.2%	--	2312	100.0	83.6	53.3	30.9	14.2	9.1	4.2
5	--	6.1%	2058	--	--	--	--	--	--	--
6	--	4.8%	2275	--	--	--	--	--	--	--
Average	6.0%	5.4%	2208	99.2	81.0	51.4	30.4	13.9	8.4	3.8
COV	4.8%	17.6%	4.5%	1.0%	5.1%	7.2%	4.1%	3.6%	6.7%	15.0%

Table 7. Volumetric Information from Cores Retrieved at Site 4.

Sample ID	AC Content	Voids in Total Mix	Modulus with Ultrasonic Device, ksi	Gradation (Percent Passing)						
				1/2 in.	3/8 in.	No. 4	No. 10	No. 40	No. 80	No. 200
1	8.1%	--	1502	91.33	76.93	53.52	35.63	19.27	11.50	4.13
2	7.6%	--	1017	100	82.73	49.91	31.99	21.68	13.96	5.30
3	5.9%	--	1300	90.02	80.99	55.42	35.99	20.45	11.85	4.99
4	7.3%	--	1647	100	83.41	55.51	34.35	25.13	11.30	4.19
5	--	6.1%	1841	--	--	--	--	--	--	--
6	--	7.5%	1022	--	--	--	--	--	--	--
Average	7.2%	6.8%	1388	95.3	81.0	53.6	34.5	21.6	12.2	4.7
COV	13.1%	14.6%	24.2%	5.7%	3.6%	4.9%	5.2%	11.7%	10.1%	12.5%

APPENDIX B – VOLUMETRIC INFORMATION

Table 8. Volumetric Information from Cores Retrieved at Site 5.

Sample ID	AC Content	Voids in Total Mix	Modulus with Ultrasonic Device, ksi	Gradation (Percent Passing)						
				1/2 in.	3/8 in.	No. 4	No. 10	No. 40	No. 80	No. 200
1	7.4%	--	2155	100	79.76	45.46	27.14	16.61	10.10	4.00
2	7.1%	--	1958	100	81.81	46.24	27.11	16.57	10.27	3.98
3	7.8%	--	2009	100	82.87	48.35	30.67	21.59	15.62	9.63
4	6.8%	--	1921	92.91	82.80	53.56	33.47	17.50	9.55	4.23
5	--	8.8%	1929	--	--	--	--	--	--	--
6	--	8.0%	1792	--	--	--	--	--	--	--
Average	7.3%	8.4%	1961	98.2	81.8	48.4	29.6	18.1	11.4	5.5
COV	5.9%	6.7%	6.1%	3.6%	1.8%	7.5%	10.4%	13.2%	24.9%	51.0%

Table 9. Volumetric Information from Cores Retrieved at Site 6.

Sample ID	AC Content	Voids in Total Mix	Modulus with Ultrasonic Device, ksi	Gradation (Percent Passing)						
				1/2 in.	3/8 in.	No. 4	No. 10	No. 40	No. 80	No. 200
1	10.1%	--	2022	100	77.7	51.93	36.50	24.21	13.24	6.08
2	8.2%	--	1789	90.68	80.70	54.59	36.70	22.62	12.13	3.34
3	8.1%	--	1897	90.79	79.11	56.18	42.62	26.94	10.51	2.24
4	8.4%	--	1720	93.98	79.43	49.96	32.99	17.93	10.09	1.97
5	--	1.6%	2123	--	--	--	--	--	--	--
6	--	2.6%	1496	--	--	--	--	--	--	--
Average	8.7%	2.1%	1841	93.9	79.2	53.2	37.2	22.9	11.5	3.4
COV	10.8%	33.7%	12.2%	4.7%	1.6%	5.2%	10.7%	16.5%	12.7%	55.1%

APPENDIX C – PSPA RESULTS

Table 10. Seismic Moduli Measured at Site 1.

Modulus Wheel path (ksi)			Modulus Midlane (ksi)		
Station No.	Longitudinal	Transverse	Station No.	Longitudinal	Transverse
1	518	645	1	866	807
	552	696		866	832
2	684	693	2	642	541
	684	726		785	541
3	679	807	3	823	645
	705	832		934	925
4	494	598	4	685	737
	529	572		615	858
5	578	957	5	879	836
	604	940		914	828
6	749	749	6	793	610
	706	758		1080	610
7	589	806	7	867	771
	598	823		875	754
8	849	685	8	901	607
	633	728		1075	615
9	815	637	9	691	761
	815	602		691	841
10	707	785	10	716	1190
	776	802		802	828
11	543	647	11	707	776
	733	647		707	742
12	892	1235	12	772	866
	678	1192		763	866
13	729	815	13	1132	798
	738	841		1192	841
14	918	806	14	832	583
	901	858		823	523
15	1152	529	15	956	649
	887	606		845	606
Average	741		Average	794	
Std Dev	155		Std Dev	150	
Cov	20.9%		COV	18.8%	

Table 11. Seismic Moduli Measured at Site 2.

Modulus Wheel path (ksi)			Modulus Midlane (ksi)		
Station No.	Longitudinal	Transverse	Station No.	Longitudinal	Transverse
1	1603	1169	1	1957	1788
	1240	1169		1974	1815
2	1062	1213	2	1027	992
	1071	1204		1027	992
3	823	814	3	904	1199
	984	832		967	1190
4	2386	2270	4	1228	1460
	2314	2261		1326	1665
5	1584	1495	5	1262	1745
	1942	1557		1298	2112
6	1844	1620	6	1038	1128
	1862	1853		958	1074
7	1029	1128	7	1298	1047
	967	1172		1378	1065
8	2349	1800	8	1233	1557
	2727	2142		1269	1557
9	2402	2256	9	1374	1283
	2402	2001		1765	1265
10	2389	2027	10	959	1294
	2045	2108		860	1249
11	2543	2324	11	732	732
	2644	2296		741	732
12	2205	2223	12	1830	1390
	2177	2186		2360	1372
13	1473	961	13	1692	1784
	1390	1519		1839	1592
14	1113	947	14	1131	1131
	1095	984		1223	1113
15	920	855	15	810	607
	874	865		819	607
Average	1645		Average	1280	
Std Dev	589		Std Dev	392	
COV	35.8%		COV	30.6%	

Table 12. Seismic Moduli Measured at Site 3.

Modulus Wheel path (ksi)			Modulus Midlane (ksi)		
Station No.	Longitudinal	Transverse	Station No.	Longitudinal	Transverse
1	1619	1711	1	1674	1711
	1583	1647		1702	1702
2	1619	1628	2	1474	1656
	1565	1574		1483	1656
3	1710	1493	3	1737	1909
	1755	1620		1728	1909
4	1611	1665	4	1737	1881
	1557	1710		1674	1863
5	1797	1629	5	1700	1842
	1850	1664		1718	1842
6	1904	2019	6	2098	2019
	1886	2001		2072	1966
7	2006	1927	7	1883	1910
	2050	1962		1910	1953
8	2009	2087	8	1940	2069
	2018	2069		1906	2095
9	2159	1826	9	2133	2176
	2099	1818		2167	2167
10	2318	2258	10	2131	2284
	2403	2182		2131	2241
11	2221	2019	11	2289	2120
	2272	2052		2238	2103
12	2331	2120	12	2500	2196
	2095	2103		2449	2036
13	2361	2378	13	2235	2370
	2412	2353		2202	2344
14	1808	2318	14	1749	2122
	1851	2428		1800	2199
15	2161	2222	15	1908	1725
	2117	2231		1839	1717
Average	1964		Average	1967	
Std Dev	271		Std Dev	239	
COV	13.8%		COV	12.2%	

Table 13. Seismic Moduli Measured at Site 4.

Modulus Wheel path (ksi)			Modulus Midlane (ksi)		
Station No.	Longitudinal	Transverse	Station No.	Longitudinal	Transverse
1	1845	2097	1	2170	2212
	1919	2160		2118	2139
2	2052	1689	2	1742	2020
	2073	1731		1892	2063
3	2052	1657	3	1854	1426
	1865	1657		1843	1426
4	1544	1420	4	1307	1567
	1555	1826		1386	1567
5	928	950	5	939	729
	939	1005		983	729
6	712	778	6	1001	367
	756	801		1045	367
7	922	1130	7	965	954
	933	1152		834	954
8	1115	1039	8	736	747
	1115	1039		758	747
9	736	725	9	920	780
	780	736		942	747
10	1343	931	10	1061	1202
	1299	931		1072	1202
11	696	696	11	1049	1027
	685	663		1038	1038
12	954	1009	12	801	1086
	976	1031		801	1053
13	834	596	13	812	812
	823	671		790	671
14	566	460	14	673	695
	566	460		695	727
15	682	628	15	855	996
	682	617		974	1061
Average	1104		Average	1119	
Std Dev	485		Std Dev	468	
COV	44.0%		COV	41.8%	

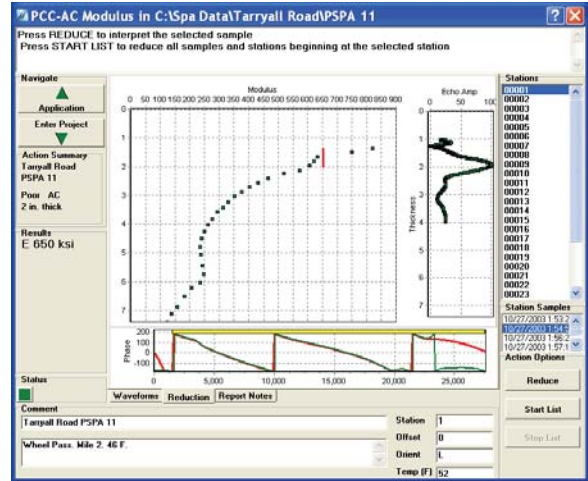
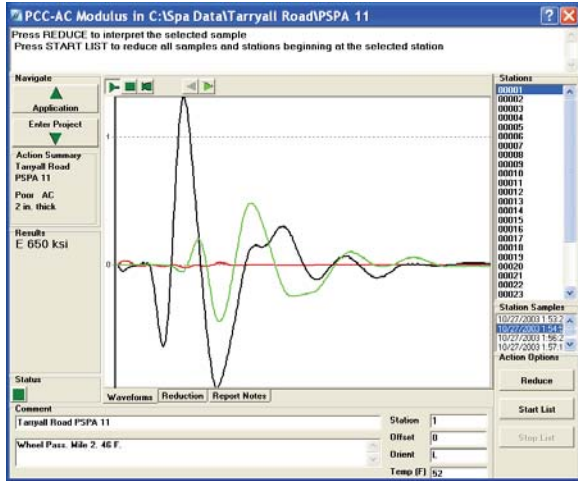
Table 14. Seismic Moduli Measured at Site 5.

Modulus Wheel path (ksi)			Modulus Midlane (ksi)		
Station No.	Longitudinal	Transverse	Station No.	Longitudinal	Transverse
1	2046	1589	1	1980	2341
	1922	1627		2103	2322
2	2080	2291	2	2176	2128
	944	2349		2705	1579
3	1560	1290	3	2118	1560
	1521	1252		1598	1579
4	1646	1983	4	1261	1993
	1126	1579		1608	1935
5	1435	2012	5	1406	1309
	1829	2320		1396	2022
6	2160	1830	6	1637	2102
	1821	1617		2208	2111
7	1811	1734	7	1995	1995
	1753	1637		2014	1433
8	1336	1714	8	2286	2053
	1327	2034		2111	2179
9	1364	2026	9	1724	1705
	1354	1831		1559	1880
10	1489	1754	10	1460	1519
	1362	1823		1823	1480
11	2231	2124	11	1403	1364
	1559	2007		1413	1461
12	2211	2221	12	2046	1968
	2280	2143		2075	1939
13	2087	1636	13	2146	1323
	1970	1646		2234	1480
14	1783	2156	14	1578	1950
	1989	2166		2019	1970
15	1881	2342	15	2283	2058
	1881	2195		1705	2146
Average	1811		Average	1849	
Std Dev	335		Std Dev	331	
COV	18.5%		COV	17.9%	

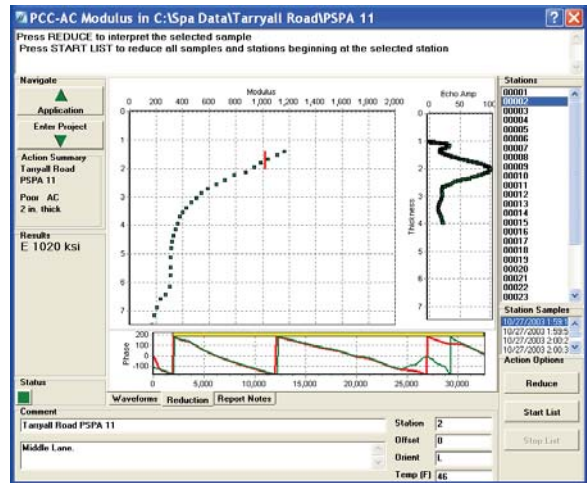
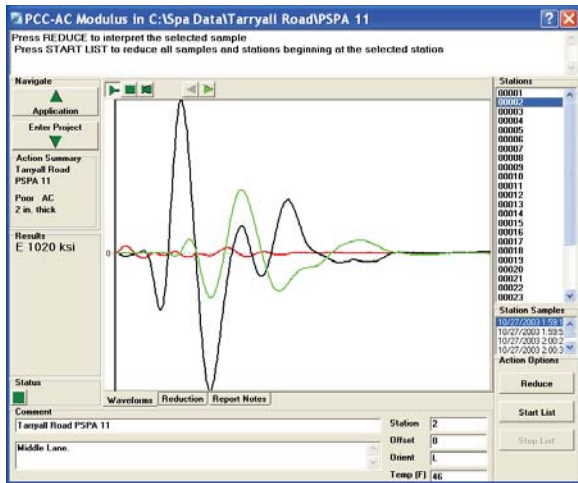
Table 15..Seismic Moduli Measured at Site 6.

Modulus Wheel path (ksi)			Modulus Midlane (ksi)		
Station No.	Longitudinal	Transverse	Station No.	Longitudinal	Transverse
1	1741	1363	1	2082	1400
	1760	1372		975	1542
2	2167	2009	2	1460	2214
	2167	1926		1470	2279
3	2015	1959	3	1817	625
	2139	2006		2044	615
4	1437	1704	4	1009	1456
	1456	1713		1266	1523
5	1863	1656	5	856	941
	2239	1477		1138	941
6	2593	1741	6	1930	1505
	2337	1741		1968	1505
7	1534	1364	7	1646	1656
	1524	1345		1628	1694
8	1375	1179	8	1375	1357
	1366	1179		1413	1394
9	1057	1029	9	1815	2058
	964	1010		1796	2068
10	2498	2021	10	2582	2114
	2545	1843		2451	2301
11	2512	1995	11	1543	1684
	2418	2032		1524	1731
12	1991	2930	12	3191	1600
	1963	3414		3154	1944
13	2102	2391	13	1265	1693
	2158	1972		1274	1572
14	1562	1431	14	1562	2423
	1562	1618		1703	2386
15	664	1684	15	1188	1160
	664	2198		1254	1123
Average	1795		Average	1648	
Std Dev	525		Std Dev	528	
COV	29.2%		COV	32.0%	

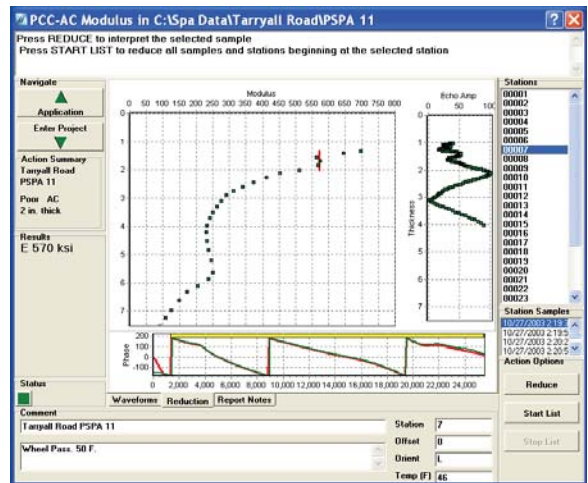
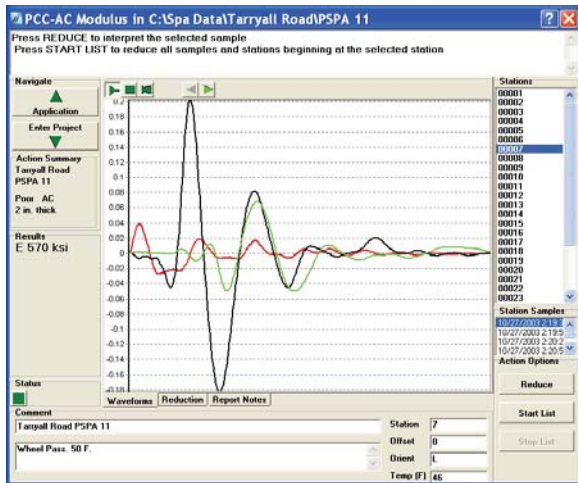
APPENDIX D – TYPICAL RESULTS FROM PSPA



a) Core 1

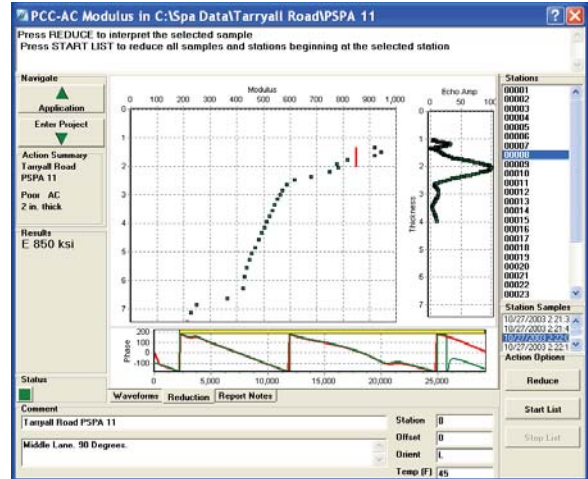
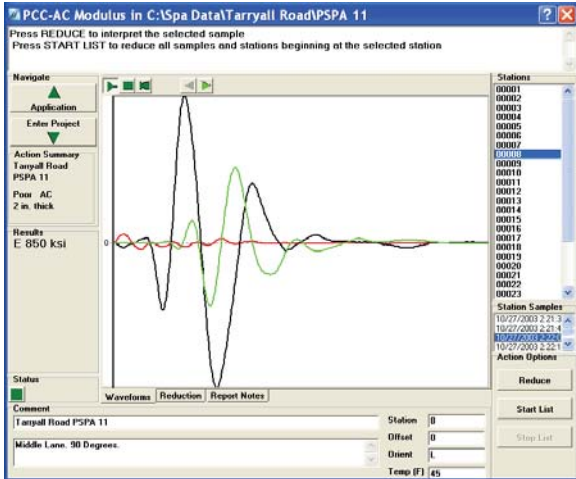


b) Core 2

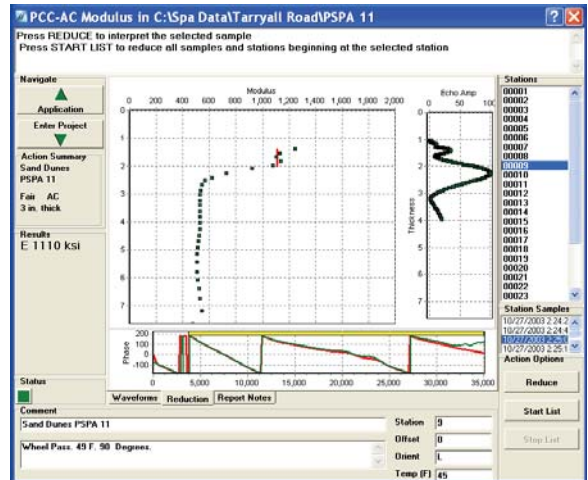
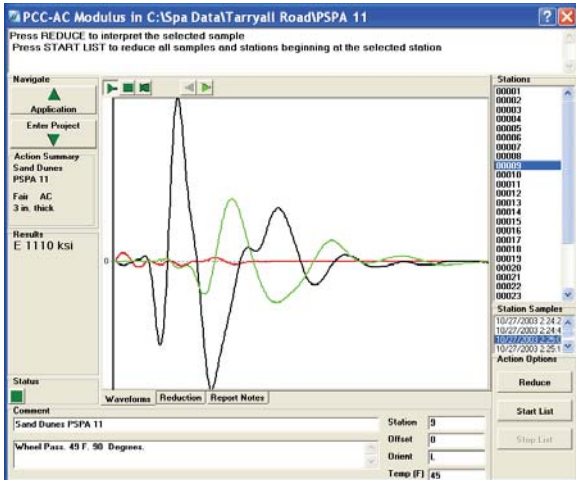


c) Core 3

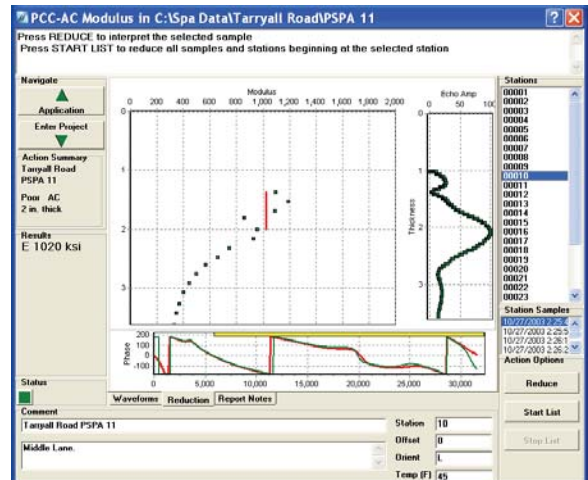
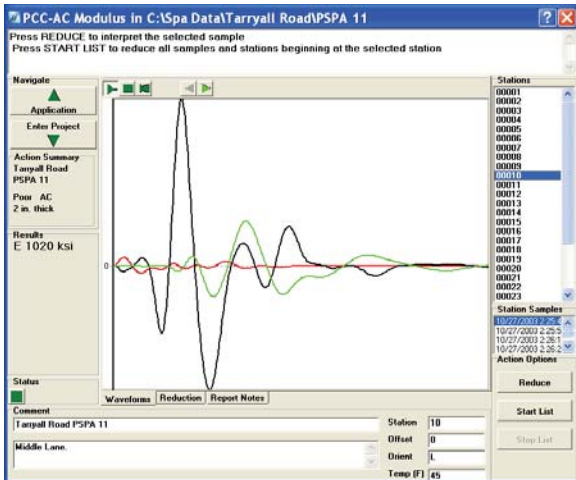
Figure 55. Graph. Typical PSPA Results at Site 1.



d) Core 4

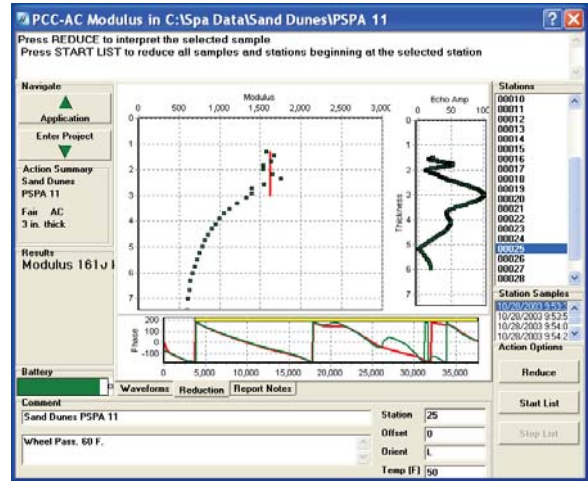
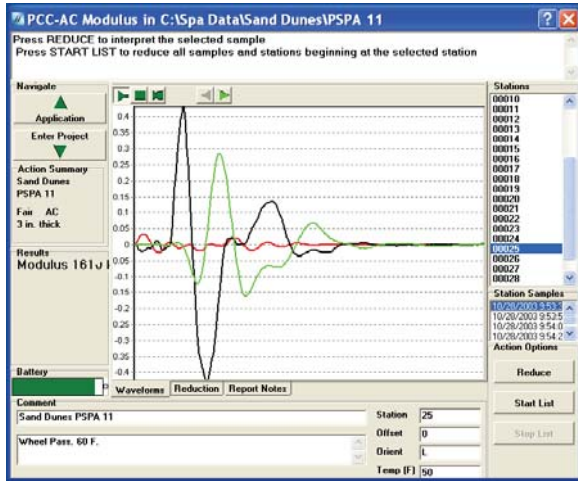


e) Core 5

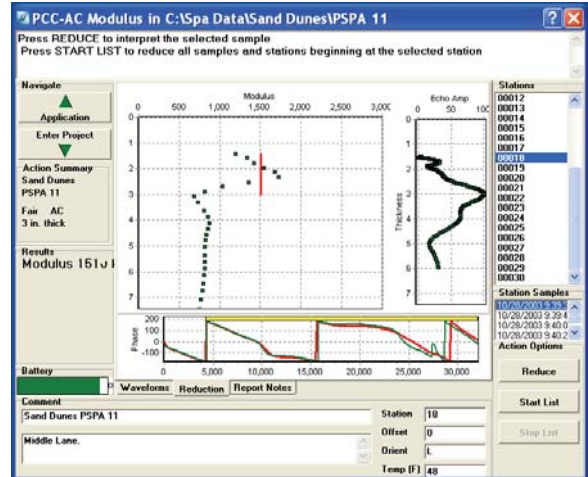
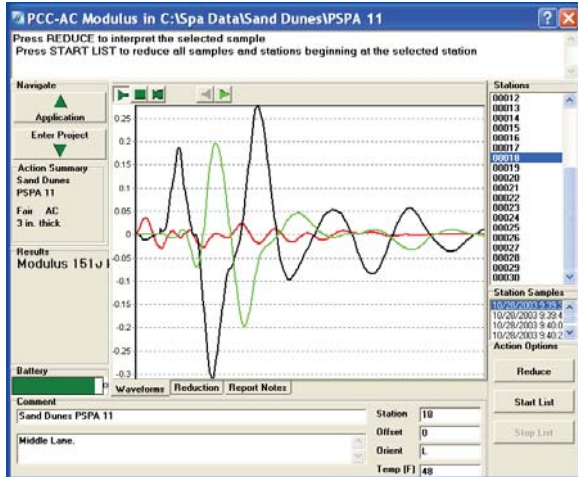


f) Core 6

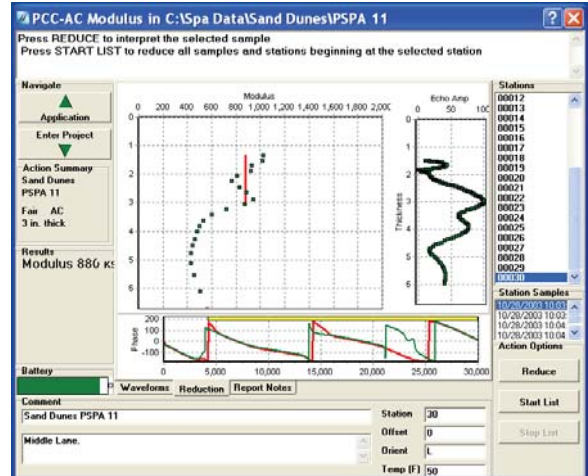
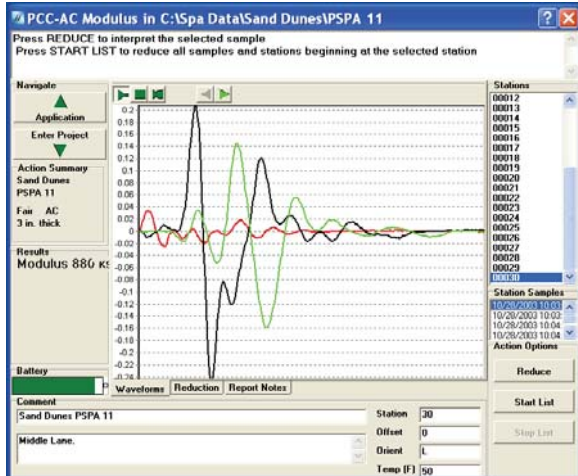
Figure 55 (Cont). Graph. Typical PSPA Results at Site 1.



a) Core 1

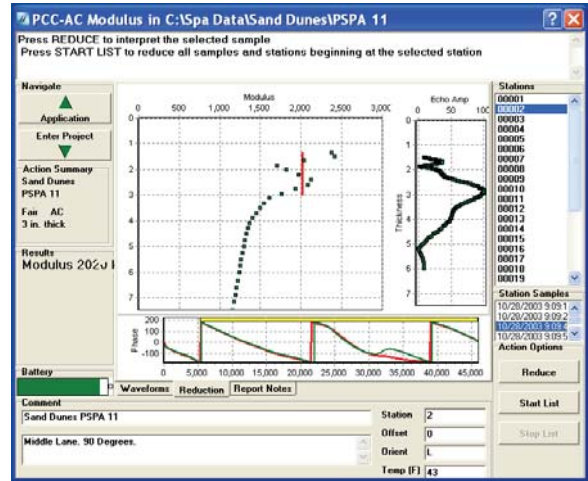
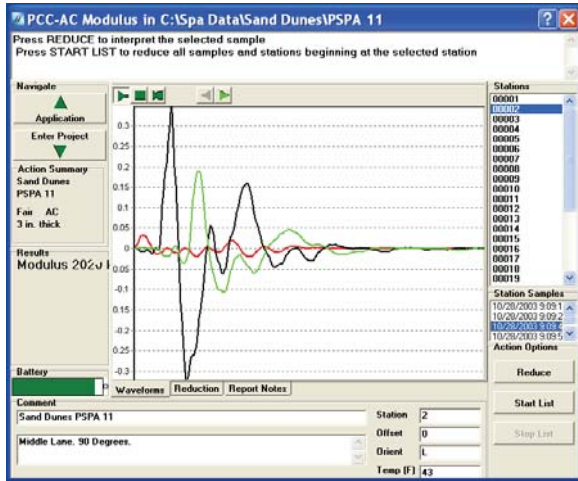


b) Core 2

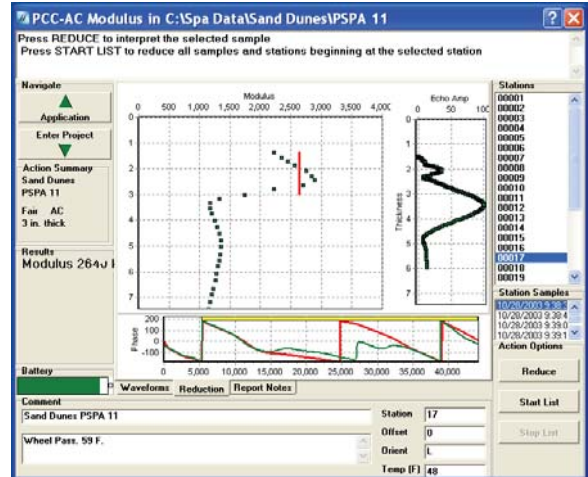
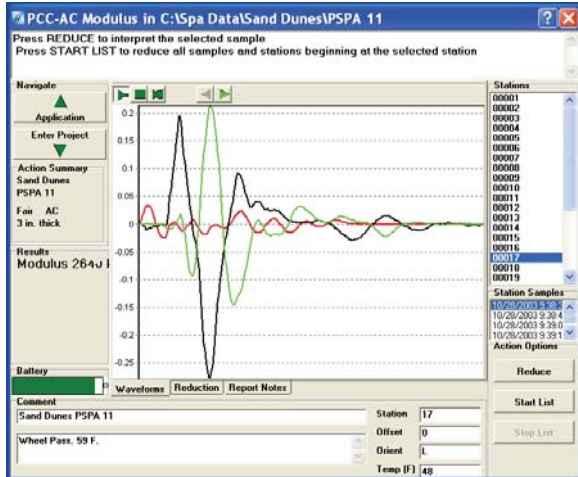


c) Core 3

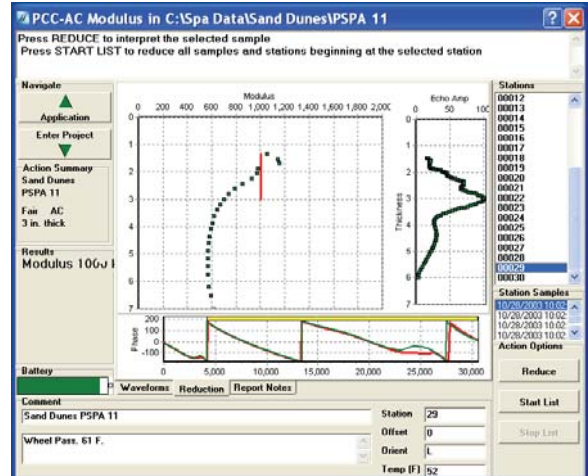
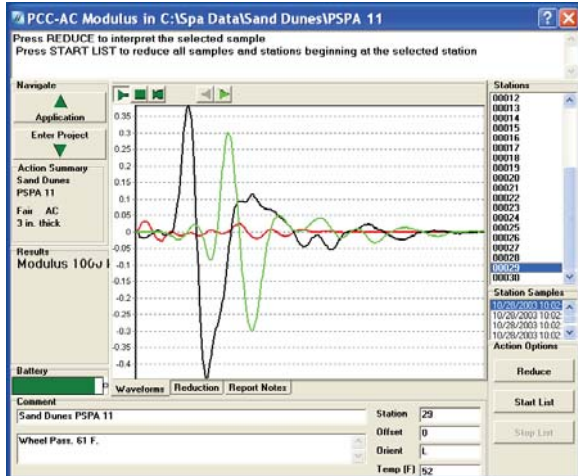
Figure 56. Graph. Typical PSPA Results at Site 2.



d) Core 4

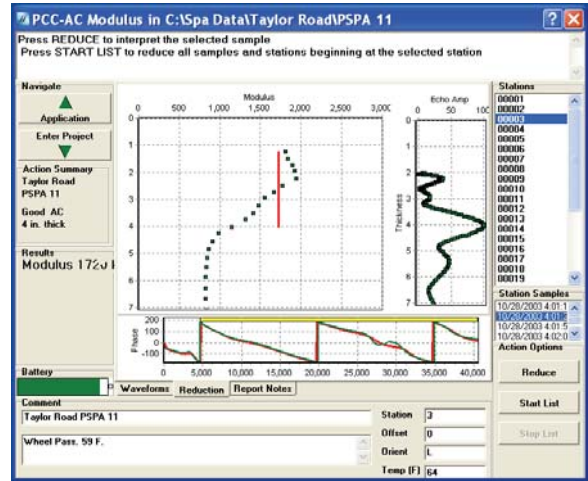
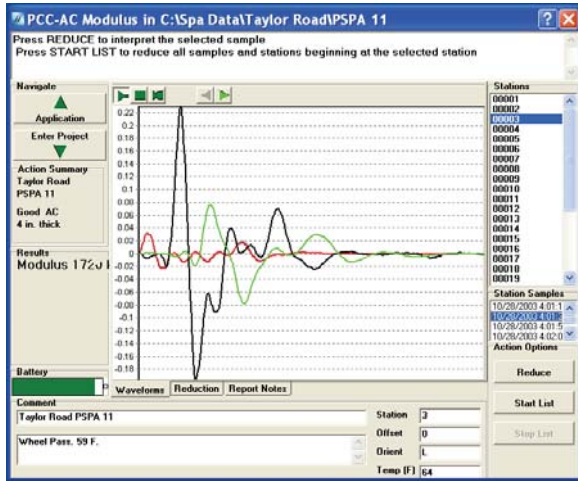


e) Core 5

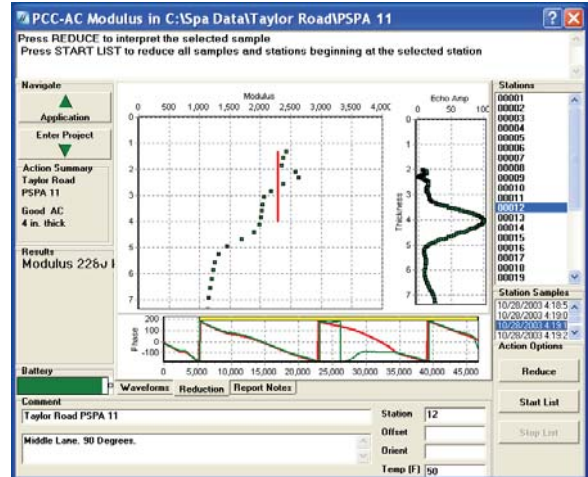
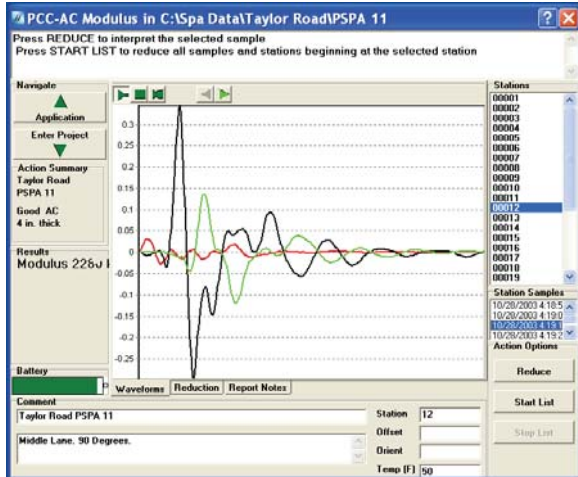


f) Core 6

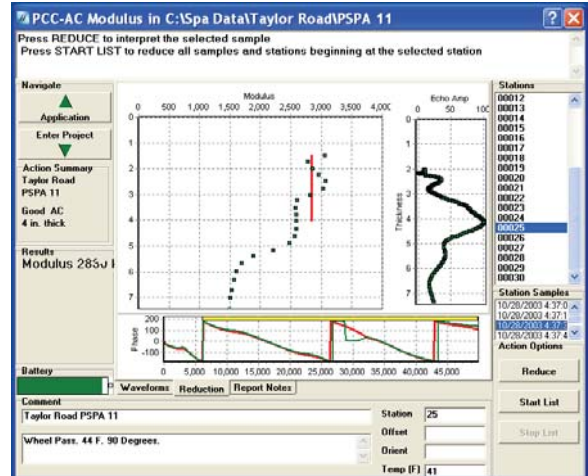
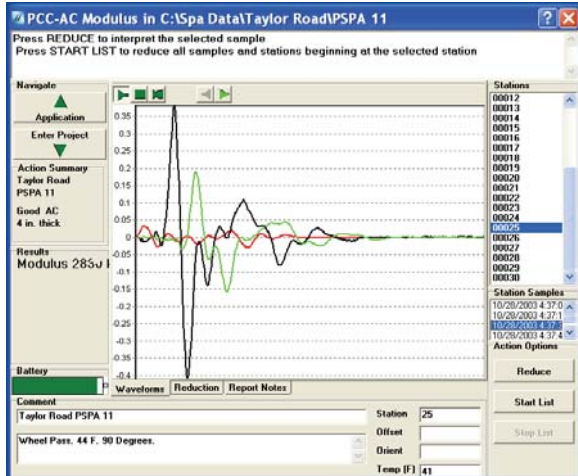
Figure 56 (cont). Graph. Typical PSPA Results at Site 2.



a) Core 1

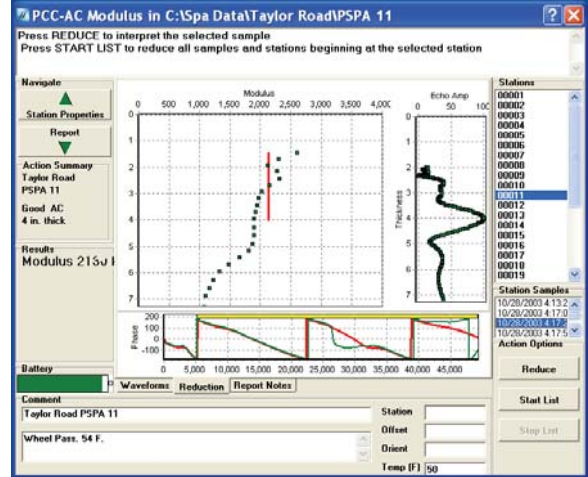
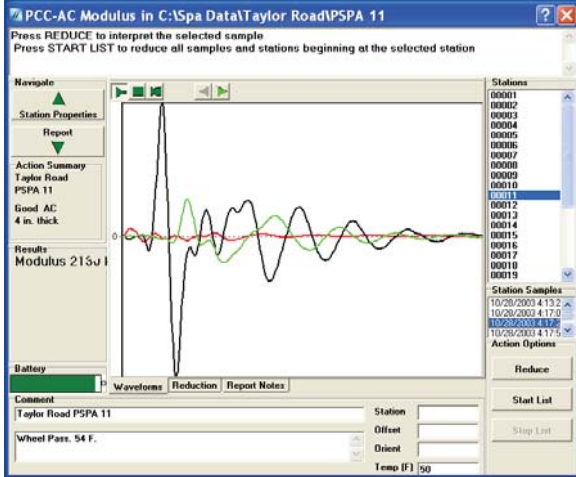


b) Core 2

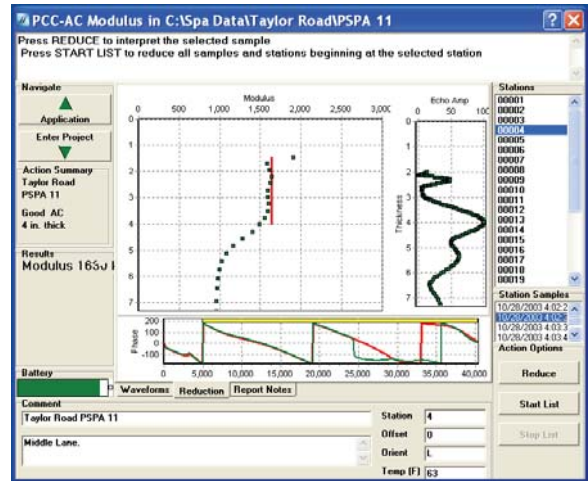
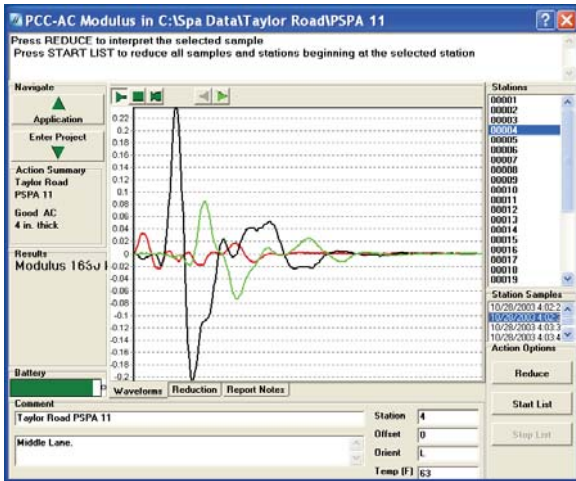


c) Core 3

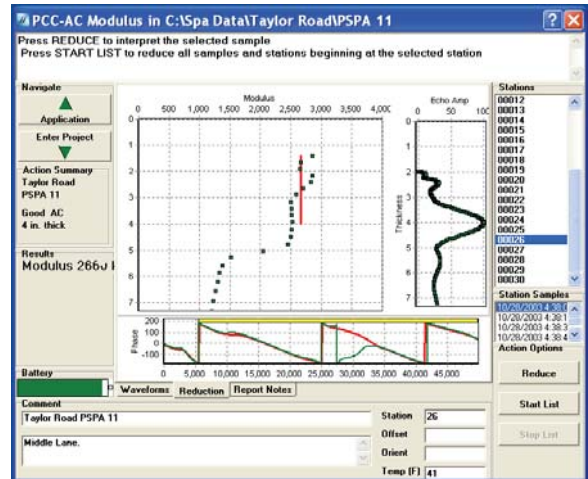
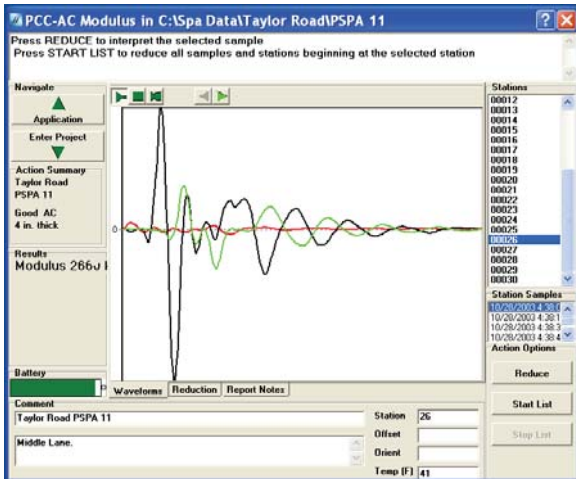
Figure 57. Graph. Typical PSPA Results at Site 3.



d) Core 4

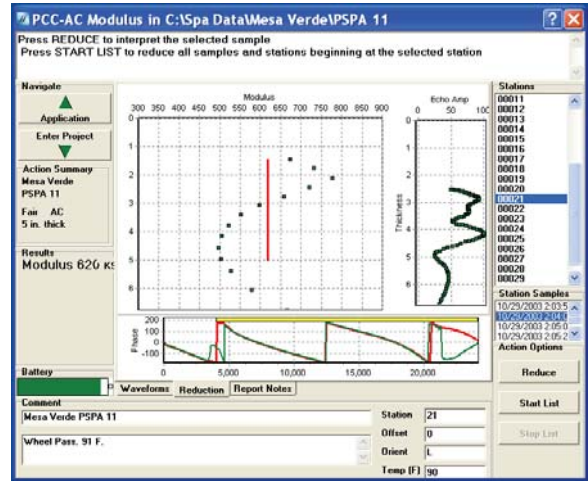
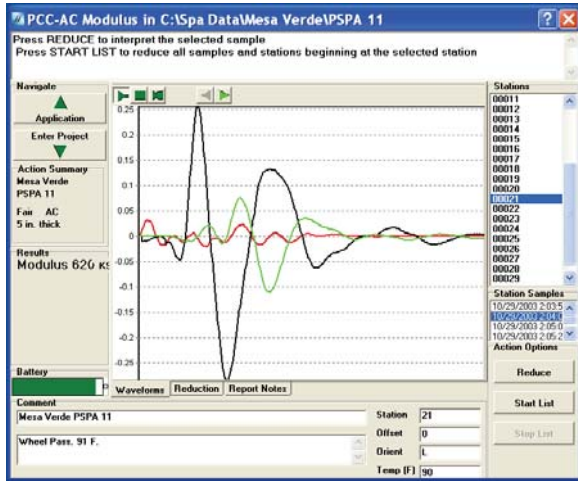


e) Core 5

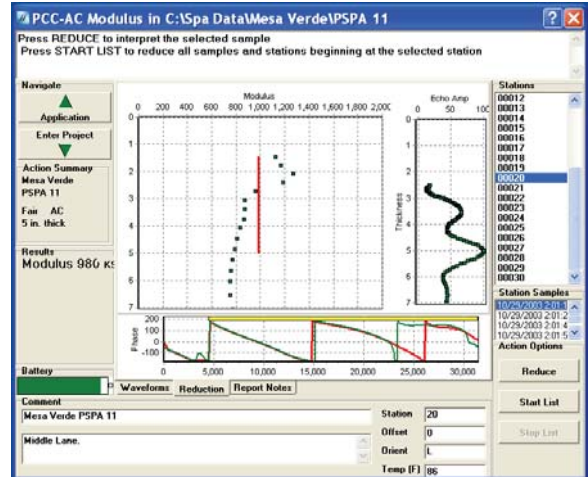
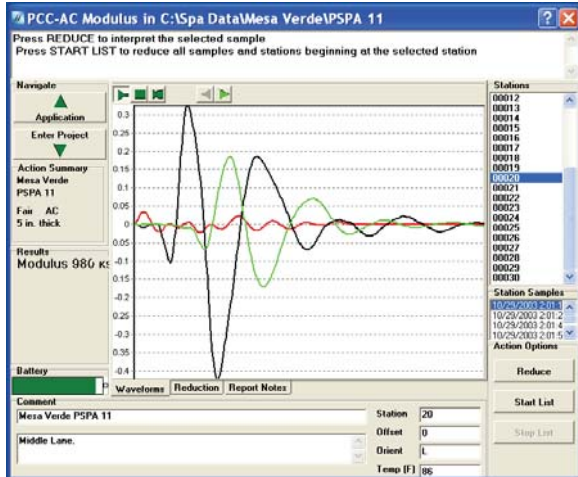


f) Core 6

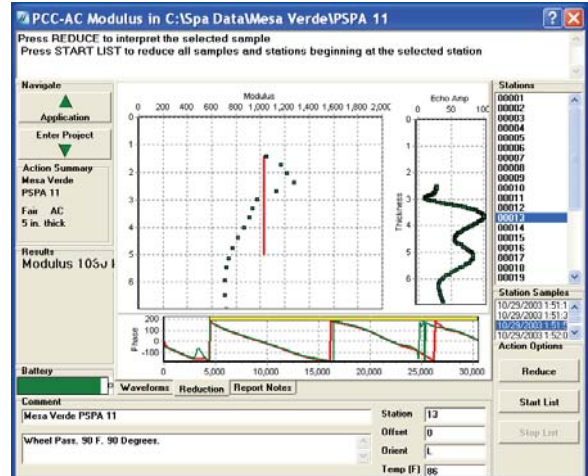
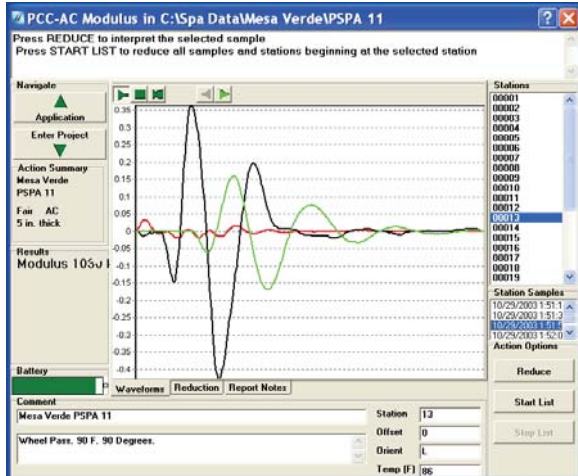
Figure 57 (cont). Graph. Typical PSPA Results at Site 3.



a) Core 1

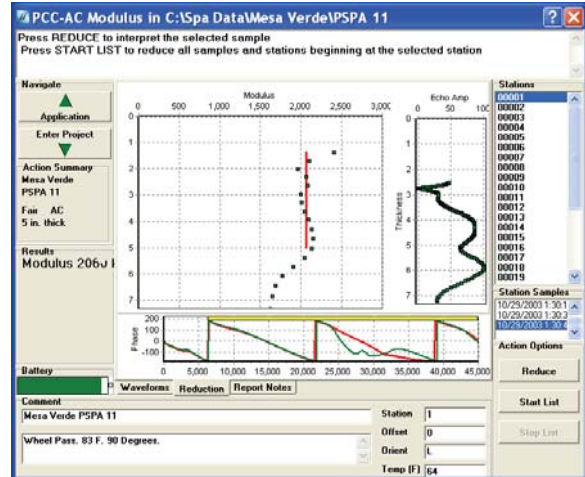
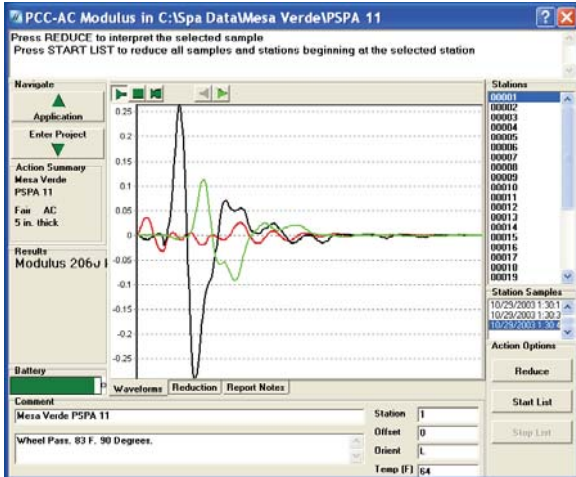


b) Core 2

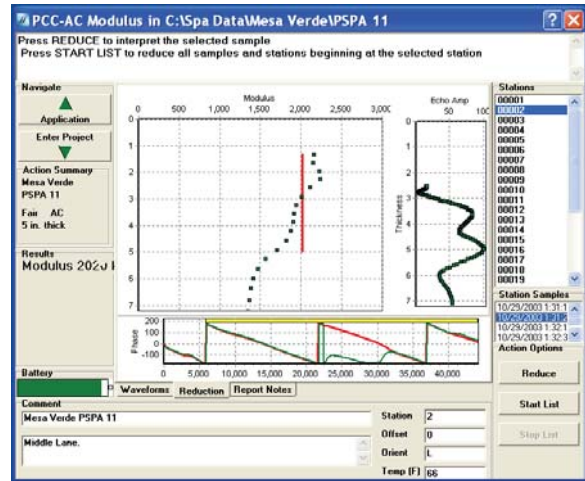
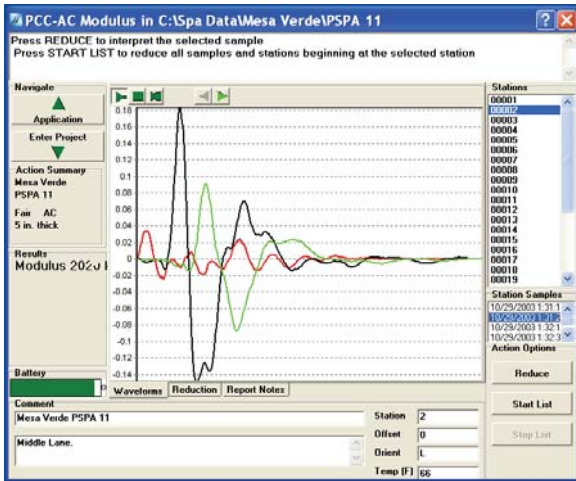


b) Core 3

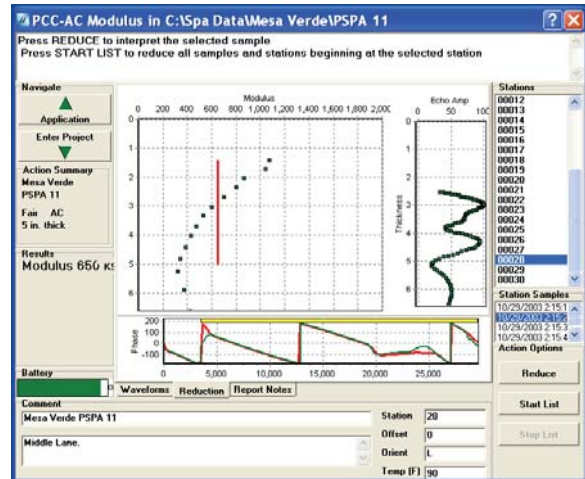
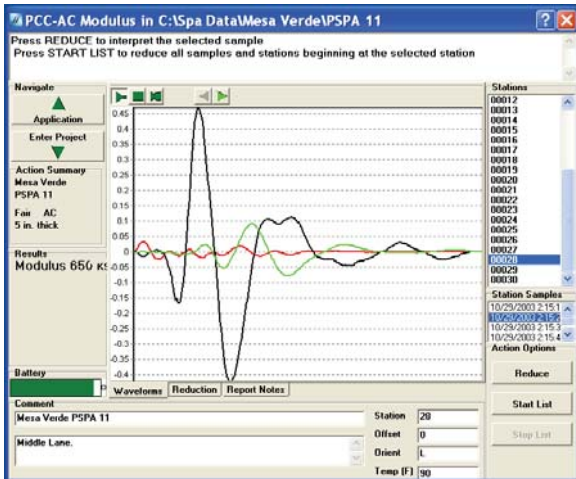
Figure 58. Graph. Typical PSPA Results at Site 4.



d) Core 4

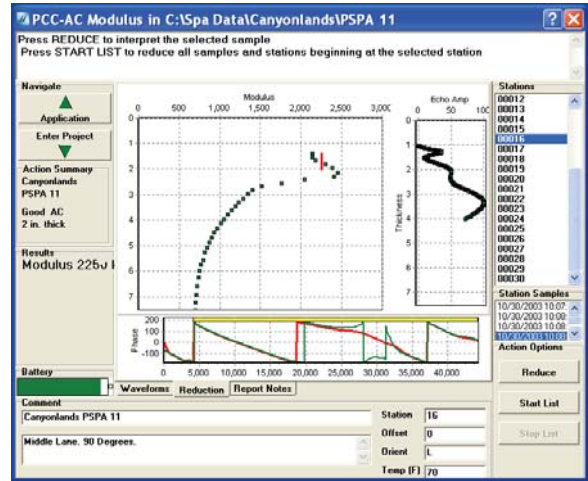
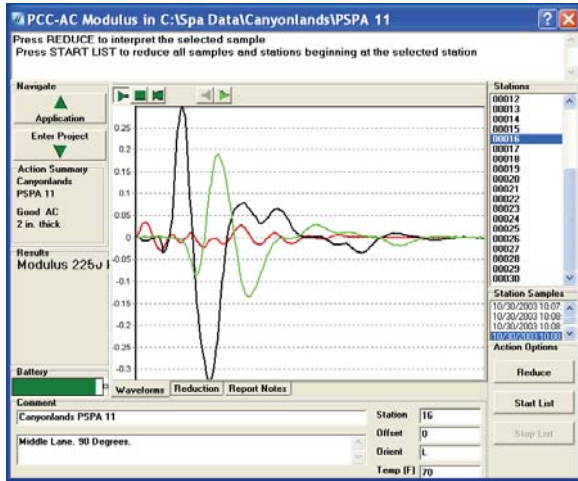


e) Core 5

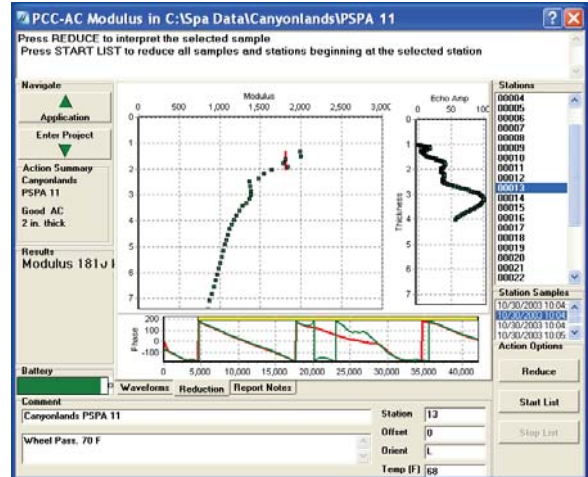
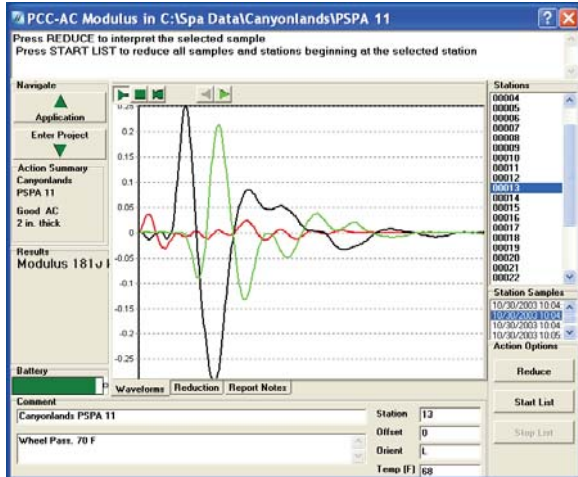


f) Core 6

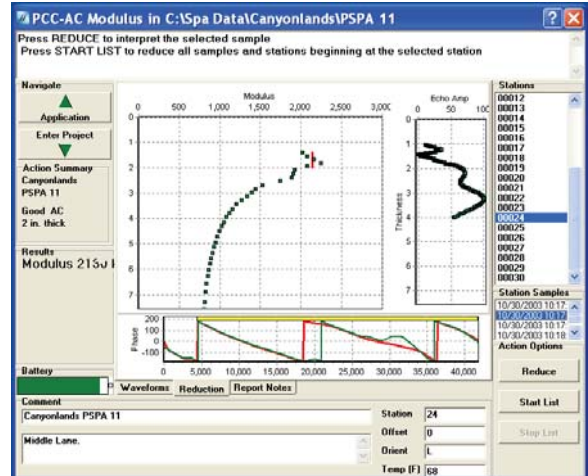
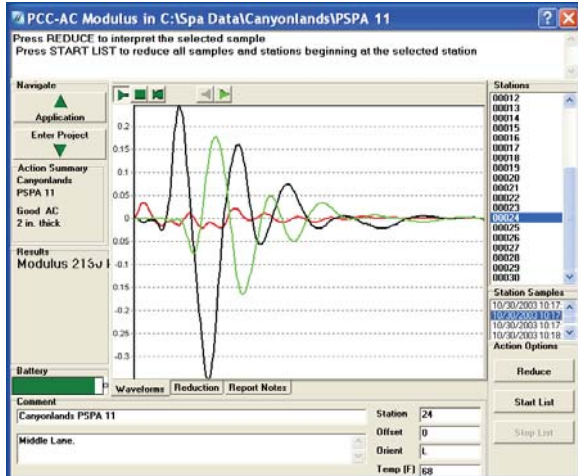
Figure 58 (cont). Graph. Typical PSPA Results at Site 4.



a) Core 1

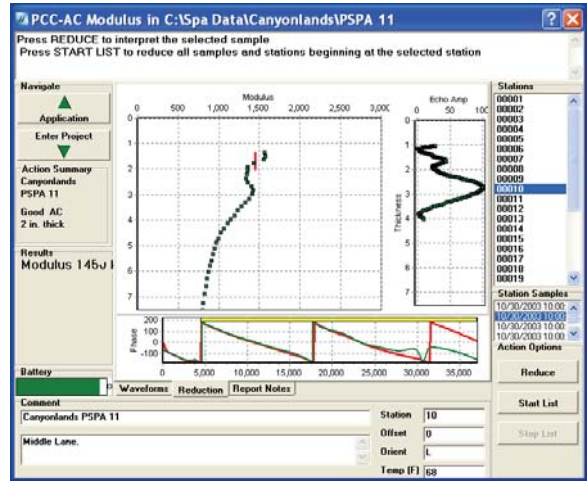
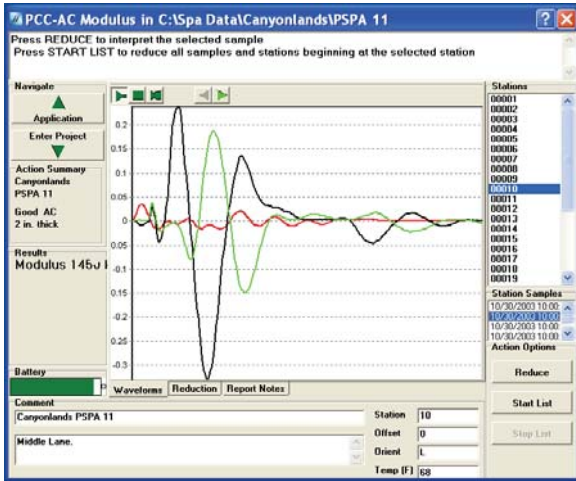


b) Core 2

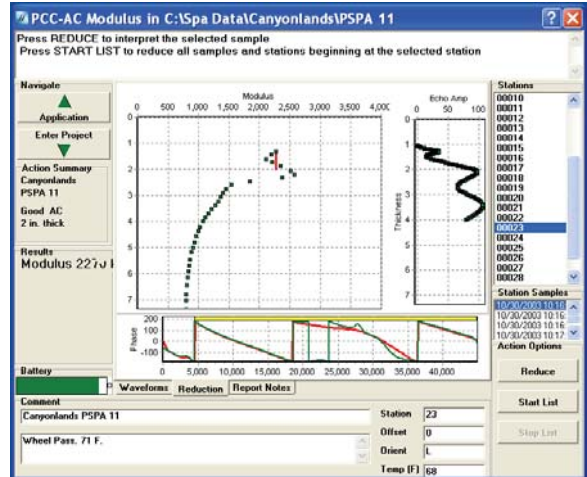
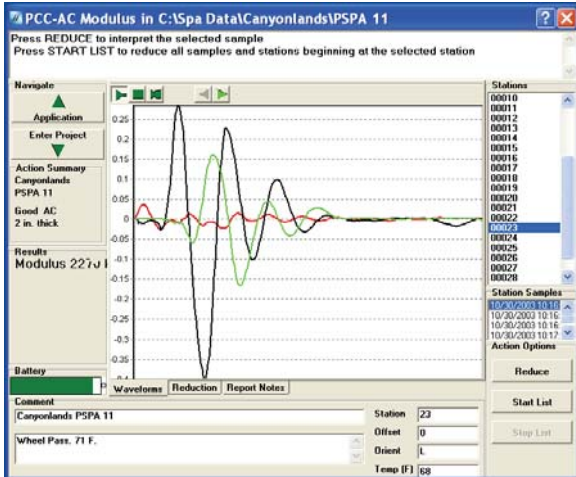


c) Core 3

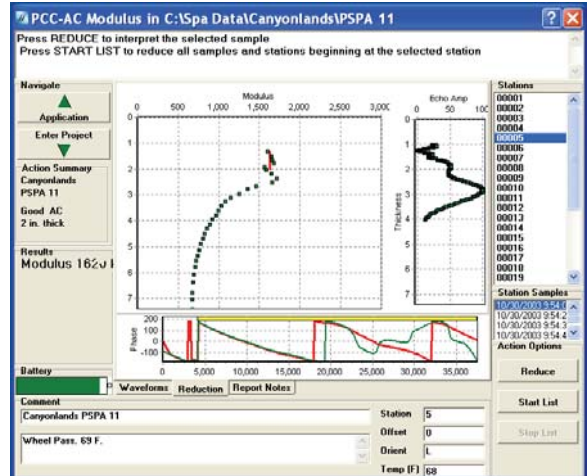
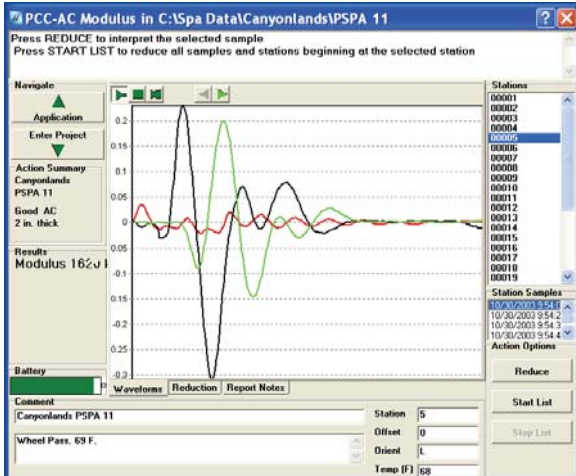
Figure 59. Graph. Typical PSPA Results at Site 5.



d) Core 4

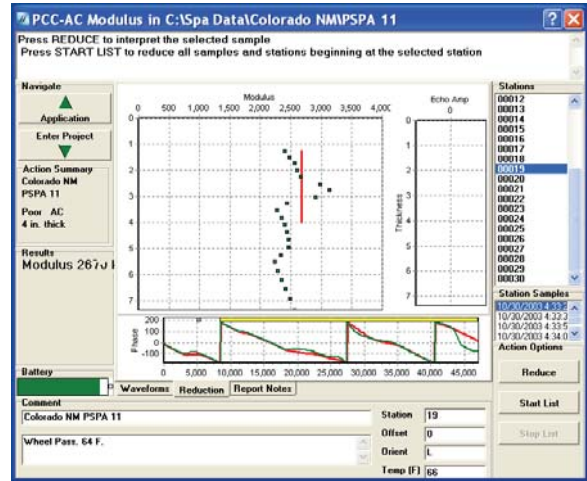
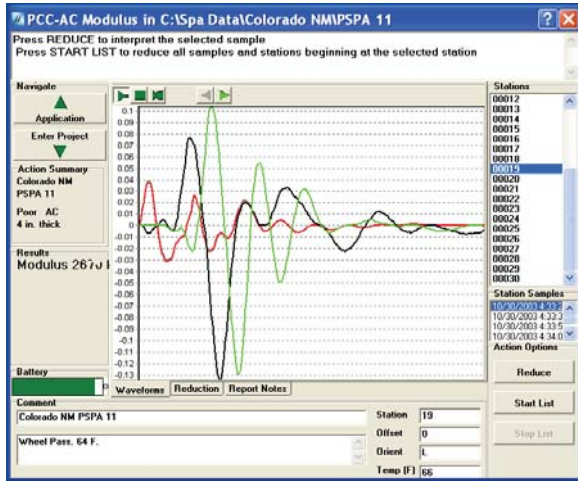


e) Core 5

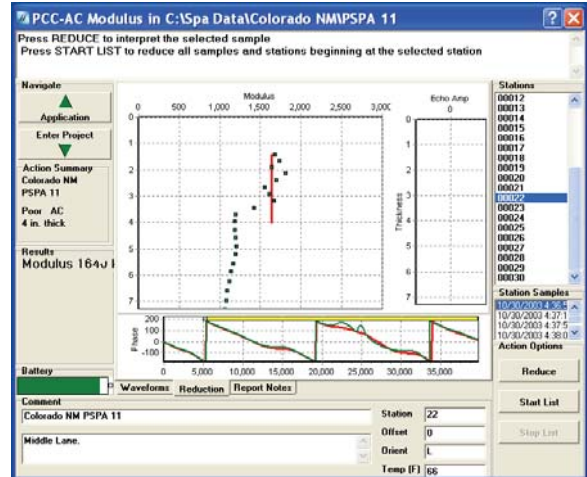
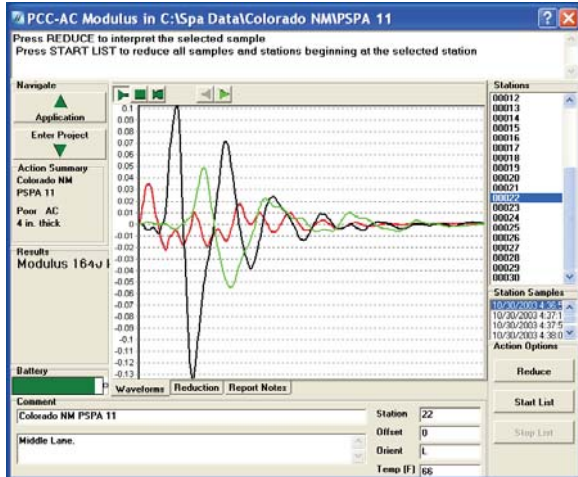


f) Core 6

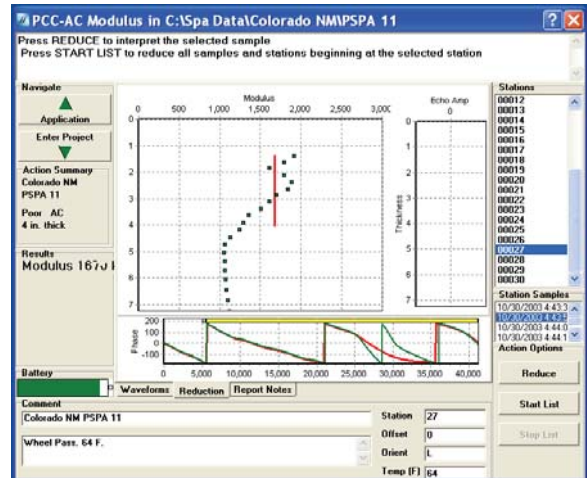
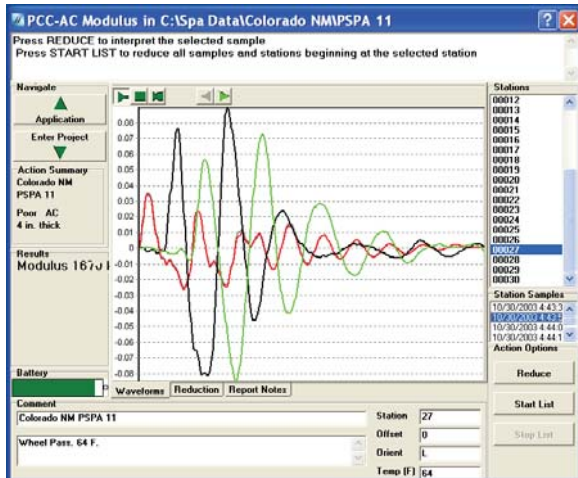
Figure 59 (cont). Graph. Typical PSPA Results at Site 5.



a) Core 1

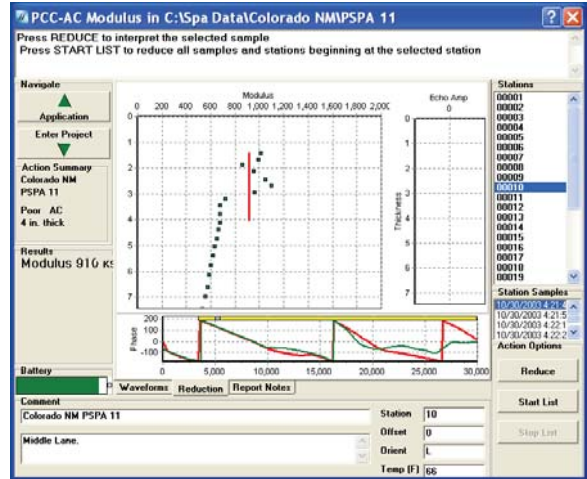
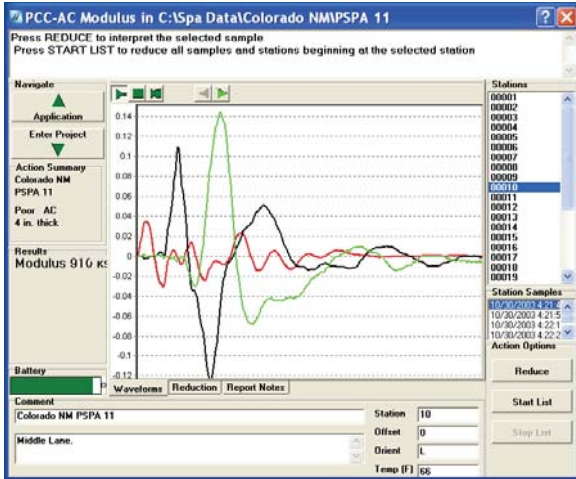


b) Core 2

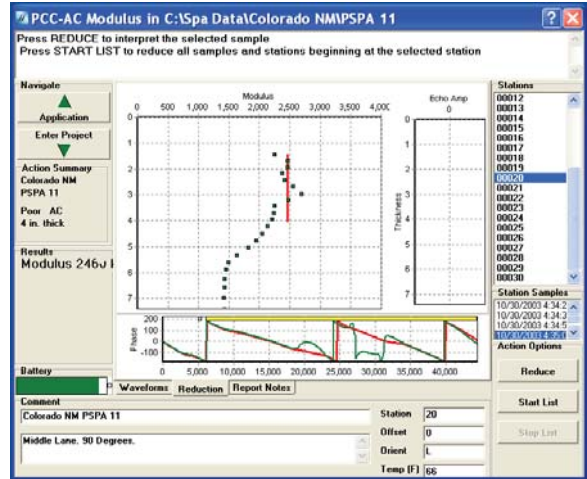
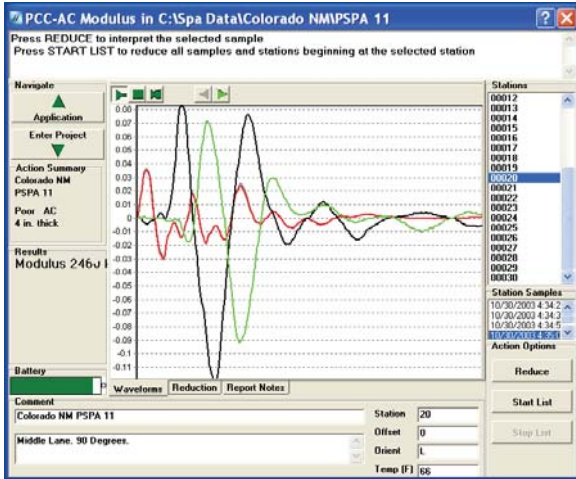


c) Core 3

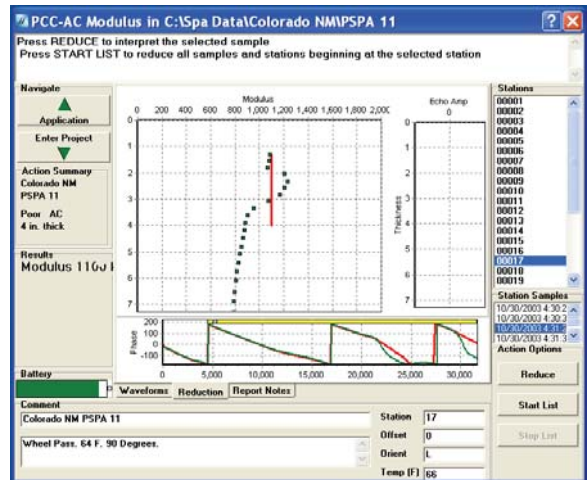
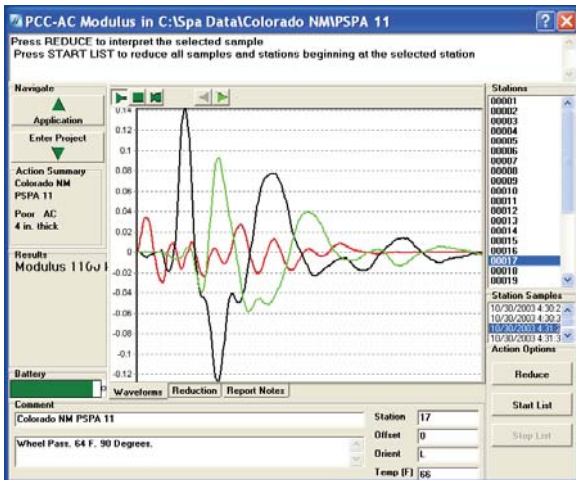
Figure 60. Graph. Typical PSPA Results at Site 6.



d) Core 4



e) Core 5



f) Core 6

Figure 60 (cont). Graph. Typical PSPA Results at Site 6.

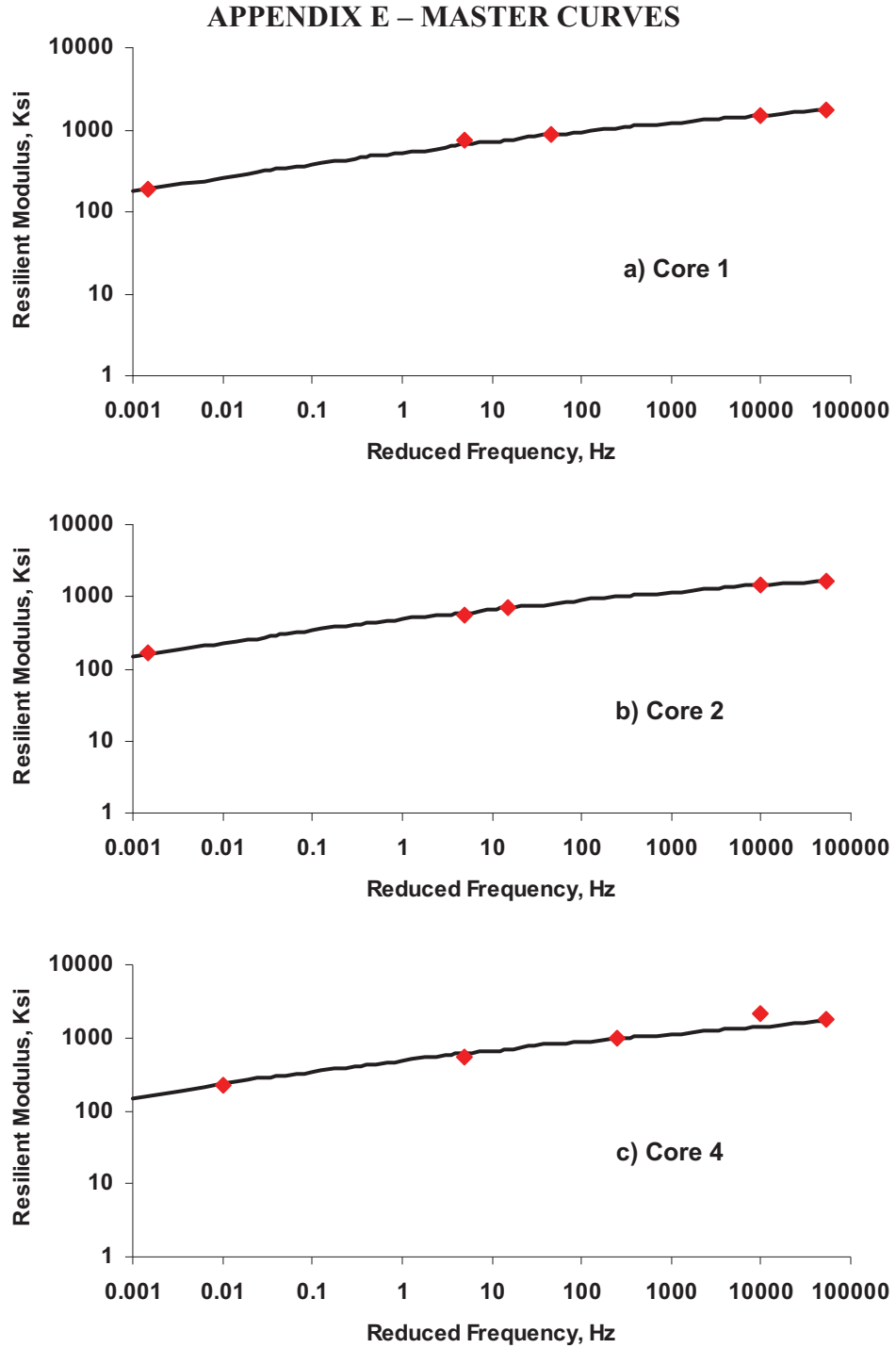


Figure 61. Graph. Master Curves for Site 2.

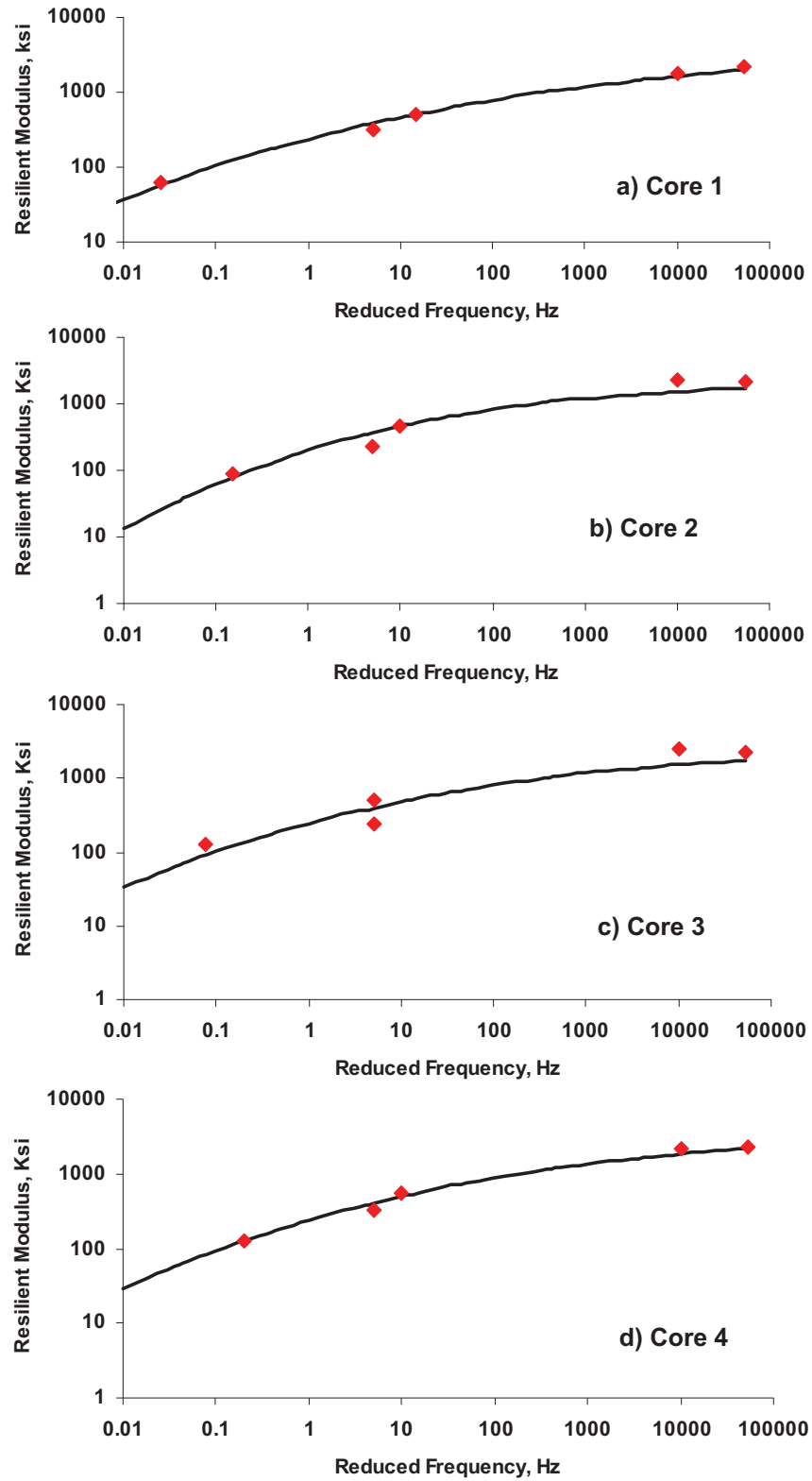


Figure 62. Graph. Master Curves for Site 3.

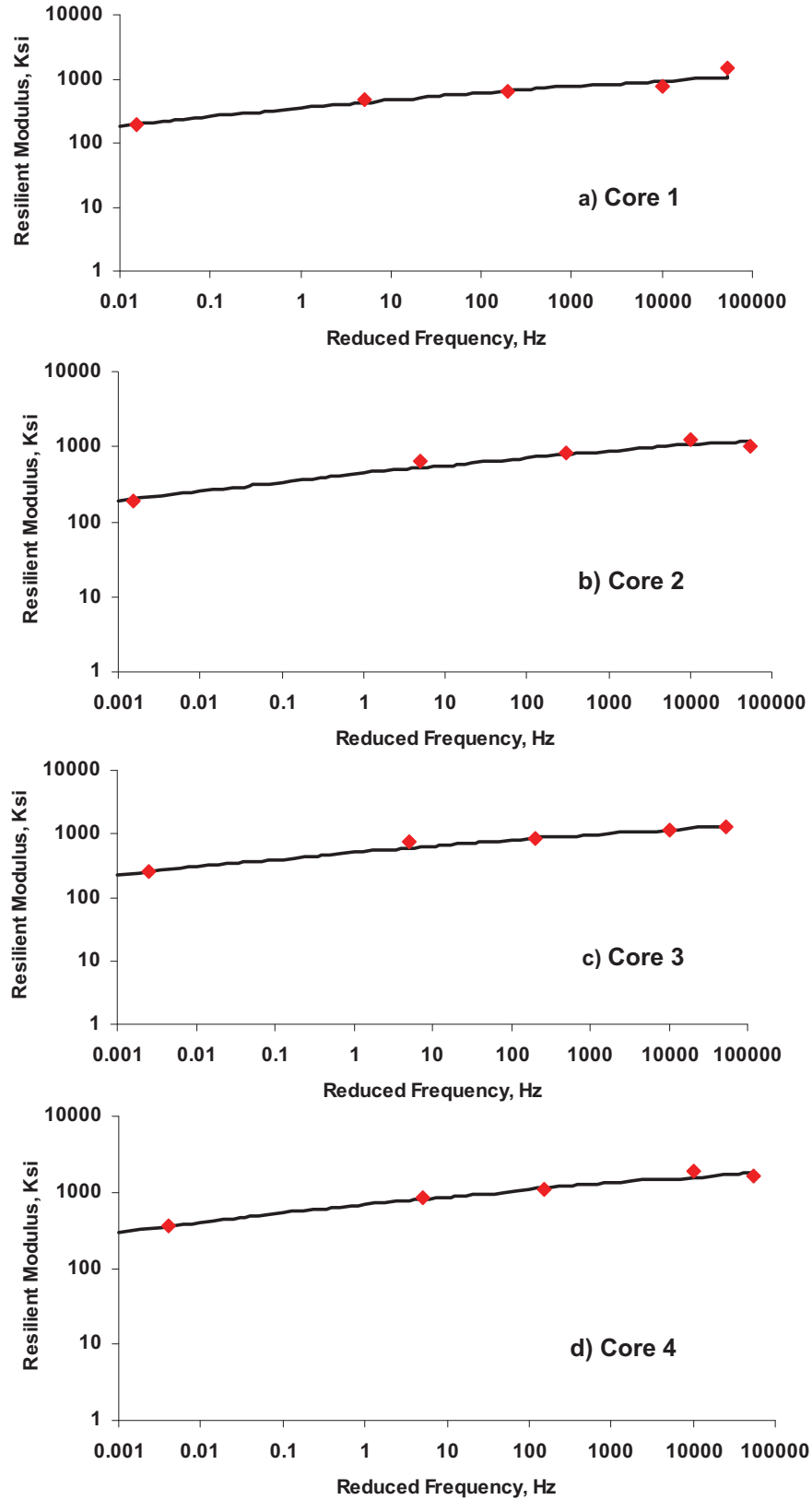


Figure 63. Graph. Master Curves for Site 4.

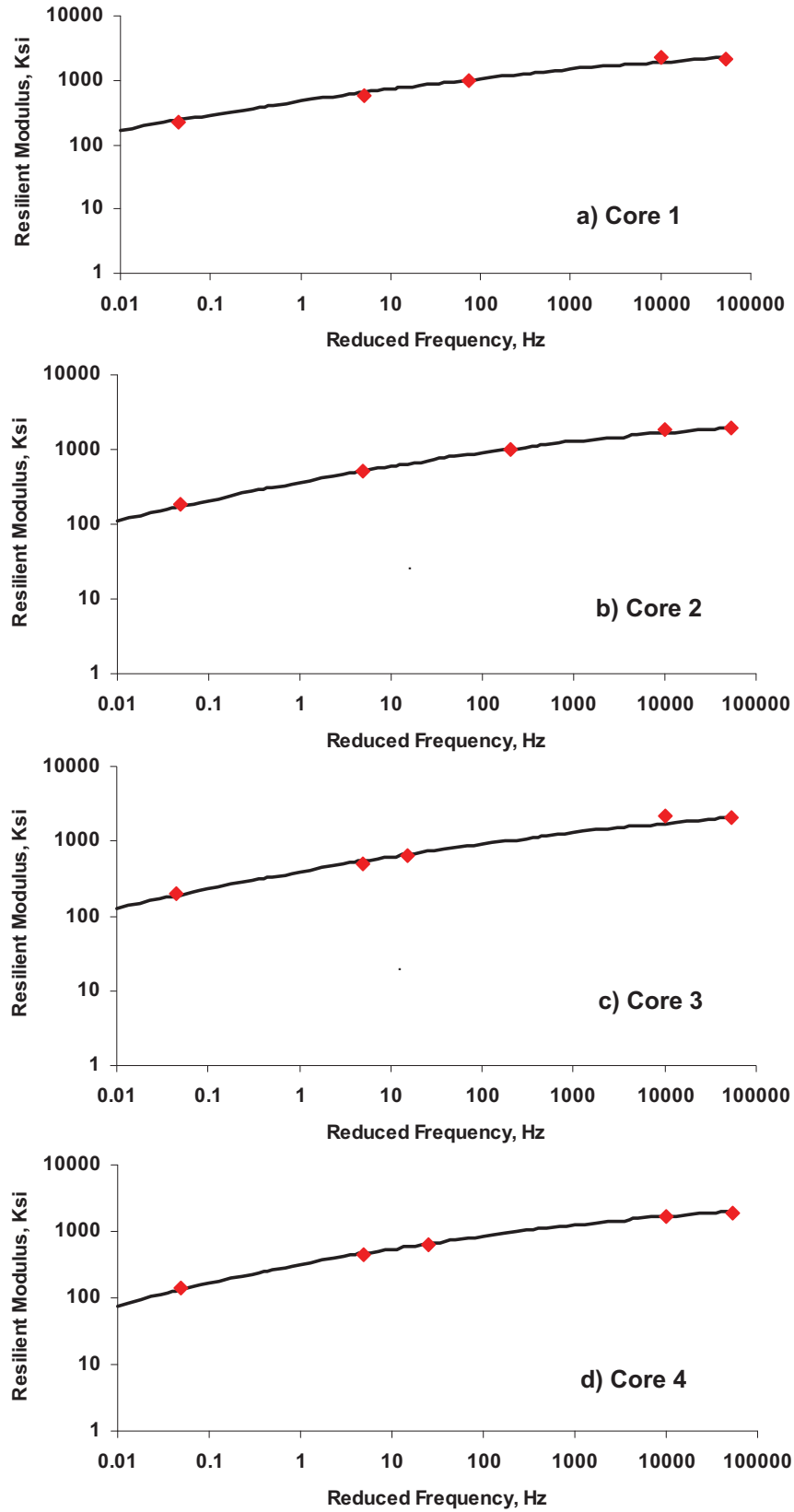


Figure 64. Graph. Master Curves for Site 5.

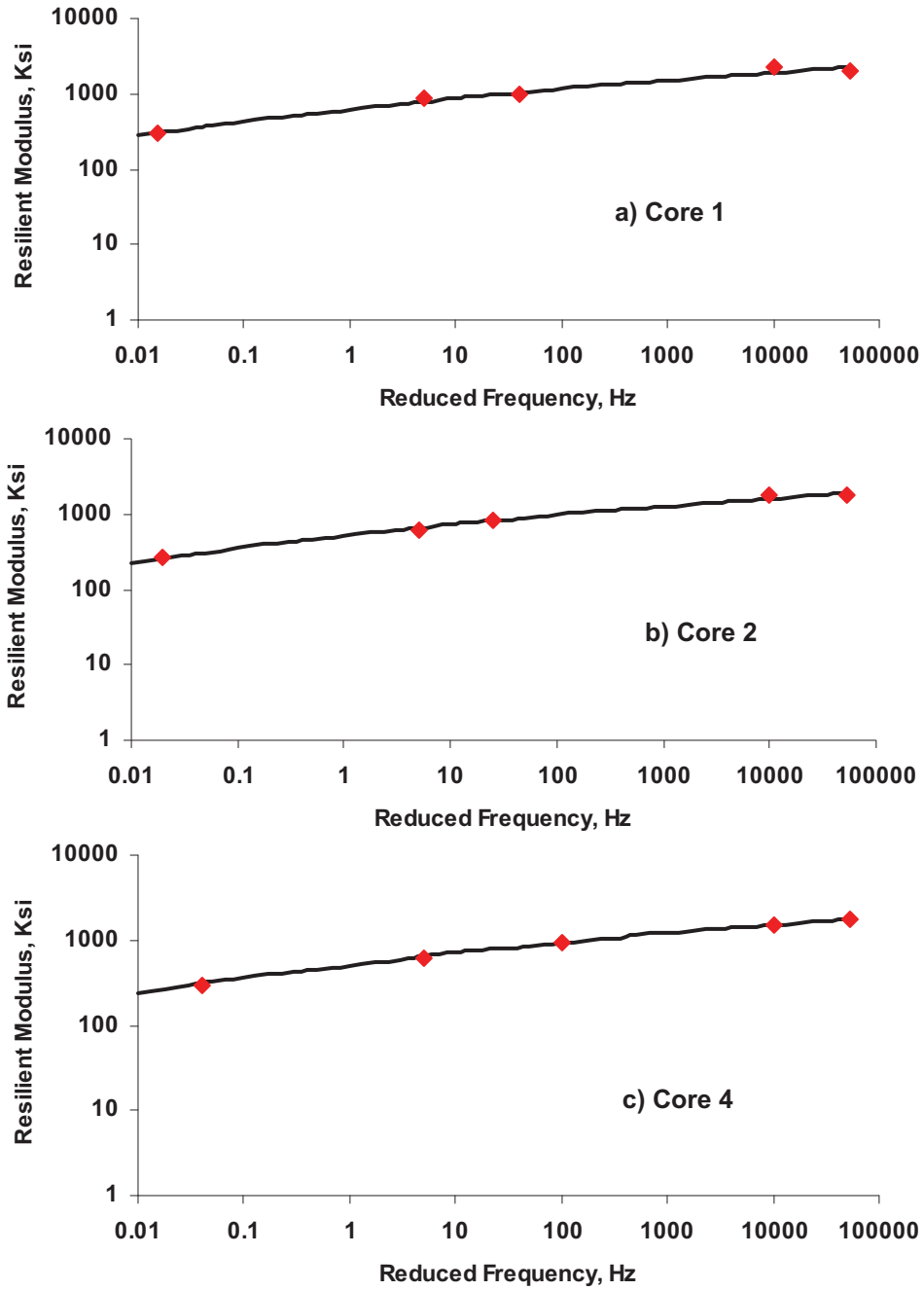


Figure 65. Graph. Master Curves for Site 6.

Table 16. Master Curve Parameters for Site 2.

Specimen Number	δ	α	β	γ	RMS Error	R^2
1	-3.100	7.000	-1.600	0.140	6%	0.970
2	-3.100	6.950	-1.600	0.150	6%	0.992
3	Could not be tested					
4	-3.100	6.950	-1.600	0.150	15%	0.973
Average	-3.100	6.967	-1.600	0.147	9%	0.978

Table 17. Master Curve Parameters for Site 3.

Specimen Number	δ	α	β	γ	RMS Error	R^2
1	-3.700	7.300	-1.600	0.320	13%	0.974
2	-2.900	6.250	-1.600	0.500	35%	0.958
3	-2.900	6.350	-1.600	0.380	39%	0.942
4	-3.700	7.300	-1.600	0.360	14%	0.967
Average	-3.300	6.800	-1.600	0.390	25%	0.960

Table 18. Master Curve Parameters for Site 4.

Specimen Number	δ	α	β	γ	RMS Error	R^2
1	-2.950	6.600	-1.600	0.140	17%	0.933
2	-3.100	6.900	-1.600	0.115	10%	0.945
3	-2.950	6.800	-1.600	0.110	13%	0.932
4	-2.950	6.950	-1.600	0.110	9%	0.965
Average	-2.988	6.813	-1.600	0.119	12%	0.944

Table 19. Master Curve Parameters for Site 5.

Specimen Number	δ	α	β	γ	RMS Error	R^2
1	-3.300	7.180	-1.600	0.200	11%	0.978
2	-3.300	7.080	-1.600	0.220	10%	0.984
3	-3.300	7.050	-1.600	0.230	5%	0.981
4	-3.450	7.150	-1.600	0.260	5%	0.980
Average	-3.338	7.115	-1.600	0.228	8%	0.981

Table 20. Master Curve Parameters for Site 6.

Specimen Number	δ	α	β	γ	RMS Error	R^2
1	-2.950	6.900	-1.600	0.160	10%	0.961
2	-2.950	6.800	-1.600	0.165	6%	0.981
3	Could not be tested					
4	-2.950	6.800	-1.600	0.155	3%	0.991
Average	-2.950	6.833	-1.600	0.160	6%	0.977